

Dissertation zur Erlangung des Doktorgrades
der Fakultät für Chemie und Pharmazie
der Ludwig-Maximilians-Universität München

**Investigation of the Sulfone Moiety
under Superacidic Conditions**

Dominik Johannes Leitz

aus Esslingen am Neckar

2018

Erklärung

Diese Dissertation wurde im Sinne von § 7 der Promotionsordnung vom 28. November 2011 von Herrn Prof. Dr. Andreas J. Kornath betreut.

Eidesstattliche Versicherung

Diese Dissertation wurde eigenständig und ohne unerlaubte Hilfe erarbeitet.

München, den 20.12.2018

.....

(Dominik Johannes Leitz)

Dissertation eingereicht am 27.12.2018

1. Gutachter: Prof. Dr. A. J. Kornath

2. Gutachter: Prof. Dr. T. M. Klapötke

Mündliche Prüfung am 28.01.2019

„What we know is a drop,
what we don't know is an ocean.“

Isaac Newton (1643–1727)

Danksagung (Acknowledgements)

An erster Stelle möchte ich meinem Doktorvater Herrn Prof. Dr. Andreas J. Kornath für die freundliche Aufnahme in den Arbeitskreis, die fortwährende Unterstützung, die interessante Aufgabenstellung und die Gewährung wissenschaftlicher Freiheit, herzlich danken.

Des Weiteren möchte ich mich bei Herrn Prof. Dr. Thomas M. Klapötke für die Übernahme des Korreferats bedanken.

Zunächst möchte ich mich bei der „alten Crew“ Alex, Can, Christian, Joe, Mathias, Nadine und Theresa für die freundliche Aufnahme in den Arbeitskreis, schon während der Bachelorarbeit, bedanken. Weiterhin gebührt Alan, Alex, Chris, Flo, Ines, Manu, Marie, Martina, Michi, Nedz, Steffi, Lukas und Yvonne ein besonderes Dankeschön für die hervorragende Arbeitsatmosphäre, die bereichernden fachlichen und fachfremden Gespräche, die Karaoke-Abende und die BBQs. Ich habe die Zeit mit euch sehr genossen.

Karin und Yvonne – ohne eure bemerkenswerte Geduld beim Picken von Einkristallen und Lösen der Kristallstrukturen, würde meine Arbeit nur halb so bunt aussehen. Tausend Dank! Ihr habt einen großen Teil zum Gelingen dieser Arbeit beigetragen. Bei Flo bedanke ich mich für die Hilfe und Unterstützung bei quanten-chemischen Fragestellungen. Du hast ebenso einen großen Beitrag zum Gelingen dieser Arbeit geleistet.

Bei meinen PraktikantInnen Jana, Marvin, Alan, Alex, Marie und Gloria möchte ich mich für die gute Zusammenarbeit und experimentellen Beiträge zu meiner Doktorarbeit bedanken.

Des Weiteren möchte ich mich beim kompletten Team der Ver- und Entsorgung bedanken: Frau Buchholz, Frau Brackelmann, Frau Reineke, Herrn Gayer und Herrn Schürer, bei Herrn Ober und der kompletten Feinmechanik 1 und 2, Herrn Obst und Herrn Wolf in der Elektrotechnik, Herrn Fuchs und dem gesamten HLS Team, Frau Geng und Frau Schöler von der Poststelle und Herrn Hartmann. Sie alle haben stets einen reibungslosen Laboralltag ermöglicht und standen für Hilfestellungen unentwegt zur Stelle.

Bei Markus und Wolfgang möchte ich mich für die großartige Nachbarschaft bedanken.

Ein herzliches Dankeschön gilt auch Dr. Guillaume Bélanger-Chabot für die finalen sprachlichen Korrekturen.

Ein ganz besonderer Dank gilt unserer Sekretärin Gaby. Deine Unterstützung in allen organisatorischen Angelegenheiten und auch auf persönlicher Ebene, ist zweifelsohne beispiellos.

Meiner Familie und meinen Freunden möchte ich für die Unterstützung, die aufmunternden Worte und ihr Verständnis ganz herzlich danken.

Im Speziellen danke ich meiner Freundin. Du warst all die Jahre immer für mich da und ein stetiger Rückhalt und hast mich aufgebaut, wenn es einmal nicht so lief. Ich bin froh, Dich in meinem Leben zu haben.

Table of Contents

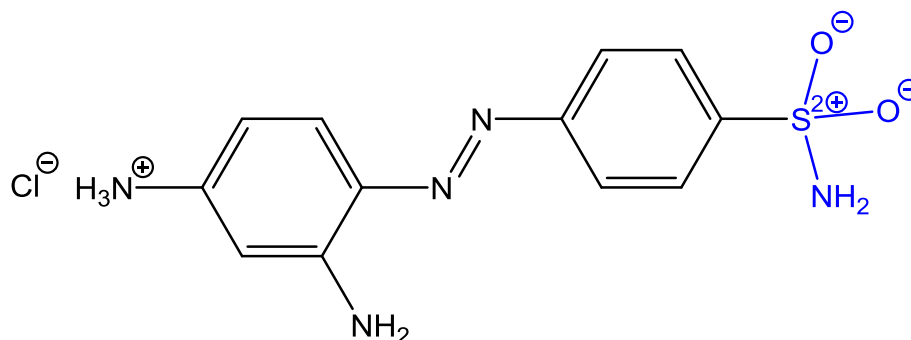
1. INTRODUCTION.....	1
2. OBJECTIVES.....	4
3. SUMMARY	6
3.1 Protonation of Dimethylsulfone.....	6
3.2 Protonation of Methanesulfonamide	7
3.3 Protonation of Chlorosulfonamide.....	9
3.4 Chlorosulfonyl isocyanate in anhydrous hydrogen fluoride.....	11
3.5 Protonation of Sulfamide	11
3.6 Protonation of Selenourea.....	13
3.7 Protonation of Thiourea dioxide.....	14
4. CONCLUSIONS.....	16
5. APPENDIX	20
5.1 Curriculum Vitae.....	20
5.2 Full list of Publications and Conference Contributions.....	21
5.2.1 Publications (peer-reviewed).....	21
5.2.2 Poster Presentations.....	22
5.2.3 Oral Presentations	22
5.3 Manuscripts, Supporting Information and Cover Pictures published in the context of this dissertation	23
5.3.1 Dimethylhydroxyoxosulfonium(VI) Hexafluoridometallates, $[(\text{CH}_3)_2\text{SO}(\text{OX})]^+[\text{MF}_6]^-$ (X = H, D; M = As, Sb	24
5.3.2 Methanesulfonamide in Superacids: Investigations of the $\text{CH}_3\text{SO}_2\text{NH}_3^+$ Cation	32
5.3.3 The Influence of the Counterions $[\text{AsF}_6]^-$ and $[\text{GeF}_6]^{2-}$ on the Structure of the $[\text{ClSO}_2\text{NH}_3]^+$ Cation	38

5.3.4	Crystal Structure and Vibrational Spectra ClSO ₂ NHC(O)F	42
5.3.5	Tuning the Anomeric Effect in Sulfamide with Superacids.....	56
5.3.6	Preparation of Protonated Selenourea	67
5.3.7	Structural Investigation of Thiourea dioxide in Superacids.....	78

1. INTRODUCTION

Compounds of the general formula $R-SO_2-R'$ ($R, R' \neq H$) are defined as sulfones.^[1] This compound class is known at least since 1867, when dimethylsulfone, its simplest representative, was synthesized by *Saytzeff*.^[2] Its synthesis was achieved by the oxidation of dimethylsulfoxide using concentrated nitric acid.^[2] In the following decades, a large number of further sulfone derivatives was developed.^[3-4] Nowadays sulfone derivatives are still of great interest for research because of their numerous applications, such as anti-infectious agents,^[5] anticancer agents^[6] and also due to their anti-inflammatory-analgesic activity.^[7] Even the above mentioned dimethylsulfone has proved to be a versatile drug for arthrosis,^[8] arthritis,^[9] or as breast cancer suppressing agent.^[10]

The formal substitution of R by an amino group in a sulfone leads to the compound class of sulfonamides ($R-SO_2-NH_2$). Here, the discovery of Prontosil has to be mentioned as a pioneering breakthrough. Just one year after its first synthesis by *Mietzsch and Klarer*^[11] in 1934, *Domagk* was able to show its antibacterial activity. For this discovery he received the Nobel Prize for Medicine in 1939.



This prompted the development of a large number of bioactive sulfonamides with multiple medical uses, such as the treatment of malaria,^[12] diabetes^[13] and epilepsy,^[14] and with applications in agriculture, because of the antifungal activity^[15] of sulfonamides. In 1940 *Mann and Keilin* discovered sulfanilamide as a carbonic anhydrase (CA) inhibitor.^[16] For a long time, it was believed that solely aromatic sulfonamides possess this property. This dogma was contradicted by *Supuran et al.* who showed that sulfamide ($H_2NSO_2NH_2$) can act as CA inhibitor as well.^[17] *Maren et al.*

reported that other aliphatic sulfonamides, such as $\text{CH}_3\text{SO}_2\text{NH}_2$ or $\text{CF}_3\text{SO}_2\text{NH}_2$, also show CA inhibitory potential.^[18] The authors of this study found that the introduction of halogen atoms to the aliphatic residue leads to a significant increase in inhibitory strength. A linear relationship between the dissociation constant (pK_a) of the sulfonamide derivative and the dissociation constant K_1 was established.^[18] This finding emphasizes the importance of the acid and base properties for a fundamental understanding of inhibitory properties. For the definitions and derivations of these essential physicochemical parameters one has to go a step back in history. Already in 1908, *Henderson* recognized the relevance of these characteristics and was the first who describe the relationship between the hydrogen ion $[\text{H}^+]$ and the composition of a buffer.^[19] For a simplified comparison of $[\text{H}^+]$ concentrations in different solutions, *Sørensen* introduced the pH value, which is defined as the negative logarithm of $[\text{H}_3\text{O}^+]$ (Equation (1)).

$$\text{pH} := -\log([\text{H}_3\text{O}^+]) \quad (1)$$

Henderson basically layed the foundation out of which *Hasselbalch*^[20] developed eight years later the following Equation (2):

$$\text{pH} := \text{pK}_a + \log\left(\frac{[\text{A}^-]}{[\text{HA}]}\right) \quad (2)$$

This equation is commonly known as ‘*Henderson-Hasselbalch* equation’, whereby a relation between pH and pK_a is given to the equilibrium concentrations of non-dissociated acid (HA) and dissociated acid (A^-).

LeMaire and *Lucas* were the first to report a photometric study on the estimation of the acid pK_a value of a sulfonamide-derivative.^[21] The authors of this study determined the pK_a value of *p*-toluenesulfonamide to be -3.2 . As a further study, *Olavi et al.* reported pK_a values for some other benzenesulfonamide derivatives with comparable values.^[22] *Laughlin et al.* investigated the basicity of aliphatic sulfonamides using NMR spectroscopy in solution showing that an *N*-protonation is favored.^[23] However, structural parameters of protonated sulfonamide derivatives have so far not been reported.

Regarding the basicity, urea derivatives represent another interesting compound class. These molecules hold two competing basic sites: the amino group and the chalcogen atom as shown in Figure 1.

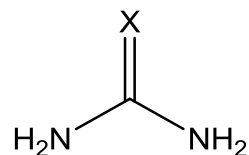


Figure 1: General structure of a urea derivative (X = chalcogen).

This issue has been intensively discussed. Based on a vibrational spectroscopic study, *Spinner* concluded that, in the case of urea and thiourea, the protonation takes place at the nitrogen atom, which leads to the formation of the $[\text{H}_2\text{NC}(\text{X})\text{NH}_3]^+$ (X = O, S) cation.^[24] This finding was disproved unanimously by two other studies.^[25-26] The characterization of urea phosphate by a single-crystal X-ray diffraction study supported this result.^[27] In 1963, *Birch* and *Gillespie* reported indications of an *N,S*-diprotonation in highly acidic media (fluorosulfonic acid) using NMR-spectroscopy.^[28] *Olah* and *Christe* confirmed the existence of the $[\text{H}_2\text{NC}(\text{SH})\text{NH}_3]^{2+}$ cation by a Raman-spectroscopic investigation.^[29] In the course of his PhD thesis, *Axhausen* investigated urea and thiourea in the binary superacidic systems HF/MF₅ (M = As, Sb).^[30] It was shown that, depending on the molar ratio of Lewis acid to starting material, salts of *X*-mono- and *X,N*-diprotonated species of the type $[\text{H}_2\text{NC}(\text{XH})\text{NH}_2]^+$ and $[\text{H}_2\text{NC}(\text{XH})\text{NH}_3]^{2+}$ (X = O, S), respectively, are selectively obtained.^[30] The corresponding cations were characterized by low temperature vibrational spectroscopy and single crystal X-ray structure analyses.

2. OBJECTIVES

Since the basicity of sulfone derivatives has not been studied systematically until now, the first project in the course of this PhD work was to examine dimethylsulfone (DMSO₂/Figure 2), the simplest sulfone representative, in the binary superacidic systems HF/AsF₅ and HF/SbF₅ with the aim to prepare and structurally characterize its protonated species.

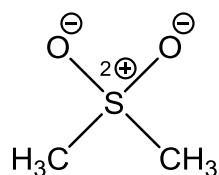


Figure 2: Structure of dimethylsulfone.

In contrast to the sulfones, a few studies on the basicity of sulfonamides were reported in the literature.^[21-23] However, the structural parameters of protonated sulfonamides are unknown to date. Furthermore, the question is raised whether a diprotonation is possible and whether the cationic structure can be influenced by the choice of counterions. Methanesulfonamide and chlorosulfonamide are therefore promising target molecules to be investigated in binary superacidic systems (Figure 3).



Figure 3: Structures of methanesulfonamide (left) and chlorosulfonamide (right).

The formal substitution of the methyl group and the chlorine atom, respectively, by an amino group constitutes the sulfamide molecule, which is another interesting species in the above-mentioned context (Figure 4).

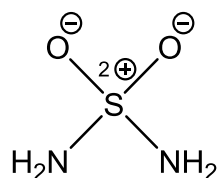


Figure 4: Structure of sulfamide.

As stated in the introduction, *Axhausen* already studied the basicity of urea and thiourea where in both cases diprotonations were detected.^[30] As a further study, it was interesting to investigate if the observed effects are also observed for the heavier homologue selenourea (Figure 5).

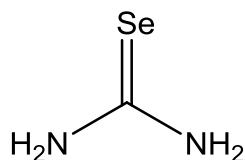


Figure 5: Structure of selenourea.

As a chimeric species between sulfone- and urea derivatives, thiourea dioxide (Figure 6) proved to be an interesting species to be investigated under the above-mentioned conditions.

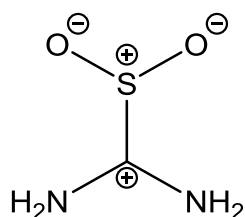
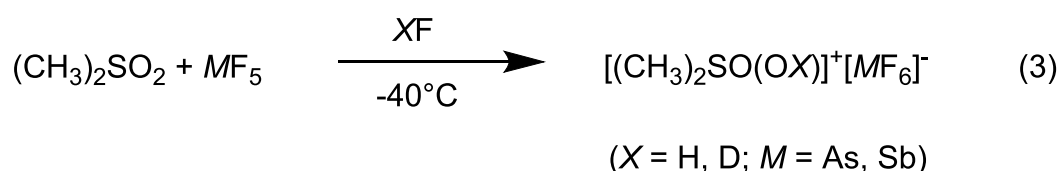


Figure 6: Structure of thiourea dioxide.

3. SUMMARY

3.1 Protonation of Dimethylsulfone

Dimethylsulfone (DMSO₂) reacts in superacidic media according to the following Equation (3)^[31]:



The vibrational spectroscopic analysis clearly shows that a monoprotection takes place. This result is supplemented by a single-crystal X-ray diffraction analysis of $[(\text{CH}_3)_2\text{SO}(\text{OH})]^+ [\text{SbF}_6]^-$. The experimental results are consistent with quantum chemical calculations as shown in Figure 7 comparing the calculated and experimental structures.

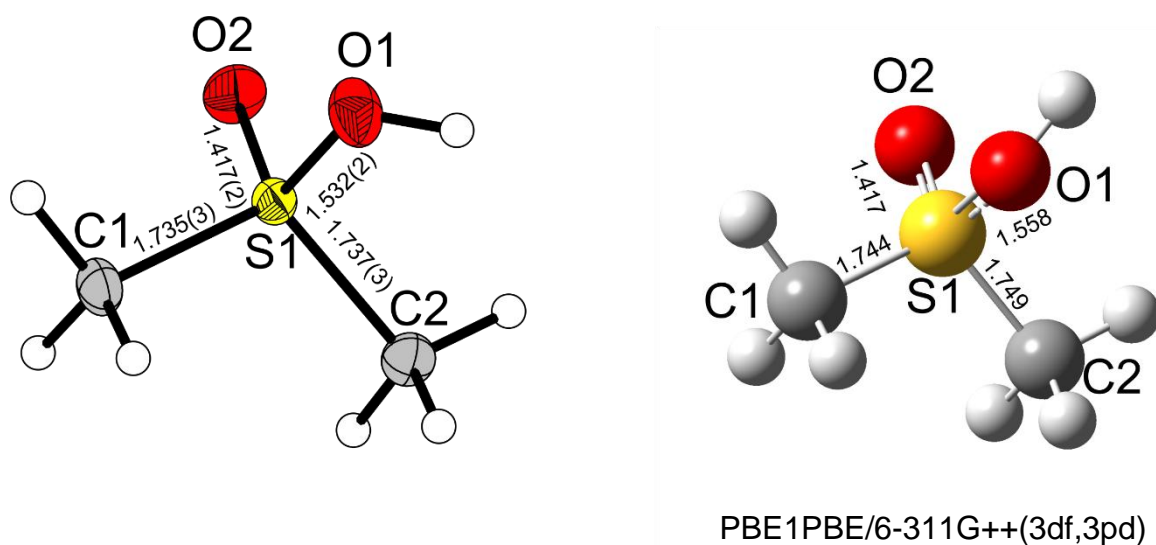


Figure 7: Comparison of the experimentally observed (left) and the calculated (right) cationic structure of $[(\text{CH}_3)_2\text{SO}(\text{OH})]^+$ (bond lengths in Å).

A diprotonation was not observed, even by employing a large excess of Lewis acid with respect to DMSO₂. In the solid state the cations form zigzag-like chains along the *a* axis, connected by weak C(-H)⋯O donor-acceptor interactions. Therefore, a further theoretical investigation of its electrostatic potential (ESP) was carried out. (Figure 8)

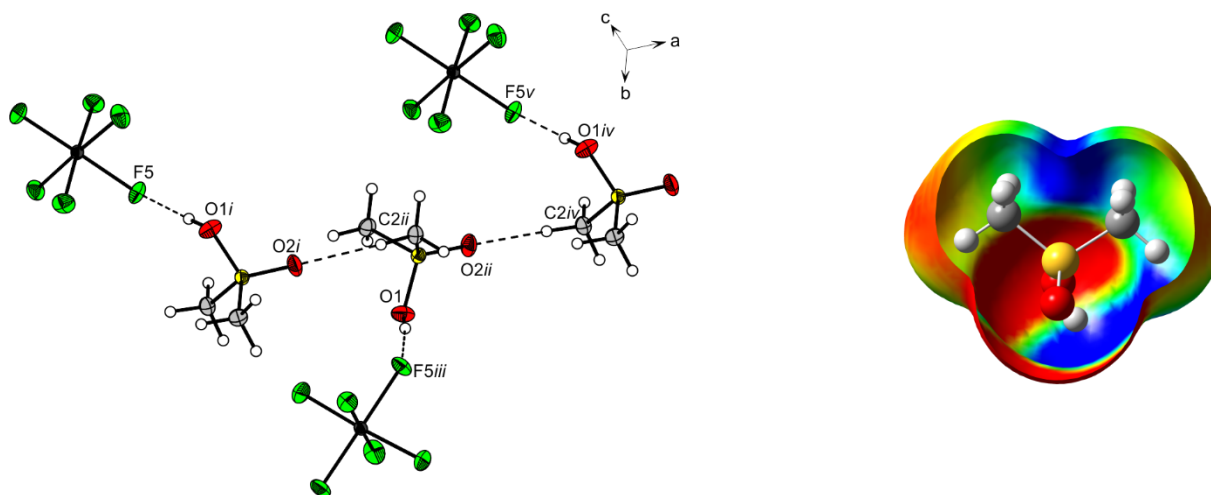
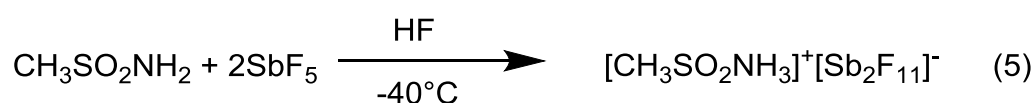
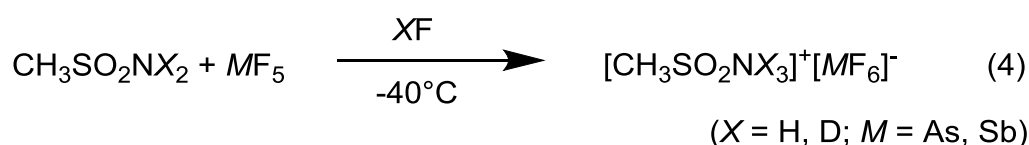


Figure 8: Connectivity of cations and anions. Hydrogen bonds represented as dashed lines. (thermal ellipsoids with 50%probability). Symmetry codes: $i=-0.5+x, y, 0.5-z$; $ii=x, 0.5-y, 0.5-z$; $iii=0.5+x, 0.5-y, -z$; $iv=0.5+x, y, 0.5-z$; $v=1+x, y, z$. (left). Gas-phase optimization of $[(\text{CH}_3)_2\text{SO}(\text{OH})]^+$. In the background an electrostatic potential (ESP) map is superimposed as a colorscale ranging from 0.170 a.u. (red) and 0.210 a.u. (blue); isoval. = 0.004.

In the course of the examination of the ESP, no significant difference in the positive polarization of the protons of both methyl groups is found. Therefore, one can conclude that the cation-cation interaction is mainly based on solid-state effects rather than by an intrinsic property of the $[(\text{CH}_3)_2\text{SO}(\text{OH})]^+$ cation.

3.2 Protonation of Methanesulfonamide

Methanesulfonamide reacts in the superacidic solutions XF/AsF_5 or XF/SbF_5 under the formation of colorless salts of the type $[\text{CH}_3\text{SO}_2\text{NX}_3]^+[\text{MF}_6]^-$ ($X = \text{H}, \text{D}$; $M = \text{As}, \text{Sb}$)^[32] (Equation 4). Adding several equivalents of the Lewis acids with respect to methanesulfonamide does not lead to an N,O -protonation but, in the case of SbF_5 , to the formation of $[\text{CH}_3\text{SO}_2\text{NH}_3]^+[\text{Sb}_2\text{F}_{11}]^-$ (Equation 5).



Quantum chemical calculations of the $[\text{CH}_3\text{SO}_2\text{NH}_3]^+$ cation predict that the protonation causes a remarkable elongation of the sulfur-nitrogen bond which is confirmed by the single-crystal X-ray structure analysis of $[\text{CH}_3\text{SO}_2\text{NH}_3]^+[\text{Sb}_2\text{F}_{11}]^-$ and consistent with the vibrational analyses. In terms of the quantum chemical calculations, the addition of three HF molecules leads to the best agreement with the experimentally determined geometry. In previous studies, this method already became apparent as a powerful tool for simulating H-bonding in the solid state.^[33-34] Figure 9 shows a comparison between the calculated and the experimental structure of the $[\text{CH}_3\text{SO}_2\text{NH}_3]^+$ cation.

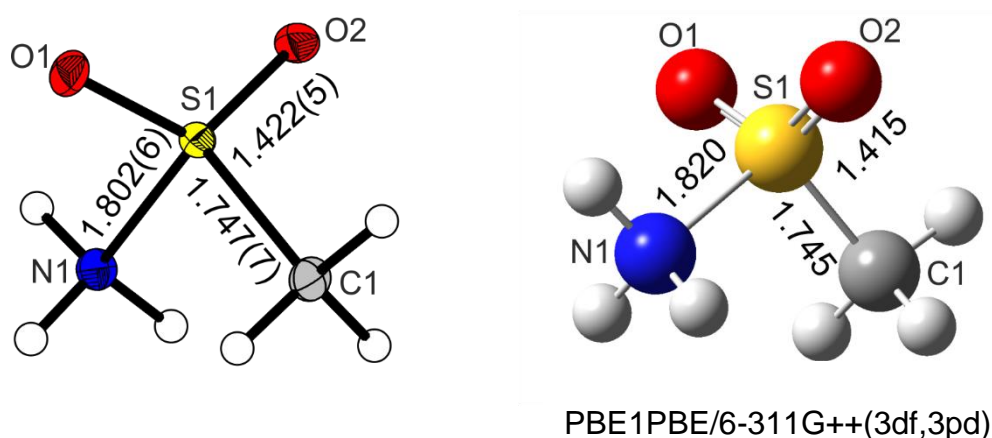


Figure 9: Comparison of the experimentally observed (left) and the calculated (right) structure of $[\text{CH}_3\text{SO}_2\text{NH}_3]^+$ (bond lengths in Å) (for the sake of clarity the HF molecules are omitted).

In addition, the single-crystal X-ray structure of the starting material methanesulfonamide was revisited. In the solid state the $\text{CH}_3\text{SO}_2\text{NH}_2$ molecules are building layers along the *b* axis. Each molecule is connected to four neighboring molecules building 14-membered rings. (Figure 10).

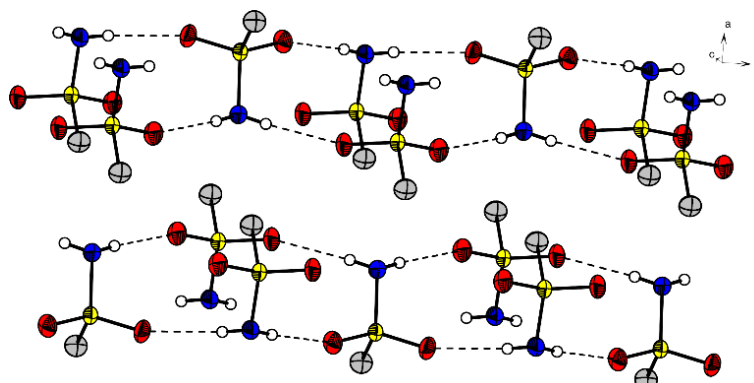


Figure 10: Crystal packing of $\text{CH}_3\text{SO}_2\text{NH}_2$. View along the *c* axis. Hydrogen bonds are drawn as dashed lines. The protons of the methyl groups are not shown (50% probability displacement ellipsoids).

3.3 Protonation of Chlorosulfonamide

Before investigating chlorosulfonamide under superacidic conditions, we determined its surprisingly hitherto unknown single-crystal X-ray structure. The ClSO₂NH₂ molecules are forming a three-dimensional network consisting of 14-membered rings as shown in Figure 11.^[35]

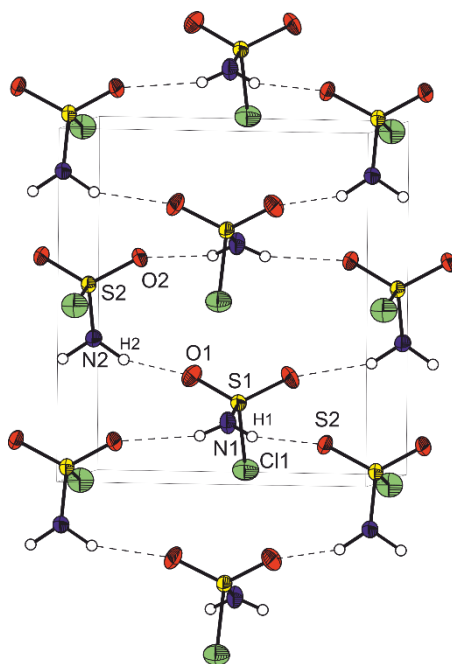
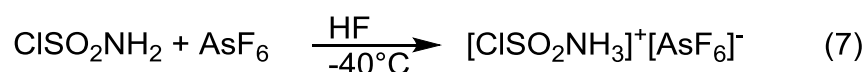


Figure 11: Crystal packing of ClSO₂NH₂ (50% probability displacement ellipsoids). View along *b* axis. Hydrogen bonds are drawn as dashed lines.

Chlorosulfonamide reacts in the superacidic systems HF/AsF₅ and HF/GeF₄ according to the following Equations (6–7).^[35]



Vibrational analyses show that the protonation selectively takes place at the nitrogen atom, which is confirmed by the single-crystal X-ray structure analyses of [ClSO₂NH₃]⁺[AsF₆]⁻ and ([ClSO₂NH₃]⁺)₂[GeF₆]²⁻. Figure 12 depicts a formula unit of the [GeF₆]²⁻ salt (left) and the asymmetric unit of the [AsF₆]⁻ salt (right).

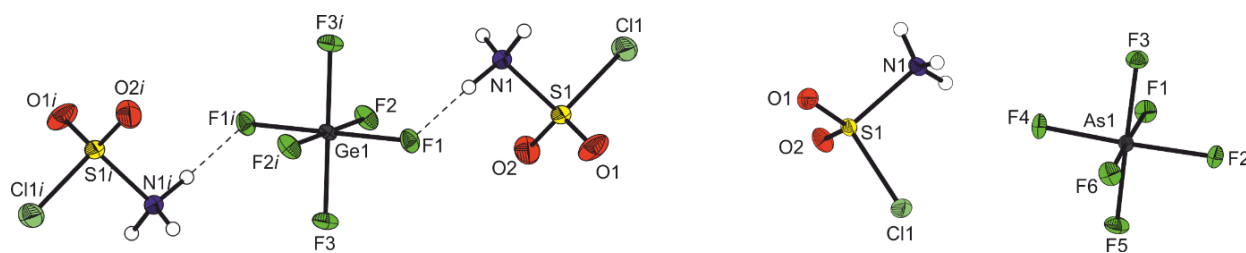


Figure 12: Formula unit of $[(\text{ClSO}_2\text{NH}_3)^+]_2[\text{GeF}_6]^{2-}$, Symmetry code: $i=-x, 1-y, -z$ (left); asymmetric unit of $[\text{ClSO}_2\text{NH}_3]^+[\text{AsF}_6]^-$ (right) (50% probability displacement ellipsoids).

Comparable to that of methanesulfonamide, the *N*-protonation of chlorosulfonamide causes a significant elongation of the nitrogen-sulfur bond. Depending on the counterion $[\text{GeF}_6]^{2-}$ and $[\text{AsF}_6]^-$, respectively, it was found that the S–N bond lengths are notably different. Therefore, further quantum chemical calculations were performed in order to investigate the influence on the counterions. The results of this investigation are illustrated in Figure 13. The geometric parameters are well reproduced by the quantum chemical calculations. This can be considered as proof for the hypothesis of the influence of the counterions on the cationic structure of the $[\text{ClSO}_2\text{NH}_3]^+$ cation.

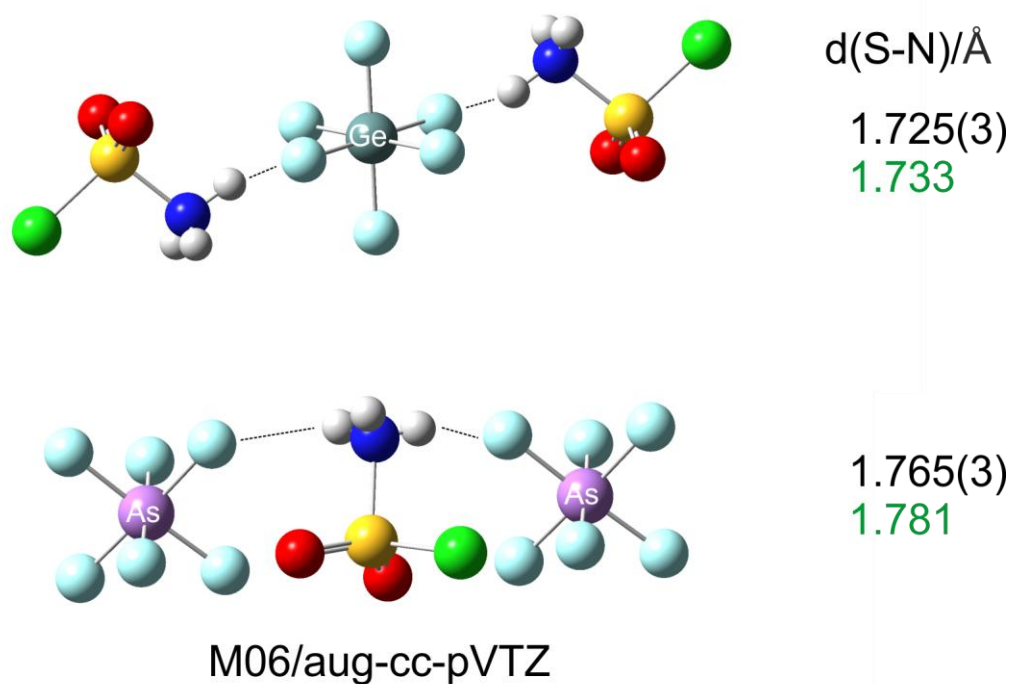


Figure 13: Calculated units of $[(\text{ClSO}_2\text{NH}_3)^+]_2[\text{GeF}_6]^{2-}$ (top) and $[(\text{ClSO}_2\text{NH}_3)^+][\text{AsF}_6]^-$ (bottom) at the M06/aug-cc-pVTZ level of theory.

3.4 Chlorosulfonyl isocyanate in anhydrous hydrogen fluoride

Chlorosulfonyl isocyanate (CSI) reacts in anhydrous hydrogen fluoride according to the following Equation (8).^[36]



The selective HF addition forming ClSO₂NHC(O)F is unambiguously shown by vibrational analyses and confirmed by a single-crystal X-ray diffraction analysis. The experimental results are in fair agreement with the calculated ones which is shown in Figure 14.

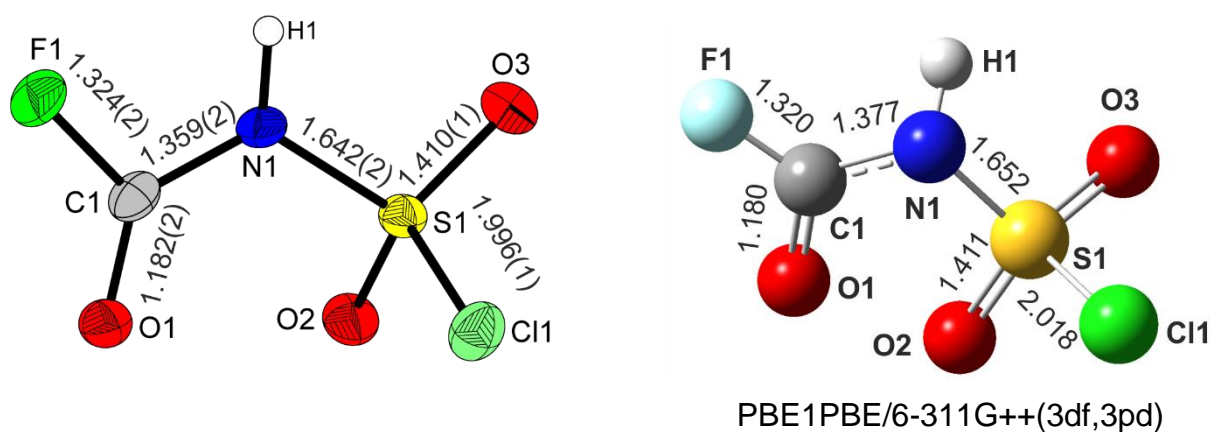
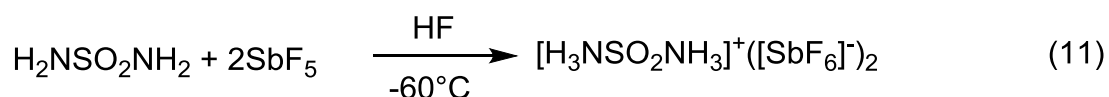
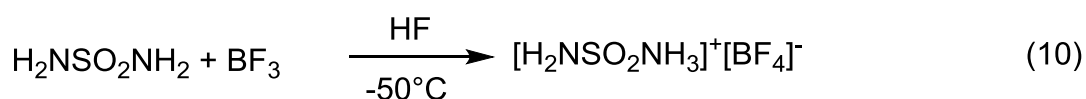
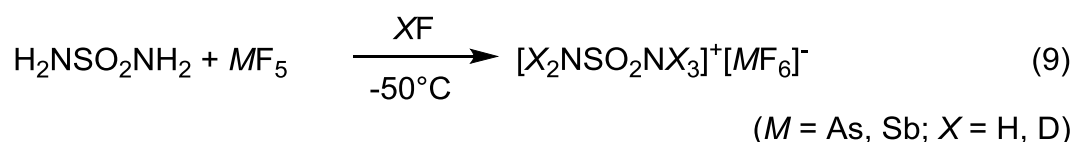


Figure 14: Comparison of the experimental (left) and calculated (right) structure of ClSO₂NHC(O)F.

3.5 Protonation of Sulfamide

Sulfamide was investigated in the binary superacidic systems HF/MF₅ (*M* = As, Sb) as well as HF/BF₃. Reactions accordingly to the following Equations (9–11) were observed.^[37]



The $[\text{H}_2\text{NSO}_2\text{NH}_3]^+[\text{BF}_4]^-$ was proved to be a remarkably stable salt showing no significant decomposition up to 60°C and has a good stability even towards moisture. An N,N' -diprotonation succeeded only in the case of the acid HF/SbF₅. A single-crystal X-ray structure was determined for $[\text{H}_2\text{NSO}_2\text{NH}_3]^+[\text{BF}_4]^-$ and $[\text{H}_3\text{NSO}_2\text{NH}_3]^{2+}2[\text{SbF}_6]^- \cdot 2\text{HF}$. The calculated and the experimentally observed cationic structures together with selected geometric parameters are summarized in Figure 15.

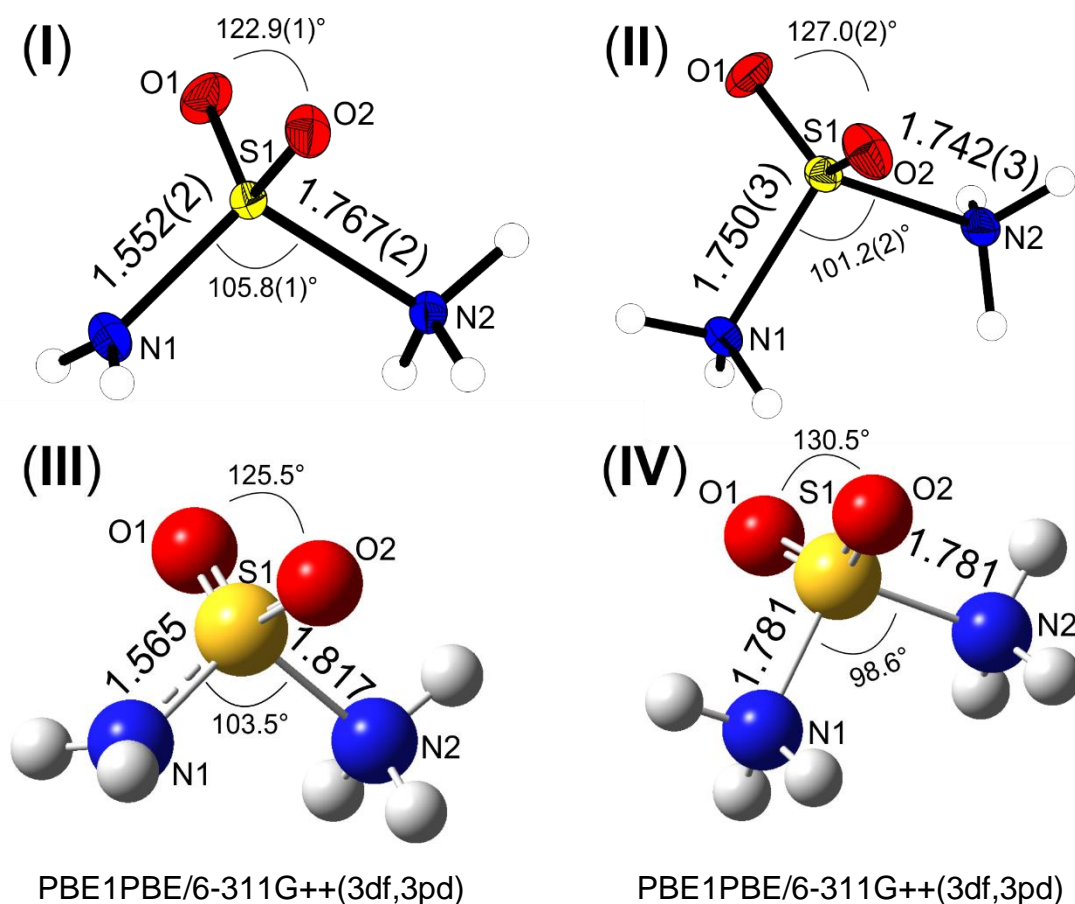
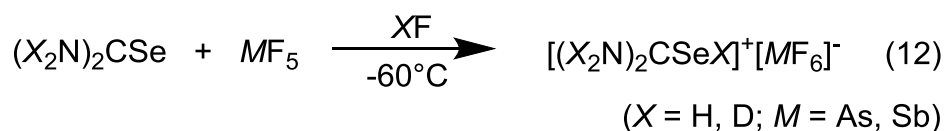


Figure 15: Comparison of the calculated (PBE1PBE/6-311++(3df, 3pd)) and experimental cationic structures of $[\text{H}_2\text{NSO}_2\text{NH}_3]^+$ [(I) and (III)] as well as $[\text{H}_3\text{NSO}_2\text{NH}_3]^{2+}$ [(II) and (IV)].

In this study it is demonstrated that the anomeric effect (negative hyperconjugation) in sulfamide, as an origin of the relatively short S–N bonds, can be tuned by the utilization of superacidic media. Interestingly, in the case of the N -monoprotonated species, the S–N bond of the amino site is significantly shortened compared to that of the starting material. Therefore, a calculation of the rotational barrier around the S–NH₂ bond was carried out, showing an approximately threefold increase compared to the starting material. This finding can be considered as a measure for the enhancement of the anomeric effect. It was shown that the occurring anomeric effect in sulfamide can be tuned by the utilization of superacidic media.

3.6 Protonation of Selenourea

Selenourea was reacted in the binary superacidic systems according to the following Equation (12).^[38]



The Se-protonation was clearly demonstrated by vibrational analyses and confirmed by a single-crystal X-ray diffraction analysis of $[(H_2N)_2CSeH]^+[SbF_6]^-$. Even employing a large excess of Lewis acid (MF_5) with respect to selenourea does not lead to a diprotonation but selectively to a monoprotonation. The experimental and the calculated results are in fair agreement as shown in Figure 16 comparing the experimental and the calculated structure.

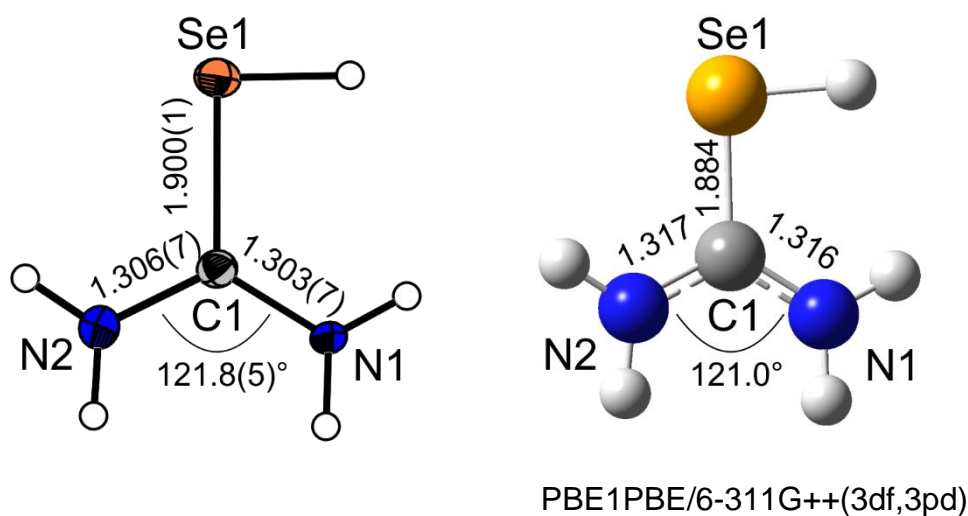


Figure 16: Comparison of the experimentally observed (left) and quantum chemically calculated (right) structure of the $[(H_2N)_2CSeH]^+$ cation.

In the solid-state, an $Se \cdots F$ contact of $2.90(1) \text{ \AA}$ was found. Therefore, a calculation of the electrostatic potential (ESP) of $[(H_2N)_2CSeH]^+$ cation was carried out. In accordance with the σ -hole concept, a positive local maximum (0.170 a.u.) on the extension of the C–Se bond was found. The contacts around the $[(H_2N)_2CSeH]^+$ cation as well as a superimposed ESP map are shown in Figure 17.

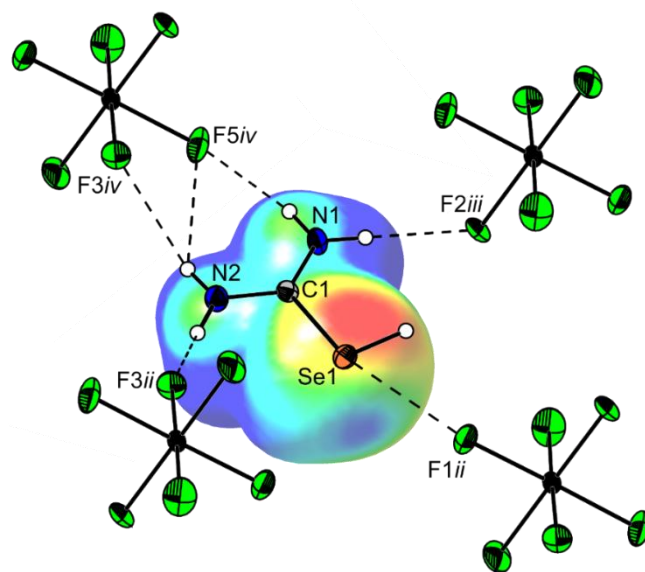
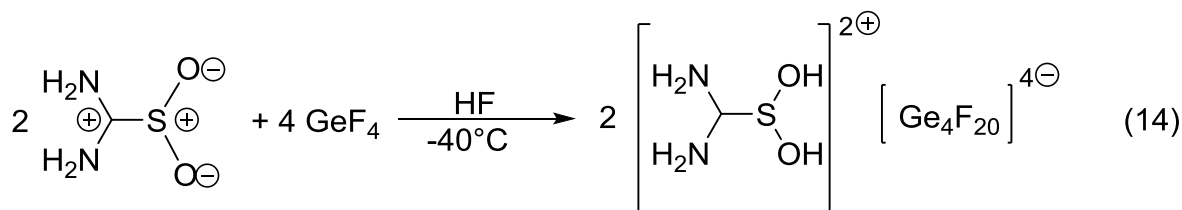
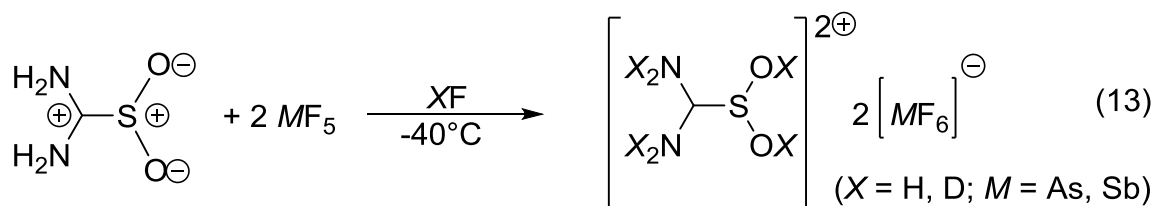


Figure 17: Cation-anion contacts in $[(\text{H}_2\text{N})_2\text{CSeH}]^+[\text{SbF}_6]^-$ (thermal ellipsoids with 50% probability). Donor-acceptor interactions are represented as dashed lines. In the background of the cation an electrostatic potential (ESP) map is superimposed as a color scale ranging from 0.145 a.u. (red) and 0.210 a.u. (blue); isoval. = 0.001; Symmetry codes: *i*: 1-*x*, 2-*y*, 1-*z*, *ii*: *x*, 1+*y*, *z*; *iii*: 1-*x*, 2-*y*, -*z*, *iv*: 1+*x*, *y*, *z*.

3.7 Protonation of Thiourea dioxide

Thiourea dioxide (TDO) reacts in superacidic media according to the following Equations (13–14).^[39]



Attempts to prepare the monoprotonated species led to mixtures containing both, the starting material and the *O,O'*-diprotonated species. The selective *O*-protonation is demonstrated by vibrational analyses and confirmed by singly-crystal X-ray structure

analysis of $2[(\text{H}_2\text{N})_2\text{CS}(\text{OH})]^{2+}_2[\text{Ge}_4\text{F}_{20}]^{4-} \cdot 4\text{HF}$ shown in Figure 18. Furthermore, this is the first example of a salt containing the $[\text{Ge}_4\text{F}_{20}]^{4-}$ anion.

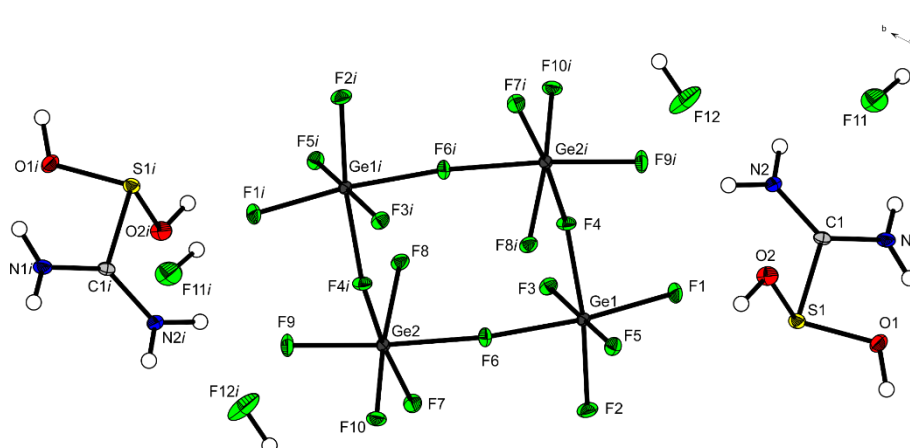


Figure 18: Formula unit of $2[(\text{H}_2\text{N})_2\text{CS}(\text{OH})_2]^{2+}_2[\text{Ge}_4\text{F}_{20}]^{4-} \cdot 4\text{HF}$ (thermal ellipsoids with 50% probability). Symmetry code: $i: -x, 1-y, 1-z$.

The O,O' -diprotonation leads to a significant shortening of the C–S bond with respect to the starting material. Based on this finding, further theoretical investigations were carried out in order to gain insight into the nature of this bond. It was found that, in the case of $(\text{H}_2\text{N})_2\text{CSO}_2$, the $\sigma^*(\text{C}-\text{S})$ orbital is occupied by 0.276 e and the p-orbitals of the oxygen atoms are occupied by 1.779 e. Considering the overlap of these orbitals, it can be concluded that the electron density of these orbitals is donated into the $\sigma^*(\text{C}-\text{S})$ orbital, which is causing a weakening of the corresponding bond. The O,O' -diprotonation results in a notably lower occupation of the $\sigma^*(\text{C}-\text{S})$ orbital [0.105 e], which is consistent with the lower overlap of the corresponding orbitals. Figure 19 shows a comparison of the calculated structures of the starting material (left) and the $[(\text{H}_2\text{N})_2\text{CS}(\text{OH})_2]^{2+}$ cation (right) together with the relevant orbitals.

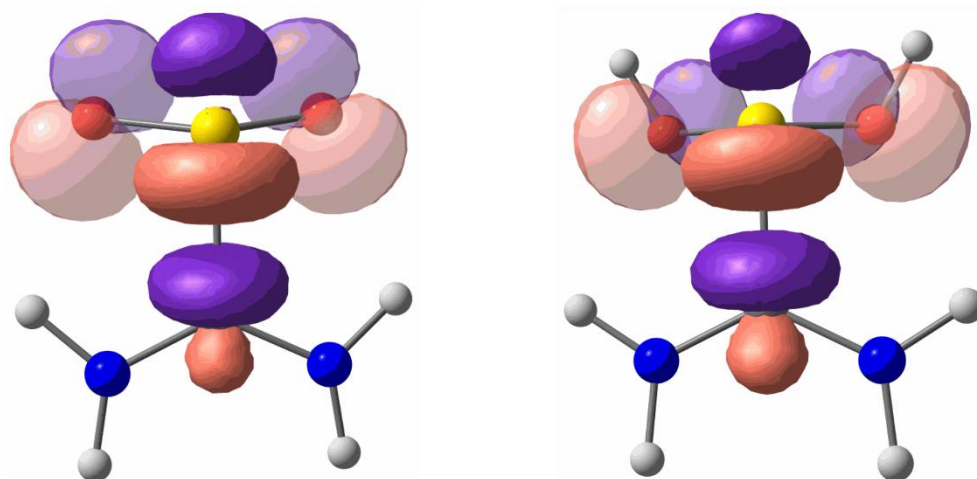


Figure 19: Calculated TDO (left) and its *O,O'*-diprotonated species (right) with illustrated $\sigma^*(\text{C-S})$ and $p(\text{O})$ orbitals.

4. CONCLUSIONS

In the scope of this PhD work, the sulfone moiety was investigated in a series of different molecules, whereby different structural aspects came to light. Starting from the protonation of the simplest representative dimethylsulfone (DMSO_2), only a monoprotection was observed. The respective diprotection was not detected, even by employing a large excess of the Lewis acids. Methanesulfonamide was then investigated, where a remarkable elongation of the sulfur-nitrogen bond took place due to the selective protonation of the nitrogen atom. This effect was also observed for chlorosulfonamide. In addition, it was shown that the counterions can influence the cationic structure of $[\text{ClSO}_2\text{NH}_3]^+$. The reaction behavior of another representative containing a sulfone-moiety, chlorosulfonyl isocyanate, was investigated in anhydrous hydrogen fluoride. HF addition was selectively leading to the novel multifunctional compound $\text{ClSO}_2\text{NHC}(\text{O})\text{F}$.

As the next target molecule, sulfamide was investigated where both a mono- and a diprotection was successfully carried out. Thereby, sulfamide undergoes notable structural changes depending on the degree of protonation. In this context, it was observed that the occurring anomeric effect, as an origin for the relatively short sulfur-nitrogen bonds, can be tuned by *N*-protonation.

Moreover, the series of chalcogen urea compounds was continued with selenourea. Here it was shown that only a monoprotection was possible. In contrast to selenourea's

lighter homologues, a diprotonation was not observed even by increasing the superacidity. Finally, thiourea dioxide, which can be considered as a chimeric species of thiourea and the sulfone moiety, was investigated. In this case an *O,O'*-diprotonation is possible and leads to a significant shortening of the carbon-sulfur bond.

- [1] A. D. McNaught, A. Wilkinson, *IUPAC*. *Compendium of Chemical Terminology, 2nd ed. (the "Gold Book")*, WileyBlackwell; 2nd Revised edition edition.
- [2] A. Saytzeff, *Justus Liebigs Ann. Chem.* **1867**, *144*, 148-156.
- [3] R. Otto, *J. Prakt. Chem.* **1889**, *40*, 505-564.
- [4] E. Stuffer, *Ber. Dtsch. Chem. Ges.* **1890**, *23*, 1408-1414.
- [5] C. Curti, M. Laget, A. O. Carle, A. Gellis, P. Vanelle, *Eur. J. Med. Chem.* **2007**, *42*, 880-884.
- [6] Y. Long, M. Yu, P. Li, S. Islam, A. W. Goh, M. Kumarasiri, S. Wang, *Bioorg Med Chem Lett* **2016**, *26*, 5674-5678.
- [7] B. Tozkoparan, E. K peli, E. Ye ilada, M. Ertan, *Bioorg. Med. Chem.* **2007**, *15*, 1808-1814.
- [8] J. I. Morton, B. V. Siegel, *Proc. Soc. Exp. Biol. Med.* **1986**, *183*, 227-230.
- [9] U. F. H. Engelke, A. Tangerman, M. A. A. P. Willemsen, D. Moskau, S. Loss, S. H. Mudd, R. A. Wevers, *NMR Biomed.* **2005**, *18*, 331-336.
- [10] E. J. Lim, D. Y. Hong, J. H. Park, Y. H. Joung, P. Darvin, S. Y. Kim, Y. M. Na, T. S. Hwang, S.-K. Ye, E.-S. Moon, B. W. Cho, K. Do Park, H. K. Lee, T. Park, Y. M. Yang, *PLoS One* **2012**, *7*, e33361.
- [11] F. Mietzsch, J. Klarer, I. G. Farbenindustrie AG, Patent DE 607537, **1937**.
- [12] B. M. D. Gupta, R. N. Chopra, *Ind. Med. Gaz.* **1938**, *73*, 665-667.
- [13] Ajeet, A. Dudhe, A. Kumar, B. Aggarwal, H. Chadha, P. K. Mishra, S. M. Jain, S. Singh, S. O. Tripathi, *Biointerface Res. Appl. Chem.* **2016**, *6*, 1345-1350.
- [14] T. Tanaka, N. Yajima, T. Kiyoshi, Y. Miura, S. Iwama, *Bioorg. Med. Chem. Lett.* **2017**, *27*, 4118-4121.
- [15] K. Szafranski, J. Slawinski, A. Kedzia, E. Kwapisz, *Molecules* **2017**, *22*, 1926/1921-1926/1917.
- [16] T. Mann, D. Keilin, *Nature* **1940**, *146*, 164.
- [17] F. Briganti, R. Pierattelli, A. Scozzafava, C. T. Supuran, *Eur. J. Med. Chem.* **1996**, *31*, 1001-1010.
- [18] T. H. Maren, C. W. Conroy, *J. Biol. Chem.* **1993**, *268*, 26233-26239.
- [19] L. J. Henderson, *Am. J. Physiol.* **1908**, *21*, 173-179.
- [20] K. A. Hasselbalch, *Biochem. Z.* **1916**, *78*, 112-144.
- [21] H. Lemaire, H. J. Lucas, *J. Am. Chem. Soc.* **1951**, *73*, 5198-5201.

- [22] P. Olavi, I. Virtanen, M. Maikkula, *Tetrahedron Lett.* **1968**, 9, 4855-4858.
- [23] R. G. Laughlin, *J. Am. Chem. Soc.* **1967**, 89, 4268-4271.
- [24] E. Spinner, *Spectrochim. Acta* **1959**, 15, 95-109.
- [25] W. Kutzelnigg, R. Mecke, *Spectrochim. Acta* **1961**, 17, 530-544.
- [26] M. J. Janssen, *Spectrochim. Acta* **1961**, 17, 475-485.
- [27] R. V. G. Sundera-Rao, J. W. Turley, R. Pepinsky, *Acta Crystallogr.* **1957**, 10, 435-436.
- [28] T. Birchall, R. J. Gillespie, *Can. J. Chem.* **1963**, 41, 2642-2650.
- [29] G. A. Olah, A. Burrichter, G. Rasul, K. O. Christe, G. K. S. Prakash, *J. Am. Chem. Soc.* **1997**, 119, 4345-4352.
- [30] J. Axhausen, *Dissertation*, LMU Munich **2013**.
- [31] D. Leitz, G. Betzenbichler, Y. Morgenstern, F. Zischka, A. J. Kornath, *Z. Anorg. Allg. Chem.* **2018**, 644, 816-820.
- [32] D. Leitz, M. Hopfinger, K. Stierstorfer, Y. Morgenstern, J. Axhausen, A. J. Kornath, *Z. Anorg. Allg. Chem.* **2017**, 643, 1202-1207.
- [33] T. Soltner, N. R. Goetz, A. Kornath, *Eur. J. Inorg. Chem.* **2011**, 20, 3076-3081.
- [34] J. Axhausen, C. Ritter, A. Kornath, *Z. Anorg. Allg. Chem.* **2013**, 639, 65-72.
- [35] D. Leitz, K. Stierstorfer, Y. Morgenstern, F. Zischka, A. J. Kornath, *Z. Anorg. Allg. Chem.* **2018**, 644, 483-488.
- [36] D. Leitz, K. Stierstorfer, A. Kornath, *Z. Anorg. Allg. Chem.* **2018**, 644, 411-414.
- [37] D. Leitz, M. C. Bayer, Y. Morgenstern, F. Zischka, A. J. Kornath, *Chem. Eur. J.* **2018**, 24, 15825-15830.
- [38] D. Leitz, A. Virmani, Y. Morgenstern, F. Zischka, A. J. Kornath, *Eur. J. Inorg. Chem.* **2018**, 47, 5053-5057.
- [39] D. Leitz, A. Nitzer, Y. Morgenstern, F. Zischka, A. J. Kornath, *Eur. J. Inorg. Chem.* **2019**, *in press*.

5. APPENDIX

The following appendix contains a curriculum vitae, a full list of publications and conference contributions, the manuscripts, supporting information and cover pictures published in the context of this dissertation. All manuscripts have been published in peer-reviewed scientific journals and are subject to copyrights. The reproduction has been carried out with the permission of the respective publisher. The manuscripts are listed without changing the format of the corresponding journal.

5.1 Curriculum Vitae

Personal Information

Name	Dominik Johannes Leitz
Born	April 15, 1987
Place of birth	Esslingen am Neckar, Germany
e-Mail	dominik.leitz@cup.uni-muenchen.de

Education

08/1994–07/1998	Elementary school , Schloss-Schule Gomaringen
09/1998–07/2007	Abitur , Karl-von-Frisch-Gymnasium, Dusslingen
10/2008–03/2012	Bachelor of Science in Chemistry and Biochemistry at LMU Munich
04/2012–09/2014	Master of Science in Chemistry at LMU Munich
10/2014–01/2019	PhD thesis at LMU Munich in the group of Prof. Dr. A. J. Kornath, Inorganic Chemistry

5.2 Full list of Publications and Conference Contributions

5.2.1 Publications

1. P. Deokar, D. Leitz, T. H. Stein, M. Vasiliu, D. A. Dixon, K. O. Christe, R. Haiges, *Preparation and Characterization of Antimony and Arsenic Tricyanide and Their 2, 2'-Bipyridine Adducts*, *Chem. Eur. J.* **2016**, *22*, 13251–13257.
DOI: 10.1002/chem.201602436
2. D. Leitz, M. Hopfinger, K. Stierstorfer, Y. Morgenstern, J. Axhausen, A. Kornath, *Methanesulfonamide in Superacids: Investigations of the $CH_3SO_2NH_3^+$ Cation*, *Z. Anorg. Allg. Chem.* **2017**, *643*, 1202–1207. (Cover Picture)
DOI: 10.1002/zaac.201700229
3. D. Leitz, K. Stierstorfer, A. Kornath, *Crystal Structure and Vibrational Spectra $ClSO_2NHC(O)F$* , *Z. Anorg. Allg. Chem.* **2018**, *644*, 411–414.
DOI: 10.1002/zaac.201800077
4. D. Leitz, K. Stierstorfer, Y. Morgenstern, F. Zischka, A. J. Kornath, *The Influence of the Counterions $[AsF_6]^-$ and $[GeF_6]^{2-}$ on the Structure of the $[ClSO_2NH_3]^+$ Cation*, *Z. Anorg. Allg. Chem.* **2018**, *644*, 483–488.
DOI: 10.1002/zaac.201800067
5. D. Leitz, G. Betzenbichler, Y. Morgenstern, F. Zischka, A. J. Kornath, *Dimethylhydroxyoxosulfonium(VI) Hexafluoridometallates, $[(CH_3)_2SO(OX)]^+[MF_6]^-$ ($X = H, D; M = As, Sb$)*, *Z. Anorg. Allg. Chem.* **2018**, *644*, 816–820. (Cover Picture)
DOI: 10.1002/zaac.201800219
6. D. Leitz, M. C. Bayer, Y. Morgenstern, F. Zischka, A. J. Kornath, *Tuning the Anomeric Effect in Sulfamide with Superacids*, *Chem. Eur. J.* **2018**, *24*, 15825–15830. (Cover Feature)
DOI: 10.1002/chem.201804009
7. D. Leitz, A. Virmani, Y. Morgenstern, F. Zischka, A. J. Kornath, *Preparation and Structure of Protonated Selenourea*, *Eur. J. Inorg. Chem.* **2018**, *47*, 5053–5057.
DOI: 10.1002/ejic.201800933

8. D. Leitz, A. Nitzer, Y. Morgenstern, F. Zischka, *Structural Investigation of Thiourea dioxide in Superacids*, *Eur. J. Inorg. Chem.* **2019**, in press.

DOI: 10.1002/ejic.201801298

5.2.2 Poster Presentations

1. D. Leitz, M. Hopfinger, K. Lux, J. Axhausen, A. J. Kornath, *The Protonation of Methanesulfonamide*, 20th International Symposium on Fluorine Chemistry, Kyoto (Japan) – July 22–27, **2012**.
2. D. Leitz, K. Stierstorfer, A. J. Kornath, *Fluorocarbonylsulfamoyl chloride – a novel multifunctional compound*, Chemistry, Environment and Nanotechnology International Science Conference, Gdańsk (Poland), April 15–17, **2015**.
3. D. Leitz, K. Stierstorfer, A. J. Kornath, *Fluorocarbonylsulfamoyl chloride – a novel multifunctional compound*, 21st International Symposium on Fluorine Chemistry & 6th International Symposium on Fluorous Technologies, Como (Italy) – August 23–28, **2015**.
4. D. Leitz, K. Stierstorfer, Y. Morgenstern, A. J. Kornath, *Crystal Structures of $ClSO_2NH_2$ and $[(ClSO_2NH_3)^+]_2[GeF_6]^{2-}$* , Pacificchem, Honolulu (USA), December 15–20, **2015**.

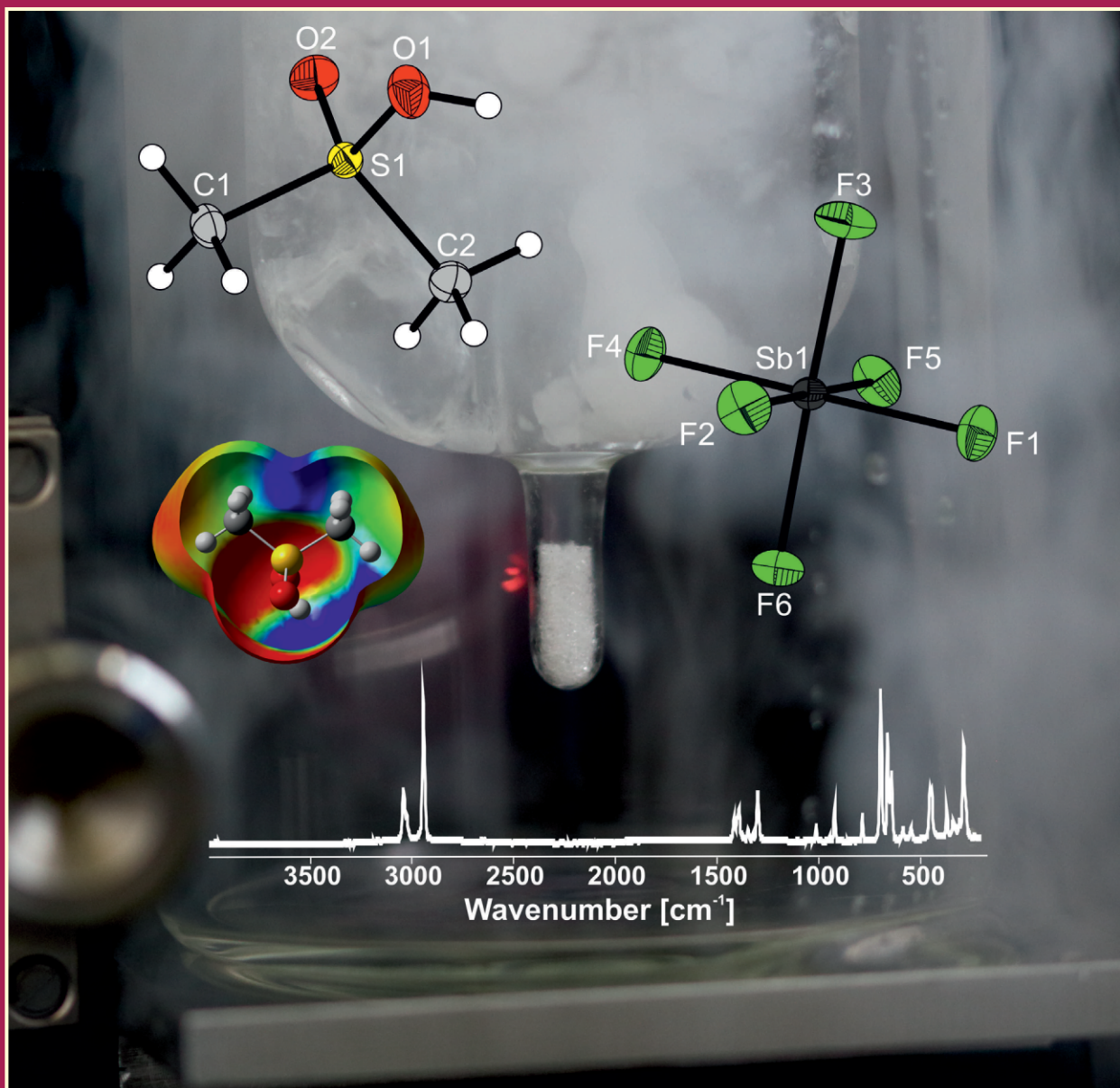
5.2.3 Oral Presentations

1. D. Leitz, A. J. Kornath, *Sulfonamid- und Harnstoff-Derivate in Supersäuren – Pnictogen- oder Chalkogen-Protonierung? (Sulfonamide- and Urea-Derivatives in Superacids – Pnictogen- or Chalcogen Protonation?)*, 17. Deutscher Fluortag, Schmitten/Ts. (Germany), September 19–21, **2016**.
2. D. Leitz, Y. Morgenstern, F. Zischka, M. C. Bayer, G. Betzenbichler, A. Virmani, A. J. Kornath, *Protonierungsreaktionen ausgewählter Sulfon(amid)-Derivate in Supersäuren (Protonation reactions of selected Sulfone(amide)-Derivatives in Superacids)*, 18. Deutscher Fluortag, Schmitten/Ts. (Germany), September 17–19, **2018**.

5.3 Manuscripts, Supporting Information and Cover Pictures published in the context of this dissertation

The manuscripts, supporting information and cover pictures, which were published within the scope of this PhD work are listed in the following. These manuscripts have been published in peer-reviewed journals and are subject to copyrights, therefore they have been reproduced with permission of the corresponding publisher.

2018
644/15



Front Cover: Dimethylhydroxyoxosulfonium(VI) Hexafluoridometallates,
 $[(\text{CH}_3)_2\text{SO}(\text{OX})]^+[\text{MF}_6]^-$ ($X = \text{H}, \text{D}; M = \text{As}, \text{Sb}$)

Dominik Leitz, Gloria Betzenbichler, Yvonne Morgenstern, Florian Zischka,
and Andreas Kornath

The front Cover shows the formula unit of $[(\text{CH}_3)_2\text{SO}(\text{OH})]^+[\text{SbF}_6]^-$ observed in the single-crystal structure analysis. The protonation of dimethylsulfone was achieved in the superacidic systems HF/AsF₅ and HF/SbF₅, representing the first examples of salts containing a protonated sulfone moiety. In the background a low temperature Raman cuvette is loaded with a sample of the above mentioned colorless salt. The crystal structure of $[(\text{CH}_3)_2\text{SO}(\text{OH})]^+[\text{SbF}_6]^-$ reveals interesting interactions in the solid state, that are discussed together with quantum chemical calculations in the article by Dominik Leitz, Gloria Betzenbichler, Yvonne Morgenstern, Florian Zischka and Andreas Kornath on page 816 ff.

Dimethylhydroxyoxosulfonium(VI) Hexafluoridometallates, $[(\text{CH}_3)_2\text{SO}(\text{OX})]^+[\text{MF}_6]^-$ ($X = \text{H}, \text{D}; M = \text{As}, \text{Sb}$)

Dominik Leitz,^[a] Gloria Betzenbichler,^[a] Yvonne Morgenstern,^[a] Florian Zischka,^[a] and Andreas Kornath*^[a]

Abstract. Dimethylsulfone reacts in the binary superacidic systems XF/MF_5 ($X = \text{H}, \text{D}; M = \text{As}, \text{Sb}$) under the formation of the corresponding salts of the type $[(\text{CH}_3)_2\text{SO}(\text{OX})]^+[\text{MF}_6]^-$. The salts are characterized by low temperature vibrational spectroscopy. In case of $[(\text{CH}_3)_2\text{SO}(\text{OH})]^+[\text{SbF}_6]^-$ a single-crystal X-ray structure analysis is

reported. The salt crystallizes in the orthorhombic space group $Pbca$ with eight formula units per unit cell [$a = 10.3281(3) \text{ \AA}$, $b = 12.2111(4) \text{ \AA}$, $c = 13.9593(4) \text{ \AA}$]. The experimental results are discussed together with quantum chemical calculations on the PBE1PBE/6-311G++(3pd,3df) level of theory.

Introduction

Dimethylsulfone (DMSO_2) is the simplest representative of sulfones ($R-\text{SO}_2-R'$). It was synthesized by *Saytzeff* in 1867 for the first time by the oxidation of dimethyl sulfoxide (DMSO) with concentrated nitric acid.^[1] DMSO_2 occurs in nature. It was discovered in 1940 as a constituent of beef blood.^[2] Later DMSO_2 was also found in vegetables, fruits,^[3] the human brain^[4] and blood plasma.^[5] DMSO_2 has a wide field of medical applications such as in drugs for arthritis,^[5] arthrosis,^[6] and allergies.^[7] In 2012 *Lim et al.* discovered DMSO_2 as a breast cancer suppressing agent.^[8] The properties of DMSO_2 are well investigated but its basicity is unknown. In the course of our studies of sulfone-derivatives we recognized that in general the basicity of the sulfone moiety has not been investigated yet. This prompted us to study the basicity of DMSO_2 in the superacids XF/MF_5 ($X = \text{D}, \text{H}; M = \text{As}, \text{Sb}$).

Results and Discussion

Dimethylsulfone was reacted with the binary superacidic systems XF/MF_5 ($X = \text{D}, \text{H}; M = \text{As}, \text{Sb}$) at $-40 \text{ }^\circ\text{C}$ accordingly to Equation (1).



($X = \text{D}, \text{H}; M = \text{As}, \text{Sb}$)

The salts are remarkably soluble in anhydrous hydrogen fluoride ($a\text{HF}$), even at low temperatures down to $-78 \text{ }^\circ\text{C}$. A slow and careful removal of the solvent in vacuo (within 72 h) led to the formation of colorless crystals. In case of $[(\text{CH}_3)_2\text{SO}(\text{OH})]^+[\text{SbF}_6]^-$ the crystals were suitable for a single-crystal X-ray structure analysis. The moisture sensitive

salts are stable up to $-25 \text{ }^\circ\text{C}$. Attempts to achieve a diprotonation by employing an excess of the Lewis acids AsF_5 or SbF_5 led only to the monoprotonated species.

Crystal Structure

$[(\text{CH}_3)_2\text{SO}(\text{OH})]^+[\text{SbF}_6]^-$ crystallizes in the orthorhombic space group $Pbca$ with eight formula units per unit cell. The formula unit is shown in Figure 1. Bond lengths and angles are given in Table 1. The cell parameters as well as measurement details are summarized in the Experimental Section.

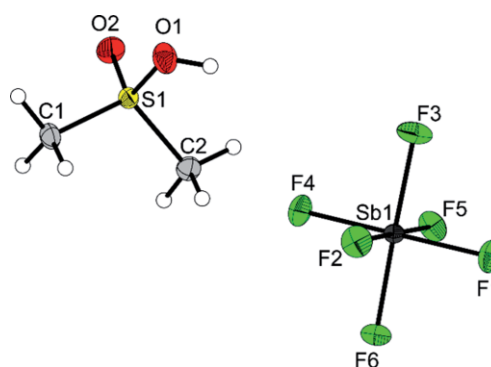


Figure 1. Formula unit of $[(\text{CH}_3)_2\text{SO}(\text{OH})]^+[\text{SbF}_6]^-$ (thermal ellipsoids with 50% probability).

Table 1. Bond lengths / \AA and angles / $^\circ$ of $[(\text{CH}_3)_2\text{SO}(\text{OH})]^+[\text{SbF}_6]^-$.

Bond lengths			
S1–O1	1.532(2)	S1–C1	1.735(3)
S1–O2	1.417(2)	S1–C2	1.737(3)
Bond angles			
O2–S1–O1	113.7(1)	O2–S1–C1	111.9(1)
O1–S1–C1	112.7(2)	O2–S1–C2	107.0(2)
O1–S1–C2	101.5(1)	C1–S1–C2	109.5(2)
Donor-acceptor distance / \AA			
O1(–H1)⋯F5	2.557(3)		
C2(–H2b)⋯O2	3.246(3)		

* Prof. Dr. A. Kornath
 E-Mail: andreas.kornath@cup.uni-muenchen.de

[a] Department Chemie
 Ludwig-Maximilians-Universität München
 Butenandtstr. 5–13
 81377 Munich, Germany

Supporting information for this article is available on the WWW under <http://dx.doi.org/10.1002/zaac.201800219> or from the author.

The coordination sphere of the sulfur atom can be described as a distorted tetrahedron, whereby the bond angle O1–S1–O2 of 113.7(1)° is decreased by 4.2° and the C1–S1–C2 bond angle is increased by 6.5° compared to the neutral compound.^[9] The S–C bonds of 1.735(3) Å and 1.737(3) Å, respectively, are slightly shorter than the S–C bonds in (CH₃)₂SO₂ [1.778(17) Å]^[9] but still in the range of regular S–C single bonds. As expected, due to the *O*-protonation the S1–O1 bond [1.532(2) Å] is significantly longer than the S1–O2 bond [1.417(2) Å]. The Sb–F bonds of the slightly distorted octahedral [SbF₆][−] anion are between 1.867(2) Å and 1.911(2) Å. The longest Sb–F bond is involved in a hydrogen bond.

The cations and anions are connected via O1(–H1)⋯F5 hydrogen bonds with a donor-acceptor distance of 2.557(3) Å indicating medium strong hydrogen bonds. The cations are connected among each other by weak C2(–H2b)⋯O2 hydrogen bonds with a donor-acceptor distance of 3.246(3) Å forming zigzag like chain structures along the *a* axis. Such weak C(–H)⋯O interactions have been reported several times, for example by *Arshad et al.*^[10] The connectivity of the cations and anions is illustrated in Figure 2.

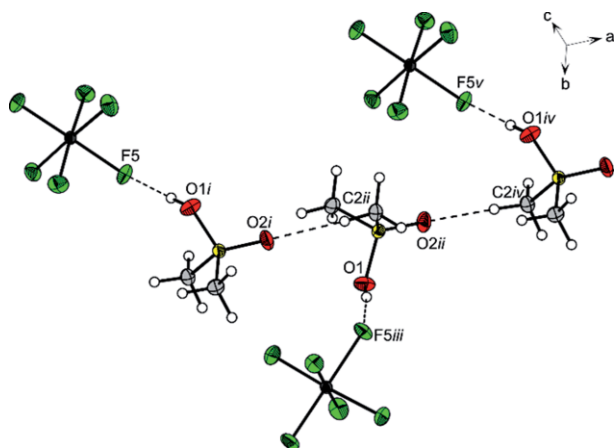


Figure 2. Hydrogen bonds in [(CH₃)₂SO(OH)]⁺[SbF₆][−], represented as dashed lines (thermal ellipsoids with 50% probability). Symmetry codes *i* = −0.5+*x*, *y*, 0.5−*z*; *ii* = *x*, 0.5−*y*, −0.5+*z*; *iii* = 0.5+*x*, 0.5−*y*, −*z*; *iv* = 0.5+*x*, *y* 0.5−*z*; *v* = 1+*x*, *y*, *z*.

Vibrational Spectra

Figure 3 shows the vibrational spectra of [(CH₃)₂SO(OH)]⁺[SbF₆][−], [(CH₃)₂SO(OH)]⁺[AsF₆][−], and [(CH₃)₂SO(OD)]⁺[AsF₆][−]. For the [(CH₃)₂SO(OX)]⁺ cation with *C*₁ symmetry 30 vibrational modes are expected displaying both Raman as well as IR activity. In Table 2 selected vibrational modes are summarized together with their assign-

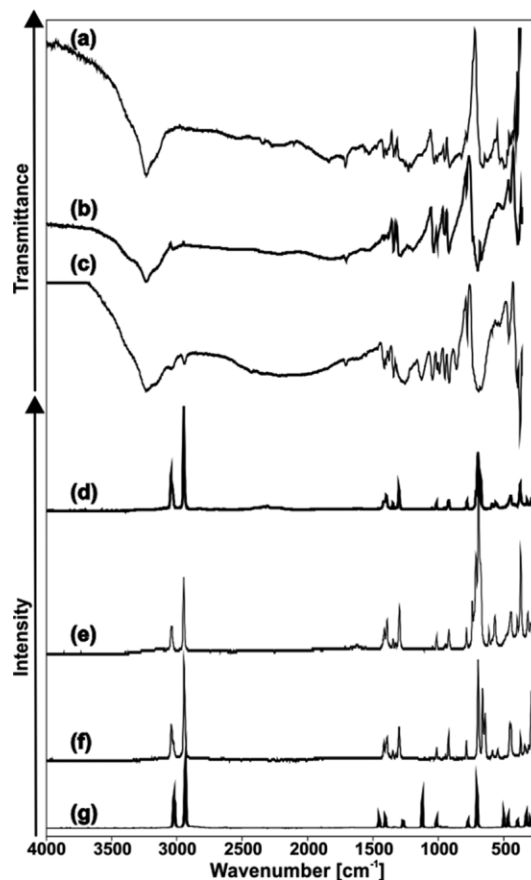


Figure 3. Low temperature vibrational spectra of [(CH₃)₂SO(OH)]⁺[SbF₆][−]: (a) IR spectrum, (f) Raman spectrum; [(CH₃)₂SO(OH)]⁺[AsF₆][−]: (b) IR spectrum, (e) Raman spectrum; [(CH₃)₂SO(OD)]⁺[AsF₆][−]: (c) IR spectrum, (d) Raman spectrum; (CH₃)₂SO₂: (g) Raman spectrum.

Table 2. Selected experimental vibrational frequencies /cm^{−1} of [(CH₃)₂SO(OH)]⁺[SbF₆][−], [(CH₃)₂SO(OH)]⁺[AsF₆][−] and [(CH₃)₂SO(OD)]⁺[SbF₆][−] and calculated vibrational frequencies /cm^{−1} of [(CH₃)₂SO(OH)]⁺ and [(CH₃)₂SO(OD)]⁺.

[(CH ₃) ₂ SO(OH)] ⁺ [SbF ₆] [−]		[(CH ₃) ₂ SO(OH)] ⁺ [AsF ₆] [−]		[(CH ₃) ₂ SO(OH)] ⁺	[(CH ₃) ₂ SO(OD)] ⁺ [AsF ₆] [−]		[(CH ₃) ₂ SO(OD)] ⁺	Assignment	
IR	Raman	IR	Raman	calcd. ^{a)} (IR/Raman)	IR	Raman	calcd. ^{a)} (IR/Raman)	b)	
3232 (s)		3238 (vs)		3729 (293/70)	2424 (w)		2607 (136/40)	<i>v</i> ₁	<i>v</i> (OX)
1322 (w)	1324 (3)	1324 (w)	1325 (1)	1394 (182/9)	1324 (w)	1325 (2)	1322 (114/9)	<i>v</i> ₁₂	<i>v</i> (S=O)
		1197 (w)		1123 (43/2)			787 (95/2)	<i>v</i> ₁₅	δ(SOX)
823 (w)				898 (143/4)	861 (m)		845 (42/5)	<i>v</i> ₂₀	<i>v</i> (S–O)
781 (w)	781 (13)	783 (w)	783 (12)	781 (14/3), 778 (10)	779 (m)	778 (10)	731 (23/4)	<i>v</i> ₂₁	<i>v</i> _{as} (SC ₂)
		671 (s)	677 (1)	691 (1/22), 683 (8)	668 (s)	683 (8)	638 (1/25)	<i>v</i> ₂₂	<i>v</i> _s (SC ₂)

a) Calculated at the PBE1PBE/6-311G++(3df,3dp) level of theory. IR intensity are in km·mol^{−1} and Raman intensity in Å⁴·μ^{−1}. Abbreviations for IR intensities: *v* = very, *s* = strong, *m* = medium, *w* = weak. *iph* = in phase, *oph* = out of phase. Raman activity is stated to a scale of 1 to 100. b) X = H, D.

ments. The complete vibrational modes are given in Table S1 (Supporting Information). The OH stretching vibration occurs at 3232 cm^{-1} and 3238 cm^{-1} and the OD-stretching mode is detected at 2424 cm^{-1} , which is in good agreement with the Teller-Redlich rule for an isotopic H/D effect.^[11] The CH stretching vibrations are detected at 3041 cm^{-1} , 3043 cm^{-1} , 3044 cm^{-1} , 3032 cm^{-1} , 3038 cm^{-1} , 3025 cm^{-1} , 2944 cm^{-1} , 2947 cm^{-1} and are slightly red-shifted compared to the neutral compound. The CH_3 deformation modes are observed at around 1416 cm^{-1} , 1395 cm^{-1} , 1341 cm^{-1} , and remain approximately unchanged.^[12] In case of the SO stretching vibrations a significant change compared to DMSO_2 is observed due to the O protonation. This causes the disappearance of the symmetric SO_2 stretching vibration.

The S=O stretching mode is detected at around 1324 cm^{-1} and is red-shifted by approximately 30 cm^{-1} compared to the antisymmetric SO stretching mode in the neutral compound. The S–O mode occurs at 823 cm^{-1} and in case of the deuterated species at 861 cm^{-1} . The antisymmetric SC_2 stretching mode is displayed at approximately 780 cm^{-1} and is blue-shifted by 90 cm^{-1} compared to DMSO_2 , whereas the symmetric SC_2 vibration of 671 , 677 , 668 , and 683 cm^{-1} is red-shifted by approximately 80 cm^{-1} , which is in good agreement with results of the quantum-chemical calculations. For the octahedral anions $[\text{AsF}_6]^-$ and $[\text{SbF}_6]^-$ more vibrations than expected are observed. This finding can be explained by distortion of the anions caused by hydrogen bonds in the solid state as observed in the crystal structure of the $[\text{SbF}_6]^-$ salt.

Theoretical Calculations

Quantum chemical calculations were performed using the hybrid method PBE1PBE with the basis set 6-311G++(3pd,3df). The calculated structure as well as vibrational frequencies satisfactorily agree with the experimental results, with exception of the OX stretching vibration, which is overestimated due to interactions in the solid state. A comparison of the experimental and calculated structure of the $[(\text{CH}_3)_2\text{SO}(\text{OH})]^+$ cation is shown in Figure 4.

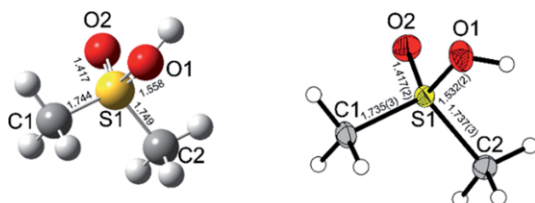


Figure 4. Comparison of the calculated (left) and the experimental (right) observed cationic structure of $[(\text{CH}_3)_2\text{SO}(\text{OH})]^+$ (bond lengths in Å).

Because of the occurrence of the weak $\text{C}(\text{--H})\cdots\text{O}$ interaction in the solid state, an analysis of the electrostatic potential (ESP) of the $[(\text{CH}_3)_2\text{SO}(\text{OH})]^+$ cation was carried out with the aim to investigate its origin. We found no significant difference in the positive polarization on the protons of both methyl groups (Figure 5). Therefore we assume that this interaction is

mainly based on solid-state effects, rather than by an intrinsic property of the cation.

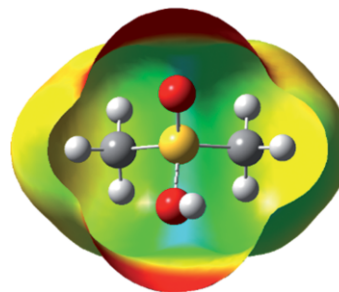


Figure 5. Gas-phase optimization of $[(\text{CH}_3)_2\text{SO}(\text{OH})]^+$. In the background an electrostatic potential (ESP) map is superimposed as a color scale ranging from 0.170 a.u. (red) and 0.210 a.u. (blue); isoval. = 0.004 .

Conclusions

In this study, salts containing the dimethylhydroxyoxo-sulfonium(VI) cation were synthesized and characterized. The salts represent the first examples of an O-protonated sulfone moiety. In case of $[(\text{CH}_3)_2\text{SO}(\text{OH})]^+[\text{SbF}_6]^-$ a single-crystal X-ray structure analysis reveals that the protonation of DMSO_2 leads to an elongation of one S–O bond and an increase of the tetrahedral distortion.

Experimental Section

Caution! Avoid contact with any of these compounds. The hydrolysis of all these salts might form HF, which burns skin and causes irreparable damage. Safety precautions should be taken using and handling these materials.

Apparatus and Materials: All reactions were performed by employing standard Schlenk techniques using a stainless-steel vacuum line. Syntheses in superacidic media were carried out in FEP/PFA reactors closed with a stainless-steel valve. All reaction vessels and the stainless-steel line were dried with fluorine prior to use. IR spectroscopic investigations were performed at low temperature with a Bruker Vertex-80V FTIR spectrometer by placing small amounts of the sample on a CsBr single-crystal plate in a cooled cell. IR spectra were recorded in a range between 350 and 4000 cm^{-1} . Raman measurements were carried out with a Bruker MultiRAM FT-Raman spectrometer at $-196\text{ }^\circ\text{C}$ with Nd:YAG laser excitation ($\lambda = 1064\text{ nm}$) in the range between 250 and 4000 cm^{-1} . The low-temperature single-crystal X-ray diffraction was performed with an Oxford XCalibur3 diffractometer equipped with a Spellman generator (50 kV , 40 mA) and a KappaCCD detector operating with Mo- $K\alpha$ radiation ($\lambda = 0.7107\text{ \AA}$). Data collection was carried out using the CrysAlis CCD software,^[13] for data reduction the CrysAlis RED software^[14] was used. The solution and refinement of the crystal structure was performed with the programs SHELXS^[15] and SHELXL-97^[16] implemented in the WinGX software package^[17] and finally checked with the PLATON software.^[18] For the absorption correction the SCALE ABSPACK multi-scan method^[19] was in use. $(\text{CH}_3)_2\text{SO}_2$ (Sigma-Aldrich) was used as received. SbF_5 (VWR) was triple-distilled prior to use. AsF_5 was synthesized from the elements and purified by fractional distillation. HF (Linde) was purified by trap-to-trap condensation under vacuum before drying with

fluorine for two weeks in a stainless-steel pressure cylinder. DF was synthesized from dried CaF_2 and D_2SO_4 . The quantum-chemical calculations were performed with the Gaussian09 package^[20] using the PBE1PBE density functional approach on the 6-311G++(3pd, 3df) level. Selected crystal data and structure refinement for $[(\text{CH}_3)_2\text{SO}(\text{OH})]^+[\text{SbF}_6]^-$ are given in Table 3.

Table 3. Crystal data and structure refinement for and $[(\text{CH}_3)_2\text{SO}(\text{OH})]^+[\text{SbF}_6]^-$.

	$[(\text{CH}_3)_2\text{SO}(\text{OH})]^+[\text{SbF}_6]^-$
Empirical formula	$\text{C}_2\text{H}_7\text{F}_6\text{O}_2\text{SSb}$
M_r	330.89
Crystal system	orthorhombic
Space Group	$Pbca$
$a/\text{Å}$	10.3281(3)
$b/\text{Å}$	12.2111(4)
$c/\text{Å}$	13.9593(4)
$V/\text{Å}^3$	1760.51(9)
Z	8
$\rho_{\text{calcd.}}/\text{g}\cdot\text{cm}^{-3}$	2.497
μ/mm^{-1}	3.432
λ (Mo- K_α)/Å	0.71073
$F(000)$	1248
T/K	143
hkl range	−14:15; −17:17; −20:17
Refl. measured	19365
Refl. unique	2967
R_{int}	0.0273
Parameters	115
$R(F)/wR(F^2)$ ^{a)} (all reflexions)	0.0444/0.0920
Weighting scheme ^{b)}	0.0452/1.8842
S(GoF) ^{c)}	1.121
Residual density $/e\cdot\text{Å}^{-3}$	3.014/−0.803
Device type	Oxford XCalibur
Solution/refinement	SHELXS-97 [15], SHELXL-97 [14], SHELXL-97 [14]

a) $R_1 = \sum |F_o| - |F_c| / \sum |F_o|$. b) $wR_2 = [\sum [w(F_o^2 - F_c^2)^2] / \sum [w(F_o^2)]]^{1/2}$; $w = [\sigma_c^2(F_o^2) + (xP)^2 + yP]^{-1}$; $P = (F_o^2 + 2F_c^2)/3$. c) $\text{GoF} = \{\sum [w(F_o^2 - F_c^2)^2] / (n - p)\}^{1/2}$ (n = number of reflexions; p = total number of parameters).

Crystallographic data (excluding structure factors) for the structure in this paper have been deposited with the Cambridge Crystallographic Data Centre, CCDC, 12 Union Road, Cambridge CB21EZ, UK. Copies of the data can be obtained free of charge on quoting the depository number CCDC-1590033 for $[(\text{CH}_3)_2\text{SO}(\text{OH})]^+[\text{SbF}_6]^-$ (Fax: +44-1223-336-033; E-Mail: deposit@ccdc.cam.ac.uk, http://www.ccdc.cam.ac.uk).

Synthesis of $[(\text{CH}_3)_2\text{SO}(\text{OH})]^+[\text{SbF}_6]^-$: Antimony pentafluoride, SbF_5 , (1.22 mmol, 115 mg) and anhydrous hydrogen fluoride, aHF , (ca. 2 mL) were condensed at -196°C into a reactor (FEP tube). In order to form the superacidic system the mixture was warmed up to -40°C . Dimethylsulfone, $(\text{CH}_3)_2\text{SO}$, (1.22 mmol, 265 mg) was added in a dry nitrogen atmosphere at -196°C . The mixture was warmed up again to -40°C for 5 min. Afterwards the reactor was cooled down to -78°C . The excess of anhydrous hydrogen fluoride and antimony pentafluoride were removed in dynamic vacuum. After 72 h, $[(\text{CH}_3)_2\text{SO}(\text{OH})]^+[\text{SbF}_6]^-$ was obtained as colorless solid.

Synthesis of $[(\text{CH}_3)_2\text{SO}(\text{OX})]^+[\text{AsF}_6]^-$ ($X = \text{H}, \text{D}$): Anhydrous hydrogen fluoride, HF, (ca. 2 mL) or deuterium fluoride, DF, (ca. 2 mL) and arsenic pentafluoride, AsF_5 , (1.22 mmol, 177 mg) were condensed into a reactor (FEP tube) at -196°C . The reactor was warmed to -40°C to allow the components to form a homogeneous

the superacidic system. Dimethylsulfone, $(\text{CH}_3)_2\text{SO}$, (1.04 mmol, 98.0 mg) was added in an inert nitrogen atmosphere at -196°C . The mixture was warmed to -40°C to form the product. Afterwards the reactor was cooled to -78°C . Excess of anhydrous hydrogen (or deuterium) fluoride was removed in dynamic vacuum. After 12 h, $[(\text{CH}_3)_2\text{SO}(\text{OH})]^+[\text{AsF}_6]^-$ was obtained as colorless solid.

Supporting Information (see footnote on the first page of this article): The Supporting Information includes the complete Table of experimental and calculated frequencies and their assignment (Table S1).

Acknowledgements

Financial support of this work by the Ludwig-Maximilian-University of Munich (LMU) by the Deutsche Forschungsgemeinschaft (DFG) and the F-Select GmbH is gratefully acknowledged.

Keywords: Dimethylsulfone; Protonation; Superacid chemistry; Low temperature vibrational spectroscopy; Single-crystal X-ray diffraction

References

- [1] A. Saytzeff, *Justus Liebigs Ann. Chem.* **1867**, *144*, 148–156.
- [2] J. J. Piffner, H. B. North, *J. Biol. Chem.* **1940**, *134*, 781–782.
- [3] A. C. Silva Ferreira, P. Rodrigues, T. Hogg, P. Guedes de Pinho, *J. Agric. Chem.* **2003**, *51*, 727–732.
- [4] S. E. Rosea, J. B. Chalk, G. J. Galloway, D. M. Doddrell, *Magn. Reson. Imaging* **2000**, *18*, 95–98.
- [5] U. F. H. Engelke, A. Tangerman, M. A. A. P. Willemsen, D. Moskau, S. Loss, S. H. Mudd, R. A. Wevers, *NMR Biomed.* **2005**, *18*, 331–336.
- [6] J. I. Morton, B. V. Siegel, *Proc. Soc. Exp. Biol. Med.* **1986**, *183*, 227–230.
- [7] R. N. Schiller, *J. Altern. Complement. Med.* **2002**, *8*, 167–173.
- [8] E. J. Lim, D. Y. Hong, J. H. Park, Y. H. Joung, P. Darvin, S. Y. Kim, Y. M. Na, T. S. Hwang, S.-K. Ye, E.-S. Moon, B. W. Cho, K. Do Park, H. K. Lee, T. Park, Y. M. Yang, *PLoS ONE* **2012**, *7*, e33361.
- [9] E. Sands Donald, *Z. Kristallogr.* **1964**, *119*, 245–251.
- [10] M. N. Arshad, A. M. Asiri, K. A. Alamry, T. Mahmood, M. A. Gilani, K. Ayub, A. S. Birinji, *Spectrochim. Acta Part A* **2015**, *142*, 364–374.
- [11] J. Weidlein, U. Müller, K. Dehnicke, *Schwingungsspektroskopie*, 2 ed., Georg Thieme Verlag, Stuttgart, Germany, **1988**.
- [12] G. Geiseler, G. Hanschmann, *J. Mol. Struct.* **1972**, *11*, 283–296.
- [13] CrysAlisCCD, Version 1.171.35.11 (release 16–05–2011 CrysAlis 171.NET), Oxford Diffraction Ltd, UK, **2001**.
- [14] CrysAlisRED, Version 1.171.35.11 (release 16–05–2011 CrysAlis 171.NET), Oxford Diffraction Ltd., UK, **2011**.
- [15] G. M. Sheldrick, *SHELXS-97*, Program for Crystal Structure Solution, University of Göttingen, Germany, **1997**.
- [16] G. M. Sheldrick, *SHELXL-97*, Program for the Refinement of Crystal Structures, University of Göttingen, Germany, **1997**.
- [17] L. Farrugia, *J. Appl. Crystallogr.* **1999**, *32*, 837–838.
- [18] A. L. Spek, *PLATON*, A Multipurpose Crystallographic Tool, U. Utrecht University, The Netherlands, **1999**.
- [19] *SCALE3 ABSPACK*, Oxford Diffraction Program, O. Diffraction, Ltd., UK, **2005**.
- [20] M. J. Frisch, G. W. Trucks, H. B. Schlegel, G. E. Scuseria, M. A. Robb, J. R. Cheeseman, J. A. Montgomery Jr., T. Vreven, K. N. Kudin, J. C. Burant, J. M. Millam, S. S. Iyengar, J. Tomasi, V. Barone, B. Mennucci, M. Cossi, G. Scalmani, N. Rega, G. A. Petersson, H. Nakatsuji, M. Hada, M. Ehara, K. Toyota, R. Fu-

kuda, J. Hasegawa, M. Ishida, T. Nakajima, Y. Honda, O. Kitao, H. Nakai, M. Klene, X. Li, J. E. Knox, H. P. Hratchian, J. B. Cross, C. Adamo, J. Jaramillo, R. Gomperts, R. E. Stratmann, O. Yazyev, A. J. Austin, R. Cammi, C. Pomelli, J. W. Ochterski, P. Y. Ayala, K. Morokuma, G. A. Voth, P. Salvador, J. J. Dannenberg, V. G. Zakrzewski, S. Dapprich, A. D. Daniels, M. C. Strain, O. Farkas, D. K. Malick, A. D. Rabuck, K. Raghavachari, J. B. Foresman, J. V. Ortiz, Q. Cui, A. G. Baboul, S. Clifford, J.

Cioslowski, B. B. Stefanov, G. Liu, A. Liashenko, P. Piskorz, I. Komaromi, R. L. Martin, D. J. Fox, T. Keith, M. A. Al-Laham, C. Y. Peng, A. Nanayakkara, M. Challacombe, P. M. W. Gill, B. Johnson, W. Chen, M. W. Wong, C. Gonzalez, J. A. Pople, Gaussian, Inc. **2003**, Pittsburgh PA.

Received: May 25, 2018

Published online: July 12, 2018

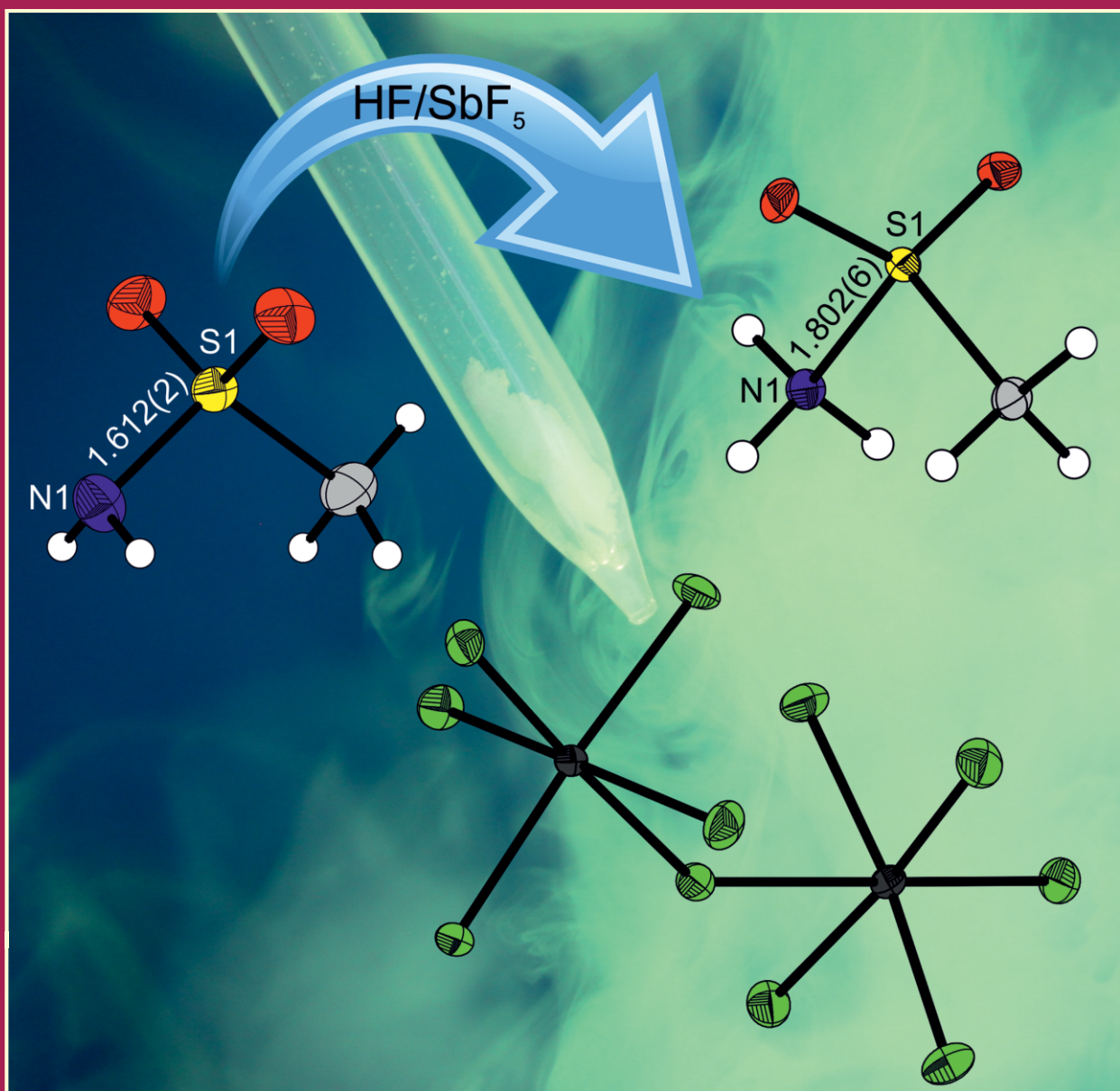
Supporting Information

Table S1. Experimental vibrational frequencies (in cm^{-1}) of $[(\text{CH}_3)_2\text{SO}(\text{OH})]^+[\text{SbF}_6]^-$, $[(\text{CH}_3)_2\text{SO}(\text{OH})]^+[\text{AsF}_6]^-$ and $[(\text{CH}_3)_2\text{SO}(\text{OD})]^+[\text{SbF}_6]^-$ and calculated vibrational frequencies (in cm^{-1}) of $[(\text{CH}_3)_2\text{SO}(\text{OH})]^+$ and $[(\text{CH}_3)_2\text{SO}(\text{OD})]^+$.

$[(\text{CH}_3)_2\text{SO}(\text{OH})]^+[\text{SbF}_6]^-$		$[(\text{CH}_3)_2\text{SO}(\text{OH})]^+[\text{AsF}_6]^-$		$[(\text{CH}_3)_2\text{SO}(\text{OD})]^+[\text{AsF}_6]^-$		$[(\text{CH}_3)_2\text{SO}(\text{OD})]^+$	$[(\text{CH}_3)_2\text{SO}(\text{OH})]^+$	Assignment	
(a)	(f)	(c)	(d)	(b)	(e)	calc. ^[a]	calc. ^[a]		
IR	Raman	IR	Raman	IR	Raman	(IR/Raman)	(IR/Raman)		
3232 (s)		3238 (vs)		2424 (w)		2607 (136/40)	3729 (293/70)	ν_1	ν (OX)
	3041 (26)		3043 (23)		3044 (27)	3108 (23/67)	3187 (26/63)	ν_2	$\nu_{\text{as,iph}}(\text{CH}_3)$
						3104 (3/14)	3183 (3/12)	ν_3	$\nu_{\text{as,oph}}(\text{CH}_3)$
				3032 (w)	3038 (1)	3098 (19/50)	3176 (21/48)	ν_4	$\nu_{\text{as}}(\text{CH}_2)$
		3025 (w)				3089 (13/43)	3169 (13/39)	ν_5	$\nu_{\text{as}}(\text{CH}_2)$
	2944 (81)		2947 (69)		2947 (100)	2992 (15/254)	3068 (13/252)	ν_6	$\nu_{\text{s,iph}}(\text{CH}_3)$
						2987 (40/34)	3063 (44/17)	ν_7	$\nu_{\text{s,oph}}(\text{CH}_3)$
1709 (w)		1707 (w)						$\nu_{16+\nu_{24}}$	
1416 (w)	1414 (14)	1415 (w)	1418 (2)	1412 (w)	1404 (9)	1397 (9/2)	1444 (1/2)	ν_8	$\delta(\text{CH}_3)$
1395 (w)	1393 (15)	1396 (w)	1394 (11)		1395 (1)	1391 (14/6)	1435 (19/5)	ν_9	$\delta(\text{CH}_3)$
		1381 (w)		1377 (w)		1376 (7/2)	1420 (6/1)	ν_{10}	$\delta(\text{CH}_3)$
1341 (m)	1345 (5)	1342 (m)	1347 (5)		1346 (4)	1373 (0/7)	1417 (1/7)	ν_{11}	$\delta(\text{CH}_3)$
1322 (w)	1324 (3)	1324 (w)	1325 (1)	1324 (w)	1325 (2)	1322 (114/9)	1394 (182/9)	ν_{12}	$\nu(\text{S}=\text{O})$
					1301 (16)	1297 (48/4)	1354 (25/1)	ν_{13}	$\delta(\text{CH}_3)$
				1286 (w)		1293 (16/1)	1347 (20/0)	ν_{14}	$\delta(\text{CH}_3)$
		1197 (w)				787 (95/2)	1123 (43/2)	ν_{15}	$\delta(\text{SOX})$
1031 (w)	1040 (1)	1035 (m)	1041 (2)	1044 (m)	1045 (1)	1005 (49/0)	1039 (101/0)	ν_{16}	$\delta(\text{CH}_3)$
1009 (w)	1010 (10)	1008 (w)	1012 (7)	992 (m)	1012 (6)	973 (22/3)	1009 (13/3)	ν_{17}	$\delta(\text{CH}_3)$
952 (m)	943 (2)	948 (m)	945 (1)	948 (w)	950 (1)	933 (56/0)	950 (55/1)	ν_{18}	$\delta(\text{CH}_3)$
911 (m)	921 (10)	918 (s)	918 (11)	916 (m)	916 (8)	904 (4/1)	935 (0/1)	ν_{19}	$\delta(\text{CH}_3)$
823 (w)				861 (m)		845 (42/5)	898 (143/4)	ν_{20}	$\nu(\text{S}-\text{O})$
781 (w)	781 (13)	783 (w)	783 (12)	779 (m)	778 (10)	731 (23/4)	781 (14/3)	ν_{21}	$\nu_{\text{as}}(\text{SC}_2)$
		671 (s)	677 (1)	668 (s)	683 (8)	638 (1/25)	691 (1/22)	ν_{22}	$\nu_{\text{s}}(\text{SC}_2)$
440 (w)		448 (m)	450 (16)	464 (m)	444 (7)	414 (31/3)	446 (50/3)	ν_{23}	$\delta(\text{SO}_2)$
371 (m)	368 (9)			361 (s)		387 (27/3)	429 (20/3)	ν_{24}	$\delta(\text{SO}_2)$
			320 (1)			332 (2/1)	350 (3/1)	ν_{25}	$\delta(\text{CSO})$
	292 (34)		285 (14)			279 (6/3)	310 (29/2)	ν_{26}	$\tau(\text{SO}_2)$
						257 (6/2)	268 (5/2)	ν_{27}	$\delta(\text{CSC})$
	228 (24)		220 (1)			210 (3/0)	228 (13/0)	ν_{28}	$\tau(\text{CH}_3)$
			152 (5)			177 (8/0)	197 (55/1)	ν_{29}	$\tau(\text{OSC})$
	161 (4)					161 (37/1)	187 (15/0)	ν_{30}	$\tau(\text{CH}_3)$
	690 (100)	734 (w)	739 (11)	733 (w)					$[\text{MF}_6]^-$
658 (m)			710 (16)		705 (6)				$[\text{MF}_6]^-$
	653 (72)	697 (s)	694 (100)	696 (m)	692 (64)				$[\text{MF}_6]^-$
389 (s)		563 (w)	585 (4)		586 (3)				$[\text{MF}_6]^-$
	292 (34)	398 (w)	395 (8)	392 (m)					$[\text{MF}_6]^-$
		381 (w)	372 (30)	380 (w)	373 (20)				$[\text{MF}_6]^-$

[a] Calculated at the PBE1PBE/6-311G++(3df,3dp) level of theory. IR intensity in km/mol and Raman intensity in $\text{\AA}^4/\mu$. Abbreviations for IR intensities: ν = very, s = strong, m = medium, w = weak. $X = \text{H, D}$. iph = in phase, oph = out of phase. Raman activity is stated to a scale of 1 to 100.

2017
643/19



Years of
ZAAC

125



Front Cover: Methanesulfonamide in Superacids: Investigations of the $\text{CH}_3\text{SO}_2\text{NH}_3^+$ Cation

Dominik Leitz, Andreas Kornath et al.

The Front Cover shows the single-crystal X-ray structure of methanesulfonamide and its protonated species. The protonation of methanesulfonamide and the isolation of corresponding salts succeeded for the first time with the superacidic systems HF/SbF₅ and HF/AsF₅. In the background of the cover picture a typical reaction vessel containing colourless crystals of [CH₃SO₂NH₃]⁺[Sb₂F₁₁]⁻ is shown. The structure analyses revealed a remarkable elongation of the sulfur-nitrogen bond due to the protonation. The reason is explained in the article by Leitz et al. on page 1202 ff.

Methanesulfonamide in Superacids: Investigations of the $\text{CH}_3\text{SO}_2\text{NH}_3^+$ Cation

Dominik Leitz,^[a] Mathias Hopfinger,^[a] Karin Stierstorfer,^[a] Yvonne Morgenstern,^[a] Joachim Axhausen,^[a] and Andreas Kornath*^[a]

Dedicated to Prof. Dr. Wolfgang Beck on the Occasion of his 85th Birthday

Abstract. The preparation of protonated methanesulfonamide was carried out using the superacidic systems HF/AsF₅ and HF/SbF₅. The vibrational spectroscopic characterization was supported by quantum chemical calculations performed with the PBE1PBE method using the 6-311G++(3df, 3pd) basis set. A remarkable long nitrogen–sulfur bond

length of 1.804(6) Å was observed in a single-crystal X-ray structure analysis of $[\text{CH}_3\text{SO}_2\text{NH}_3]^+[\text{Sb}_2\text{F}_{11}]^-$. It crystallizes in the orthorhombic space group $P2_1/c$ with four formula units in the unit cell. Furthermore the crystal structure of $\text{CH}_3\text{SO}_2\text{NH}_2$ was revisited.

Introduction

Sulfonamides are of remarkable research interest due to their high biological activity.^[1,2] Despite their common applications, the acid/base properties of sulfonamides are rarely described in literature. The first study was reported by *LeMaire* and *Lucas*, who estimated the $\text{p}K_{\text{a}}$ value of the conjugate acid of *p*-toluenesulfonamide to be ca. 3.2.^[3] *Laughlin* investigated the basicity of aliphatic sulfonamides based on the determination of the NMR chemical shifts as a function of solvent acidity. He found that the protonation of sulfonamides takes place at the nitrogen atom.^[4] *Bagno* et al. confirmed these findings by other NMR spectroscopic investigations.^[5] Additionally, it was found that the basicity of the nitrogen as a function of the hydrogen acceptor power is 2.8 kcal·mol⁻¹ higher than that of the oxygen atom. These experimental results are supported by quantum chemical calculations comparing the total energies of the *O*-protonated species with the *N*-protonated species.^[6] In the course of our investigations it was interesting for us to study methanesulfonamide as one of the simplest representatives of sulfonamides in the superacidic solutions HF/MF₅ ($M = \text{As}; \text{Sb}$) with the aim to isolate and characterize the hitherto structural unknown $\text{CH}_3\text{SO}_2\text{NH}_3^+$ cation. Furthermore we present a reinvestigation of the crystal structure of $\text{CH}_3\text{SO}_2\text{NH}_2$, which has been reported in a previous work.^[7]

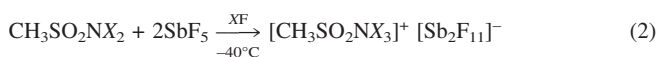
Results and Discussion

The preparation of salts containing the $[\text{CH}_3\text{SO}_2\text{NH}_3]^+$ cation was carried out by the reaction of methanesulfonamide with the superacidic solutions HF/AsF₅ and HF/SbF₅. For a

detailed vibrational spectroscopic investigation the corresponding D-isotopomers were prepared [Equation (1)]. An excess of SbF₅ does not lead to a diprotonation of methanesulfonamide but to a formation of $\text{Sb}_2\text{F}_{11}^-$ salts [Equation (2)].



($X = \text{H}, \text{D}; M = \text{As}, \text{Sb}$)



($X = \text{H}, \text{D}$)

The reactions were performed at -40°C . The solvent was removed at -78°C in dynamic vacuum overnight. The formed salts remaining as colorless crystalline precipitates are stable under dry inert gas atmosphere up to room temperature.

Vibrational Spectroscopy

The low temperature infrared and Raman spectra of $[\text{CH}_3\text{SO}_2\text{NH}_3]^+[\text{AsF}_6]^-$, $[\text{CH}_3\text{SO}_2\text{ND}_3]^+[\text{AsF}_6]^-$, $[\text{CH}_3\text{SO}_2\text{NH}_3]^+[\text{SbF}_6]^-$, and $\text{CH}_3\text{SO}_2\text{NH}_2$ are shown in Figure 1. In Table 1 the observed frequencies of the protonated species are summarized together with the quantum chemically calculated frequencies of $[\text{CH}_3\text{SO}_2\text{NH}_3]^+\cdot 3\text{HF}$ and $[\text{CH}_3\text{SO}_2\text{ND}_3]^+\cdot 3\text{HF}$.

For the $[\text{CH}_3\text{SO}_2\text{NH}_3]^+$ cation with C_s symmetry 27 fundamental vibrations are expected. All modes are both Raman and infrared active. The $\nu_{\text{as}}(\text{NH}_2)$ are detected at 3191 cm⁻¹ (a), 3197 cm⁻¹ (f), and 3196 cm⁻¹ (e) and are about 200 cm⁻¹ red-shifted compared to the amino group in the neutral compound. The corresponding $\nu_{\text{as}}(\text{ND}_2)$ are observed at 2394 cm⁻¹ (c) and 2399 cm⁻¹ (d), respectively, and they are in fair agreement with the Teller-Redlich rule for an H/D isotopic effect.^[8] The frequencies of the CH_3 group remain approximately un-

* Prof. Dr. A. Kornath
E-Mail: andreas.kornath@cup.uni-muenchen.de

[a] Department Chemie
Ludwig-Maximilians-Universität München
Butenandtstr. 5–13(D)
81377 Munich, Germany

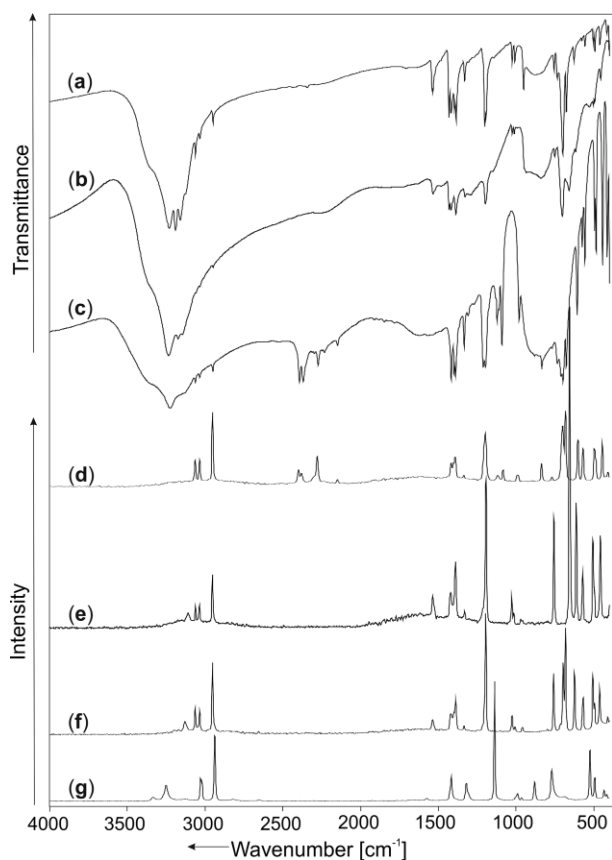


Figure 1. Low temperature vibrational spectra of $[\text{CH}_3\text{SO}_2\text{NH}_3]^+[\text{AsF}_6]^-$: (a) IR spectrum, (f) Raman spectrum; $[\text{CH}_3\text{SO}_2\text{NH}_3]^+[\text{SbF}_6]^-$: (b) IR spectrum, (e) Raman spectrum; $[\text{CH}_3\text{SO}_2\text{ND}_3]^+[\text{AsF}_6]^-$: (c) IR spectrum, (d) Raman spectrum; $\text{CH}_3\text{SO}_2\text{NH}_2$: (g) Raman spectrum.

changed in all cases and are comparable to $\text{CH}_3\text{SO}_2\text{NH}_2$.^[9] The SO_2 stretching vibrations occur at 1400 cm^{-1} and 1200 cm^{-1} and are blue-shifted by approximately 60 cm^{-1} compared to $\text{CH}_3\text{SO}_2\text{NH}_2$. The $\nu(\text{SN})$ mode at around 500 cm^{-1} is blue-shifted by approximately 270 cm^{-1} . This is in accordance with the significant elongation of the S–N bond in the protonated species found in the crystal structure, which is discussed later. For the anions AsF_6^- and SbF_6^- with ideal octahedral symmetry more vibrations are observed than expected. This can be explained by distortion of the anions in the solid state, which leads to a lower symmetry.

Crystal Structure of $[\text{CH}_3\text{SO}_2\text{NH}_3]^+[\text{Sb}_2\text{F}_{11}]^-$

$[\text{CH}_3\text{SO}_2\text{NH}_3]^+[\text{Sb}_2\text{F}_{11}]^-$ crystallizes in the monoclinic space group $P2_1/c$ with four formula units in the unit cell. Selected geometric parameters are summarized in Table 3. In Figure 2 an asymmetric unit of $[\text{CH}_3\text{SO}_2\text{NH}_3]^+[\text{Sb}_2\text{F}_{11}]^-$ is illustrated.

The sulfur atom shows a distorted tetrahedral coordination. Compared to the starting material the bond angles C1–S1–N1 [$101.7(3)^\circ$] and N1–S1–O1 [$103.5(3)^\circ$] are decreased by 6.6° and 3.6° , respectively, and the bond angles C1–S1–O1 [$112.2(3)^\circ$] and O1–S1–O2 [$122.0(3)^\circ$] are increased by 4.3°

and 3.6° , respectively. The short S–N bond observed in the starting material [$1.612(2)\text{ \AA}$] can be explained by negative hyperconjugation as previously discussed for other sulphonamide derivatives.^[10] Due to the *N*-protonation this effect seems to be revoked, resulting in a significant S–N bond elongation to $1.804(6)\text{ \AA}$ in the protonated species. The S–C bond lengths of $1.747(7)\text{ \AA}$ as well as the S–O bond lengths [$1.416(5)\text{ \AA}$ / $1.422(5)\text{ \AA}$] are slightly shorter than in $\text{CH}_3\text{SO}_2\text{NH}_2$. Experimental bond lengths and angles of the $\text{CH}_3\text{SO}_2\text{NH}_3^+$ cation are in good agreement with the quantum chemical calculations (Table 2). The observation, that the experimental and calculated S–N and S–C bond lengths are in good accordance to the theoretical values, can be considered as another proof for the correct assignment of the nitrogen and carbon atom in the crystal structure. Furthermore, hydrogen bonds are only observed for the NH_3 group. The $\text{Sb}_2\text{F}_{11}^-$ anion possesses a staggered conformation. The Sb1–F6–Sb2 bond angle [$145.3(2)^\circ$] is comparable to the corresponding Sb–F–Sb bond angle observed in $[\text{XeCl}]^+[\text{Sb}_2\text{F}_{11}]^-$.^[11] The terminal Sb–F bond lengths in the $\text{Sb}_2\text{F}_{11}^-$ anion are in the range from $1.844(4)$ to $1.896(4)\text{ \AA}$, whereas the bridging Sb–F bond lengths are $2.033(4)\text{ \AA}$ and $2.049(4)\text{ \AA}$, respectively.

In the crystal structure of $[\text{CH}_3\text{SO}_2\text{NH}_3]^+[\text{Sb}_2\text{F}_{11}]^-$ the ions are connected via $\text{N–(H)}\cdots\text{F}$ hydrogen bonds, which are marked as dashed lines in Figure 3. A three-dimensional network is formed through the connection of each cation to four anions. The medium strong^[12] hydrogen bonds have donor-acceptor distances ranging from $2.762(7)\text{ \AA}$ to $3.098(7)\text{ \AA}$.

Crystal Structure of $\text{CH}_3\text{SO}_2\text{NH}_2$

The crystal structure of $\text{CH}_3\text{SO}_2\text{NH}_2$ has previously been reported by Vorontsova in 1963.^[7] The structure was determined using an RGK camera. The reported space group $Pnma$ can be confirmed by this study. However, due to an *R* value of 0.174, the previous measurement was not suitable to determine bond lengths and bond angles accurately. In Figure 4 the asymmetric unit is shown.

Selected bond lengths and bond angles are summarized in Table 2. The S–N bond length of $1.612(3)\text{ \AA}$ is comparable to the S–N bond in sulfamide [$1.620(1)\text{ \AA}$].^[13] The S–C bond length of $1.756(3)\text{ \AA}$ and the S–O bond length of $1.435(2)\text{ \AA}$ are slightly shorter than dimethyl sulfone.^[14] In contrast to the calculation the S–O bond was found to be slightly longer. This can be explained by the participation of the oxygen atom in hydrogen bonds. In the crystal structure of $\text{CH}_3\text{SO}_2\text{NH}_2$ each molecule is connected to four neighboring molecules by medium strong hydrogen bonds along the *b* axis with a donor-acceptor distance of $2.459(1)\text{ \AA}$ (Figure 5). This linkage leads to 14-membered rings, which are condensed to $(\text{CH}_3\text{SO}_2\text{NH}_2)_n$ layers in the $[100]$ plane.

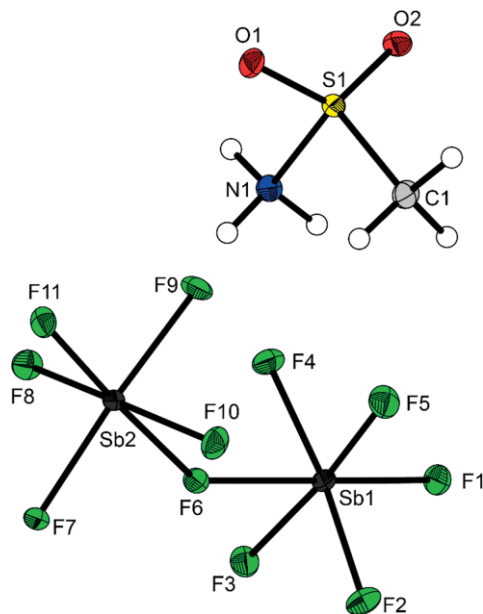
Theoretical Calculations

The quantum chemical calculations were performed with the PBE1PBE method using the 6-311G++(3df,3pd) basis set. In case of the $[\text{CH}_3\text{SO}_2\text{NH}_3]^+$ cation it was found that the ad-

Table 1. Experimental vibrational frequencies ^{a)} /cm⁻¹ of [CH₃SO₂NH₃]⁺[AsF₆]⁻, [CH₃SO₂ND₃]⁺[AsF₆]⁻ and [CH₃SO₂NH₃]⁺[SbF₆]⁻ (see Figure 1) and calculated vibrational frequencies /cm⁻¹ of [CH₃SO₂NH₃]⁺+3HF and [CH₃SO₂ND₃]⁺+3HF.

[CH ₃ SO ₂ NH ₃] ⁺ [AsF ₆] ⁻		[CH ₃ SO ₂ ND ₃] ⁺ [AsF ₆] ⁻		[CH ₃ SO ₂ NH ₃] ⁺ [SbF ₆] ⁻		[CH ₃ SO ₂ ND ₃] ⁺ +3HF		[CH ₃ SO ₂ NH ₃] ⁺ +3HF		Assignment ^{c)}	
(a)	(f)	(c)	(d)	(b)	(e)	calcd. ^{b)}		calcd. ^{b)}			
IR	Raman	IR	Raman	IR	Raman	(IR / Raman)		(IR / Raman)			
3191 (s)	3197(3)	2394 (s)	2399(20)		3196(3)	2441 (243/31)	3411 (506/51)	v ₁₇	A''	v _{as} (NX ₂)	
3161 (s)	3129(16)	2371 (s)	2379(6)	3174 (s)		2399 (341/37)	3364 (549/69)	v ₁	A'	v _{oph} (NX ₃)	
		2274 (m)				2265 (244/31)	3269 (500/148)	v ₂	A'	v _{iph} (NX ₃)	
3063 (m)	3063(20)	3064 (s)	3063(23)		3036(5)	3118 (9/37)	3198 (8/34)	v ₁₈	A''	v _{as} (CH ₂)	
	3035(13)		3035(19)			3092 (15/48)	3171 (14/43)	v ₃	A'	v _{oph} (CH ₃)	
2951 (m)	2952(58)	2952 (m)	2952(77)	2951 (m)	2952(14)	2994 (15/150)	3071 (18/133)	v ₄	A'	v _{iph} (CH ₃)	
1535 (m)	1536(14)	1122 (s)	1119(7)	1534 (w)	1535(10)	1145 (14/1)	1638 (29/2)	v ₅	A'	δ(NX ₃)	
		1092 (w)	1083(11)			1140 (1/1)	1633 (8/2)	v ₁₉	A''	δ(NX ₃)	
1418 (s)	1419(4)	1417 (s)	1418(6)	1420 (w)		1421 (111/6)	1504 (193/5)	v ₂₀	A''	v _{as} (SO ₂)	
						1028 (61/3)	1449 (93/0)	v ₆	A'	δ(NX ₃)	
						1393 (8/3)	1436 (23/3)	v ₇	A'	δ(CH ₃)	
1387 (m)	1388(53)	1399 (s)	1390(58)	1388 (w)	1389(20)	1386 (71/7)	1433 (37/6)	v ₂₁	A''	δ(CH ₃)	
1332 (m)	1334(4)	1335(m)	1335 (4)	1329 (w)	1330(2)	1301 (15/1)	1357 (31/1)	v ₈	A'	δ(CH ₃)	
1203 (s)	1195(100)	1199 (s)	1197(100)	1200 (w)	1193(49)	1177 (107/22)	1255 (125/18)	v ₉	A'	v _s (SO ₂)	
1027 (w)	1025(15)			1026 (w)	1027(7)	785 (41/5)	1057 (16/3)	v ₁₀	A'	ρ(NX ₃)	
1008 (w)	1006(2)			1013 (w)	1014(1)	949 (2/1)	1022 (11/1)	v ₂₂	A''	τ(NX ₃)	
954 (m)	958(5)			956 (w)		719(1/1)	963 (0/1)	v ₂₃	A''	τ(NX ₃)	
		981 (w)	993(13)			946 (24/1)	956 (60/0)	v ₁₁	A'	ρ(CH ₃)	
757 (w)	758(43)		769(5)	752 (m)	756(28)	785 (41/5)	757 (26/11)	v ₁₂	A'	v (SC)	
	506(39)	496 (m)	497(4)		505(22)	510 (97/4)	585 (92/9)	v ₁₃	A'	v (SN)	
495 (w)	495(5)	487 (m)	487(4)			455 (20/5)	499 (18/5)	v ₁₄	A'	δ (SO ₂)	
		445 (w)			458(24)	389 (14/7)	454 (26/4)	v ₁₅	A'	ρ(CH ₃)	
	410(4)	417 (w)				325 (2/0)	403 (2/1)	v ₂₄	A''	τ(NX ₃)	
			316(8)			338 (2/3)	374 (4/2)	v ₂₅	A''	δ(CSO)	
						272 (2/1)	308 (4/2)	v ₂₆	A''	τ(SO ₂)	
			117(73)			263 (19/1)	289 (43/1)	v ₁₆	A'	δ(NSC)	
702 (s)	697(22)	701 (w)				198 (2/0)	208 (5/0)	v ₂₇	A''	δ(CH ₃)	
678 (m)			682(76)							[AsF ₆] ⁻	
	568(36)									[AsF ₆] ⁻	
	374(34)									[AsF ₆] ⁻	
379 (w)				660 (m)						[SbF ₆] ⁻	
					656(100)					[SbF ₆] ⁻	
					571(28)					[SbF ₆] ⁻	

a) Abbreviations for IR intensities: v = very, s = strong, m = medium, w = weak. IR intensity in km²mol⁻¹ and Raman intensity in Å⁴μ⁻¹; Raman activity is stated to a scale of 1 to 100. b) Calculated at the PBE1PBE/6-311G++(3df,3dp) level of theory. c) X = H, D.

**Figure 2.** Asymmetric unit of [CH₃SO₂NH₃]⁺[Sb₂F₁₁]⁻ (50% probability displacement ellipsoids).**Table 2.** Selected bond lengths /Å and angles /° of [CH₃SO₂NH₃]⁺[Sb₂F₁₁]⁻ and the calculated [CH₃SO₂NH₃]⁺+3HF.

	CH ₃ SO ₂ NH ₂	[CH ₃ SO ₂ NH ₃] ⁺ Sb ₂ F ₁₁ ⁻	[CH ₃ SO ₂ NH ₃] ⁺ +3HF ^{a)}
Bond length			
S1-N1	1.612(2)	1.804(6)	1.820
S1-O1	1.435(1)	1.416(5)	1.415
S1-O2	1.435(1)	1.422(5)	1.415
S1-C1	1.756(3)	1.747(7)	1.749
Donor-acceptor distance			
N1-(H1D)⋯F9		2.762(7)	
N1-(H1E)⋯F3		2.942(7)	
N1-(H1E)⋯F4		2.839(7)	
N1-(H1F)⋯F8		2.782(7)	
N1-(H1F)⋯F1		3.098(7)	
Bond angle			
C1-S1-N1	108.3(2)	101.7(3)	100.5
C1-S1-O1	107.9(1)	112.2(3)	111.7
N1-S1-O1	107.1(1)	103.5(3)	102.6
O1-S1-O2	118.3(1)	122.0(3)	123.9

a) Calculated on the PBE1PBE/6-311G++(3pd,3df)-level of theory.

dition of three HF molecules leads to the most closely match with the experimentally determined geometry in the crystal

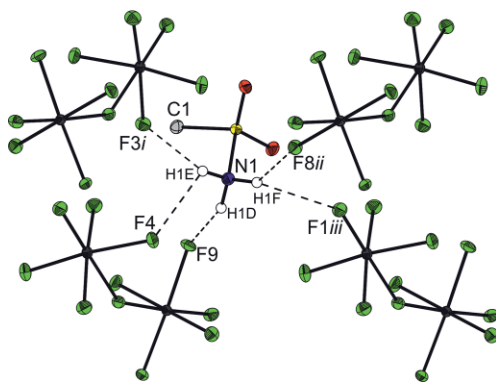


Figure 3. View of the packing along the *b* axis (50% probability displacement ellipsoids). Hydrogen bonds are drawn as dashed lines. Methyl protons are not shown in this figure. Symmetry codes: *i*: 1 - *x*, 0.5 + *y*, 0.5 - *z*; *ii*: 2 - *x*, 0.5 + *y*, 0.5 - *z*; *iii*: 1 + *x*, *y*; *z*.

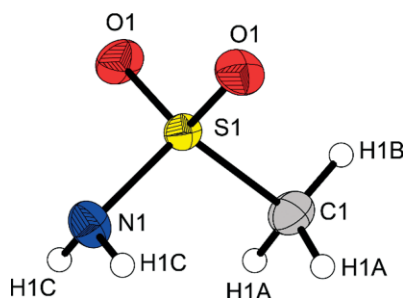


Figure 4. Molecular unit of $\text{CH}_3\text{SO}_2\text{NH}_2$ (50% probability displacement ellipsoids).

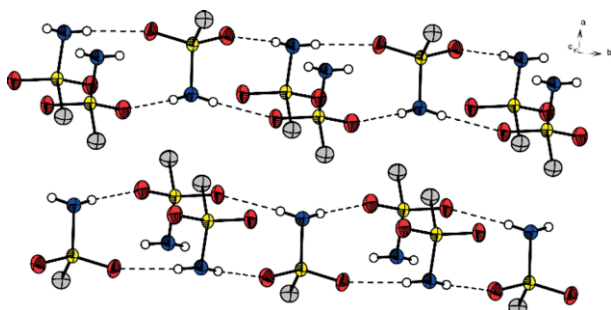


Figure 5. Crystal packing of $\text{CH}_3\text{SO}_2\text{NH}_2$. View along the *c* axis. Hydrogen bonds are drawn as dashed lines. The protons of the methyl group are not shown (50% probability displacement ellipsoids).

structure. Therefore the calculated frequencies as well as Raman and IR intensities of $[\text{CH}_3\text{SO}_2\text{NX}_3]^+ \cdot 3\text{HF}$ ($X = \text{D}, \text{H}$), which were carried out in the harmonic approximation and taken into account for the vibrational assignments. In previous studies the method of adding HF molecules to the naked cation already became apparent as a powerful tool for the simulation of hydrogen bonds in the solid state.^[15,16]

Conclusions

In the course of this study the $\text{CH}_3\text{SO}_2\text{NH}_3^+$ cation was isolated as AsF_6^- and SbF_6^- salt, respectively, for the first time.

For a complete vibrational analysis, the isotomeres $[\text{CH}_3\text{SO}_2\text{ND}_3]^+[\text{MF}_6]^-$ ($M = \text{As}; \text{Sb}$) were synthesized. It was shown that an *N*-protonation of methanesulfonamide exclusively takes place. The vibrational assignments are supported by quantum chemical calculations. An excess of SbF_5 does not lead to a diprotonation of methanesulfonamide but to the formation of $\text{Sb}_2\text{F}_{11}^-$ salts. $[\text{CH}_3\text{SO}_2\text{NH}_3]^+[\text{Sb}_2\text{F}_{11}]^-$ and $\text{CH}_3\text{SO}_2\text{NH}_2$ were characterized by single-crystal X-ray structure analysis. This study shows that the *N*-protonation causes a remarkable elongation of the S–N bond length from 1.612(2) Å in the neutral compound to 1.804(6) Å in the protonated species. This observation is in accordance with the hypothesis that the appearance of negative hyperconjugation is the reason for the short S–N bonds observed in sulfonamides.

Experimental Section

Caution! The hydrolysis of AsF_5 and SbF_5 as well as the reported salts might form HF, which burns skin and causes irreparable damage. Avoid contact with any of these compounds. Safety precautions should be taken when using and handling these materials.

Apparatus and Materials: All reactions were carried out by employing standard Schlenk techniques using a stainless-steel vacuum line. Reactions in superacidic media were performed in FEP/PFA reactors, which were closed with a stainless-steel valve. All reaction vessels were dried with fluorine prior to use. Raman spectroscopic investigations were performed at -196°C with a Bruker MultiRAM FT-Raman spectrometer with Nd:YAG laser excitation up to 1000 mW ($\lambda = 1064 \text{ nm}$) in the range between 250 and 4000 cm^{-1} . Low-temperature IR measurements were performed with a Bruker Vertex-80V FTIR spectrometer. For the measurements in a cooled cell small amounts of the sample were placed on a CsBr single-crystal plate. IR spectra were recorded in a range between 350 and 4000 cm^{-1} . The single-crystal X-ray structure analysis was carried out with an Oxford Xcalibur3 diffractometer, which is equipped with a Spellman generator (50 kV, 40 mA, with Mo- K_α radiation of $\lambda = 0.7107 \text{ \AA}$) and a KappaCCD detector. The measurement was performed at a temperature of 173 K. Data collection was carried out using the CrysAlis CCD software,^[17] and for its reduction the program CrysAlis RED software^[18]. The solution and refinement of the structure was performed with the programs SHELXS^[19] and SHELXL-97^[20] implemented in the WinGX software package^[21] and finally checked with the PLATON software^[22]. The absorption correction was carried out by employing the SCALE3 ASPACK multi scan method.^[23] $\text{CH}_3\text{SO}_2\text{NH}_2$ (Alfa Aesar) was used as received. $\text{CH}_3\text{SO}_2\text{ND}_2$ was prepared by several recrystallizations from D_2O (Euriso-Top). SbF_5 (Merck) was triple distilled prior to use. AsF_5 was synthesized from the elements and purified by several condensations. HF (Linde) was first purified by trap-to-trap condensation under vacuum and then dried with fluorine for two weeks in a stainless-steel pressure cylinder. DF was prepared from dried CaF_2 and D_2SO_4 . Quantum-chemical calculations were carried out using the Gaussian09 package^[25] using the PBE1PBE density functional approach with a 6-311GG++(3pd, 3df). Crystal data and structure refinement for $\text{CH}_3\text{SO}_2\text{NH}_2$ and $[\text{CH}_3\text{SO}_2\text{NH}_3]^+[\text{Sb}_2\text{F}_{11}]^-$ are listed in Table 3.

Crystallographic data (excluding structure factors) for the structures in this paper have been deposited with the Cambridge Crystallographic Data Centre, CCDC, 12 Union Road, Cambridge CB21EZ, UK. Copies of the data can be obtained free of charge on quoting the depository numbers CCDC-1555583 (for $[\text{CH}_3\text{SO}_2\text{NH}_3]^+[\text{Sb}_2\text{F}_{11}]^-$) and CCDC-

Table 3. Crystal data and structure refinement for CH₃SO₂NH₂ and [CH₃SO₂NH₃]⁺[Sb₂F₁₁]⁻.

	CH ₃ SO ₂ NH ₂	[CH ₃ SO ₂ NH ₃] ⁺ [Sb ₂ F ₁₁] ⁻
<i>M_r</i>	95.12	548.63
Crystal system	orthorhombic	monoclinic
Space group	<i>Pnma</i>	<i>P2₁/c</i>
<i>a</i> / Å	9.9598(5)	7.7391(3)
<i>b</i> / Å	7.4262(4)	9.8130(3)
<i>c</i> / Å	5.3555(3)	15.8449(6)
<i>α</i> / °	90	90
<i>β</i> / °	90	96.024(4)
<i>γ</i> / °	90	90
<i>V</i> / Å ³	396.11(4)	1196.68(7)
<i>Z</i>	4	4
<i>ρ</i> _{calcd.} / g·cm ⁻³	1.595	3.045
<i>μ</i> / mm ⁻¹	0.637	4.826
<i>λ</i> (Mo-K _α) / Å	0.71073	0.71073
<i>F</i> (000)	200	1008
<i>T</i> / K	173(2)	173(2)
<i>hkl</i> range	-9:12; -9:8; -6:5	-4:9; -12:11; -19:18
Refl. measured	1518	5947
Refl. unique	439	2335
<i>R</i> _{int}	0.0284	0.0252
Parameters	39	165
<i>R</i> (<i>F</i>)/ <i>wR</i> (<i>F</i> ²) ^a	0.0338	0.0359
(all reflexions)		
Weighting scheme ^b	0.0502/0.0727	0.0071/12.9881
<i>S</i> (GoF) ^c	1.145	1.240
Residual density	0.390/-0.336	1.151/-0.720
/e·Å ⁻³		
Device type	Oxford XCalibur	Oxford XCalibur
Solution/refinement	SHELXS-97 ^[21] , SHELXL-97 ^[14]	SHELXS-97 ^[21] , SHELXL-97 ^[14]

a) $R_1 = \sum |F_o| - |F_c| / \sum |F_o|$. b) $wR_2 = [\sum [w(F_o^2 - F_c^2)^2] / \sum [w(F_o^2)^2]]^{1/2}$; $w = [\sigma_c^2(F_o^2) + (xP)^2 + yP]^{-1}$; $P = (F_o^2 + 2F_c^2) / 3$. c) GoF = $\{\sum [w(F_o^2 - F_c^2)^2] / (n-p)\}^{1/2}$ (n = number of reflexions; p = total number of parameters).

1555585 (for CH₃SO₂NH₂) (Fax: +44-1223-336-033; E-Mail: deposit@ccdc.cam.ac.uk, http://www.ccdc.cam.ac.uk).

Synthesis of [CH₃SO₂NX₃]⁺[AsF₆]⁻ (*X* = H, D). Anhydrous hydrogen fluoride, HF, (ca. 2 mL) or deuterium fluoride, DF, (ca. 2 mL) and arsenic pentafluoride, AsF₅, (1.10 mmol, 187 mg) were condensed at -196 °C into a reactor (FEP tube). The mixture was allowed to warm up to 0 °C to mix the components and form the superacid system. Methanesulfonamide, CH₃SO₂NH₂, (95 mg, 1.00 mmol) or its isotopomere, CH₃SO₂ND₂, (98 mg, 1.00 mmol) were added in an inert nitrogen atmosphere at -196 °C. The mixture was warmed to -50 °C for 10 min. A colorless precipitate was formed. Afterwards the reactor was cooled to -78 °C. Excess anhydrous hydrogen fluoride (or deuterium fluoride) and arsenic pentafluoride were removed in dynamic vacuum. After 12 h, [CH₃SO₂NH₃]⁺[AsF₆]⁻ (or [CH₃SO₂ND₃]⁺[AsF₆]⁻) was obtained as colorless solid. The moisture sensitive salts are stable up to room temperature.

Synthesis of [CH₃SO₂NX₃]⁺[SbF₆]⁻ (*X* = H, D) and [CH₃SO₂NH₃]⁺[Sb₂F₁₁]⁻: Antimony pentafluoride, SbF₅, (0.35 mmol, 76 mg), and anhydrous hydrogen fluoride (ca. 2 mL) were condensed into a reactor (FEP tube) at -196 °C. The reactor was warmed for 10 min to 0 °C to allow the mixture of the components and form the superacid system. Methanesulfonamide, CH₃SO₂NH₂, (0.35 mmol, 33 mg), or its isotopomere, CH₃SO₂ND₂, (0.35 mmol, 34 mg) were added in an inert nitrogen atmosphere at -196 °C. The mixture was warmed to -50 °C for 10 min. Afterwards the reactor was cooled to -78 °C. Excess anhydrous hydrogen fluoride was removed in dynamic

vacuum. After 12 h, [CH₃SO₂NX₃]⁺[SbF₆]⁻ (*X* = H, D), was obtained as a colorless solid. The synthesis of [CH₃SO₂NH₃]⁺[Sb₂F₁₁]⁻ was carried out by the reaction of 9 equiv. of SbF₅ under analogous conditions. The obtained colorless salts are stable up to room temperature.

Acknowledgements

Financial support of this work by the Ludwig-Maximilian-University Munich (LMU) by the Deutsche Forschungsgemeinschaft (DFG) and F-Select GmbH is gratefully acknowledged.

Keywords: Methanesulfonamide; Protonation; Superacid chemistry; Vibrational spectroscopy; X-ray diffraction

References

- [1] V. Padmavathi, P. Thriveni, G. Sudhakar Reddy, D. Deepti, *Eur. J. Med. Chem.* **2008**, *43*, 917–924.
- [2] G. L. Grunewald, M. R. Seim, R. C. Regier, J. L. Martin, C. L. Gee, N. Drinkwater, K. R. Criscione, *J. Med. Chem.* **2006**, *49*, 5424–5433.
- [3] H. LeMaire, H. J. Lucas, *J. Am. Chem. Soc.* **1951**, *73*, 5198–5201.
- [4] R. G. Laughlin, *J. Am. Chem. Soc.* **1967**, *89*, 4268–4271.
- [5] A. Bagno, B. Bujnicki, S. Bertrand, C. Comuzzi, F. Dorigo, P. Janvier, G. Scorrano, *Chem. Eur. J.* **1999**, *5*, 523–536.
- [6] B. A. Shainyan, N. N. Chipanina, L. P. Oznobikhina, *J. Phys. Org. Chem.* **2012**, *25*, 738–747.
- [7] L. G. Vorontsova, *J. Struct. Chem.* **1966**, *7*, 275–277.
- [8] J. Weidlein, U. Müller, K. Dehnicke, *Schwingungsspektroskopie*, 2nd ed., Georg Thieme Verlag, Stuttgart, Germany **1988**, p. 30.
- [9] A. Blaschette, H. Bürger, *Z. Anorg. Allg. Chem.* **1970**, *378*, 104–116.
- [10] L. M. Lyapalo, H.-U. Reissig, A. Schäfer, A. Wagner, *Helv. Chim. Acta* **2002**, *85*, 4206–4215.
- [11] S. Seidel, K. Seppelt, *Angew. Chem. Int. Ed.* **2001**, *40*, 4225–4227.
- [12] G. A. Jeffrey, *An Introduction to Hydrogen Bonding*, Oxford University Press, Oxford, UK **1997**.
- [13] F. Belaj, C. Kratky, E. Nachbaur, A. Popitsch, *Monatsh. Chem.* **1987**, *118*, 427–433.
- [14] D. E. Sands, *Z. Kristallogr.* **1963**, *119*, 245–251.
- [15] T. Soltner, N. R. Goetz, A. Kornath, *Eur. J. Inorg. Chem.* **2011**, *20*, 3076–3081.
- [16] J. Axhausen, C. Ritter, A. Kornath, *Z. Anorg. Allg. Chem.* **2013**, *639*, 65–72.
- [17] *CrysAlisCCD*, Version 1.171.35.11 (release 16–05–2011 CrysAlis 171.NET), Oxford Diffraction Ltd., UK, **2011**.
- [18] *CrysAlisRED*, Version 1.171.35.11 (release 16–05–2011 CrysAlis 171.NET), Oxford Diffraction Ltd., UK, **2011**.
- [19] G. M. Sheldrick, *SHELXS-97*, Program for Crystal Structure Solution, University of Göttingen, Germany, **1997**.
- [20] G. M. Sheldrick, *SHELXL-97*, Program for the Refinement of Crystal Structures, University of Göttingen, Germany, **1997**.
- [21] L. J. Farrugia, *J. Appl. Crystallogr.* **1999**, *32*, 837–838.
- [22] A. L. Spek, *PLATON*, A Multipurpose Crystallographic Tool, Utrecht University, Utrecht, The Netherlands, **1999**.
- [23] *SCALE3 ABSPACK*, an Oxford Diffraction Program, Oxford Diffraction Ltd., UK, **2005**.
- [24] G. W. T. M. J. Frisch, H. B. Schlegel, G. E. Scuseria, M. A. Robb, J. R. Cheeseman, J. A. Montgomery, T. V. K. N. Kudin Jr., J. C. Burant, J. M. Millam, S. S. Iyengar, J. Tomasi, V. Barone, B. Mennucci, M. Cossi, G. Scalmani, N. Rega, G. A. Petersson, H. Nakatsuji, M. Hada, M. Ehara, K. Toyota, R. Fukuda, J. Hasegawa, M. Ishida, T. Nakajima, Y. Honda, O. Kitao, H. Nakai, M. Klene, X. Li, J. E. Knox, H. P. Hratchian, J. B. Cross, C. Adamo,

J. Jaramillo, R. Gomperts, R. E. Stratmann, O. Yazyev, A. J. Austin, R. Cammi, C. Pomelli, J. W. Ochterski, P. Y. Ayala, K. Morokuma, G. A. Voth, P. Salvador, J. J. Dannenberg, V. G. Zakrzewski, S. Dapprich, A. D. Daniels, M. C. Strain, O. Farkas, D. K. Malick, A. D. Rabuck, K. Raghavachari, J. B. Foresman, J. V. Ortiz, Q. Cui, A. G. Baboul, S. Clifford, J. Cioslowski, B. B. Stefanov, G. Liu, A. Liashenko, P. Piskorz, I. Komaromi, R. L. Mar-

tin, D. J. Fox, T. Keith, M. A. Al-Laham, C. Y. Peng, A. Nanayakara, M. Challacombe, P. M. W. Gill, B. Johnson, W. Chen, M. W. Wong, C. Gonzalez, J. A. Pople, Gaussian, Inc. **2003**, Pittsburgh PA.

Received: July 17, 2017

Published Online: August 28, 2017

The Influence of the Counterions $[\text{AsF}_6]^-$ and $[\text{GeF}_6]^{2-}$ on the Structure of the $[\text{ClSO}_2\text{NH}_3]^+$ Cation

Dominik Leitz,^[a] Karin Stierstorfer,^[a] Yvonne Morgenstern,^[a] and Florian Zischka,^[a] Andreas J. Kornath*^[a]

Abstract. Chlorosulfonamide reacts in the superacidic solutions HF/GeF₄ and HF/AsF₅ under the formation of $([\text{ClSO}_2\text{NH}_3]^+)_2[\text{GeF}_6]^{2-}$ and $[\text{ClSO}_2\text{NH}_3]^+[\text{AsF}_6]^-$, respectively. The chlorosulfonamide salts were characterized by X-ray single crystal structure analysis as well as vibrational spectroscopy and discussed together with quantum chemical calculations. $([\text{ClSO}_2\text{NH}_3]^+)_2[\text{GeF}_6]^{2-}$ crystallizes in the triclinic space group $P\bar{1}$ with one formula unit in the unit cell. $[\text{ClSO}_2\text{NH}_3]^+[\text{AsF}_6]^-$ crystallizes in the monoclinic space

group $P2_1/n$ with four formula units in the unit cell. Dependent on the counterion, $[\text{AsF}_6]^-$ or $[\text{GeF}_6]^{2-}$, considerable structural differences of the $[\text{ClSO}_2\text{NH}_3]^+$ cation are observed. Furthermore, the hitherto unknown X-ray single crystal structure of chlorosulfonamide is determined in the course of this study. Chlorosulfonamide crystallizes in the orthorhombic space group $Pmc2$ with four formula units per unit cell.

Introduction

Chlorosulfonamide is one of the simplest representatives of sulfonamides and was synthesized by Graf for the first time.^[1] The title compound is well characterized by vibrational^[2,3] and theoretical studies.^[4] However, surprisingly a single-crystal X-ray diffraction study has not been reported so far. Despite the numerous studies on sulfonamide derivatives investigations of its protonation sites are rarely described in the literature.^[5–7] In these studies protonations at the nitrogen site are indicated, which is in agreement with a theoretical study where it was confirmed that the nitrogen site is favorable to the protonation.^[8] In a previous study methanesulfonamide was investigated in the superacidic systems HF/MF₅ ($M = \text{As}, \text{Sb}$).^[9] It was found that the protonation takes place selectively at the nitrogen atom.

Herein we present a study of chlorosulfonamide in the superacidic solutions HF/GeF₄ and HF/AsF₅. While the superacidic system HF/AsF₅ is well established the superacidic system HF/GeF₄ is rarely described in literature. However, it showed an acidity beyond sulfuric acid and demonstrated an interesting structural versatility of the formed fluoridogermanate anions.^[10,11] We present the structural investigations of $([\text{ClSO}_2\text{NH}_3]^+)_2[\text{GeF}_6]^{2-}$ and $[\text{ClSO}_2\text{NH}_3]^+[\text{AsF}_6]^-$ by vibrational spectroscopy and single-crystal X-ray structure analyses. Furthermore the structural influence of the counterions $[\text{AsF}_6]^-$ and $[\text{GeF}_6]^{2-}$ is discussed together with quantum chemical calculations.

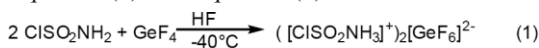
* Prof. Dr. A. Kornath
E-Mail: andreas.kornath@cup.uni-muenchen.de

[a] Department Chemie
Ludwig-Maximilians-Universität München
Butenandtstr. 5–13
81377 Munich, Germany

Results and Discussion

Synthesis and Properties of $([\text{ClSO}_2\text{NH}_3]^+)_2[\text{GeF}_6]^{2-}$ (I) and $[\text{ClSO}_2\text{NH}_3]^+[\text{AsF}_6]^-$ (II)

The salts **I** and **II** were obtained quantitatively according to Equation (1) and Equation (2):



In the first step ClSO_2NH_2 was synthesized in situ in an FEP reaction vessel. The synthesis was carried out by the reaction of chlorosulfonyl isocyanate and formic acid as described in a previous study.^[12] An excess of anhydrous HF (*a*HF), which serves as reagent as well as solvent, was condensed into the reaction vessel followed by three equivalents of GeF₄ or AsF₅, respectively. The reaction mixtures were allowed to warm up to -40°C and stored for 72 h. Colorless crystals were obtained and characterized by single-crystal X-ray structure analyses and vibrational spectroscopy.

Crystal Structure of $([\text{ClSO}_2\text{NH}_3]^+)_2[\text{GeF}_6]^{2-}$ (I)

Compound **I** crystallizes in the triclinic space group $P\bar{1}$ with one formula unit in the unit cell. Figure 1 depicts the formula

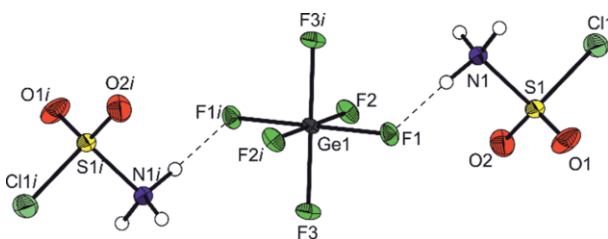


Figure 1. Formula unit of $([\text{ClSO}_2\text{NH}_3]^+)_2[\text{GeF}_6]^{2-}$ (50% probability displacement ellipsoids). Symmetry code: $i: -x, 1 -y, -z$.

Table 1. Selected bond lengths /Å and bond angles /° of $[(\text{ClSO}_2\text{NH}_3)^+]_2[\text{GeF}_6]^{2-}$ and $[\text{ClSO}_2\text{NH}_3]^+[\text{AsF}_6]^-$.

	$[\text{ClSO}_2\text{NH}_3]^+[\text{GeF}_6]^{2-}$ (obsd.)	$[\text{AsF}_6]^-$ (obsd.)	$[\text{ClSO}_2\text{NH}_3]^+\text{HF}$ HF (calcd.) ^{a)}	$[\text{ClSO}_2\text{NH}_3]^+$ (calcd.) ^{a)}
Bond lengths				
S1–O1	1.417(3)	1.406(2)	1.405	1.404
S1–N1	1.725(3)	1.765(3)	1.820	1.854
S1–Cl1	1.956(1)	1.945(1)	1.964	1.959
Bond angles				
O1–S1–O2	122.7(2)	123.6(1)	126.3	126.3
O1–S1–N1	107.2(2)	104.9(1)	102.6	102.8
O1–S1–Cl1	108.6(2)	111.0(1)	110.9	110.9
N1–S1–Cl1	99.6 (1)	100.3(1)	98.0	98.4

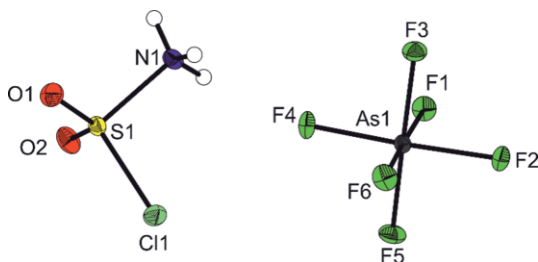
a) Calculated at the PBE1PBE 6-311G++(3pd,3df) level of theory.

unit of **I**. In Table 1 bond lengths and bond angles are summarized.

The coordination sphere of the sulfur atom can be described as a strong distorted tetrahedron. Compared to the neutral compound the bond angles O1–S1–O2 [122.7(2)°] and Cl1–S1–O1 [108.6(1)°] are increased by approximately 2° and the bond angles Cl1–S1–N1 [99.6(1)°] and N1–S1–O1 [107.2(2)°] are decreased by 7.2° and 1.8°, respectively. The S–Cl bond length of 1.956(1) Å is slightly shorter than the S–Cl bond in SO_2Cl_2 (1.980 Å).^[13] The S–N bond length of 1.725(3) Å is significantly elongated with respect to the starting material [1.571(4)/1.583(4) Å] and slightly shorter than the S–N bond in the $\text{CH}_3\text{SO}_2\text{NCl}_2^+$ cation.^[14] The S–O bond lengths of 1.417(3) Å are comparable to the S–O bonds in SO_2Cl_2 (1.418 Å).^[13] In terms of the approximately octahedral $[\text{GeF}_6]^{2-}$ anion the Ge–F bond lengths are in the range from 1.783(2) Å to 1.789(2) Å, which is in accordance to a previous study describing $[\text{GeF}_6]^{2-}$.^[10]

Crystal Structure of $[\text{ClSO}_2\text{NH}_3]^+[\text{AsF}_6]^-$ (**II**)

Compound **II** crystallizes in the monoclinic space group $P2_1/n$ with four formula units in the unit cell (see Figure 2). Bond lengths and bond angles are summarized in Table 1.

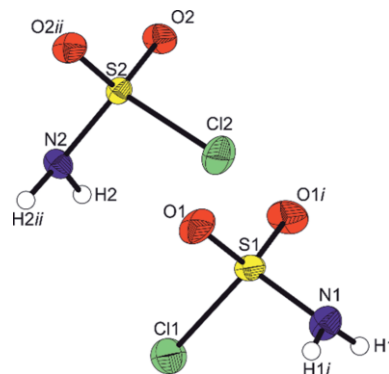
**Figure 2.** Asymmetric unit of $[\text{ClSO}_2\text{NH}_3]^+[\text{AsF}_6]^-$ (50% probability displacement ellipsoids).

In comparison to **I** the distorted tetrahedral coordination of the sulfur atom is slightly different. The S–O bond lengths are slightly shorter whereas the S–N bond of 1.765(3) Å is significantly longer than in **I**. Each cation is connected with two $[\text{AsF}_6]^-$ anions by medium strong hydrogen bonds with N(–H)⋯F donor-acceptor distances of 2.894 Å and 2.953 Å, respectively. The cations are connected by N(–H)⋯O hydrogen

bonds of donor-acceptor distances of 3.139(3) Å forming zig-zag chains.

Crystal Structure of ClSO_2NH_2 (**III**)

Single crystals of **III** were grown by slow evaporation of the solvent benzene in dynamic vacuum. The compound crystallizes in the orthorhombic space group $Pmc2$ with four formula units in the unit cell. Figure 3 shows a view of the two symmetrically independent molecules. Selected bond lengths and angles of **III** are summarized in Table 2.

**Figure 3.** Section of the crystal structure of ClSO_2NH_2 (50% probability displacement ellipsoids). Symmetry codes: *i*: 1 –*x*, *y*, *z*; *ii*: –*x*, *y*, *z*.**Table 2.** Selected bond lengths /Å and bond angles /° of ClSO_2NH_2 .

Bond lengths	obsd.	calcd. ^{a)}
S1–O1 / S2–O2	1.424(2) / 1.425(2)	1.416
S1–N1 / S2–N2	1.571(4) / 1.583(4)	1.617
S1–Cl1 / S2–Cl2	2.018(1) / 2.014(1)	2.052
Bond angles		
O1–S1–O1 / O2–S2–O2	120.7(1) / 119.8(1)	123.8
O1–S1–N1 / O1–S1–N1	109.0(1) / 108.9(1)	107.8
O1–S1–Cl1 / O2–S2–Cl2	105.3(1) / 105.8(1)	105.7
N1–S1–Cl1 / N2–S2–Cl2	106.8(1) / 106.9(1)	104.4

a) Calculated at the PBE1PBE 6-311G++(3pd,3df) level of theory.

The S–Cl bond lengths of 2.018(1) and 2.014(3) Å, respectively, are in the range of regular S–Cl single bonds observed for SO_2Cl_2 .^[13] The S–N bond lengths of 1.571(4) Å and

1.583(4) Å, respectively, are in the region between regular S–N single and double bonds. The short S–N distance can be explained by $n_N \rightarrow \sigma^*(S-O)$ and $n_N \rightarrow \sigma^*(S-N)$ interactions, where the molecule is predicted to provide 18 kJ·mol⁻¹. This is in good agreement to a previous study where sulfamide was theoretically investigated.^[15] The S–O bonds of 1.424(2) Å and 1.425(2) Å are slightly longer than observed for the [ClSO₂NH₃]⁺ cation.

Figure 4 shows the crystal packing of ClSO₂NH₂ molecules connected by donor-acceptor interactions [N(–H)⋯O] of 2.926(3) Å and 2.952(3) Å, respectively, forming 14-membered rings.

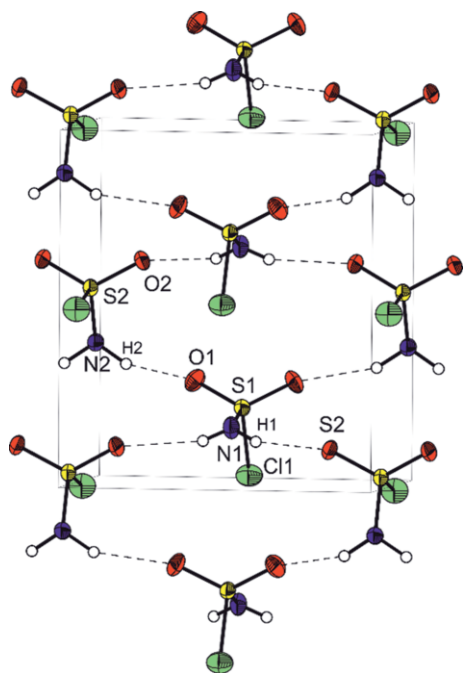


Figure 4. Crystal packing of ClSO₂NH₂ (50% probability displacement ellipsoids). View along the *b* axis. Hydrogen bonds are represented by dashed lines.

Vibrational Spectroscopy of ([ClSO₂NH₃]⁺)₂[GeF₆]²⁻ (I) and [ClSO₂NH₃]⁺[AsF₆]⁻ (II)

The Raman and infrared spectra of **I** and **II** are shown in Figure 5. In Table 3 the observed and quantum-chemically calculated frequencies are summarized. For [ClSO₂NH₃]⁺ with approximately C_s symmetry 18 fundamental vibrations are expected. The assignment of the vibrational frequencies is supported by quantum chemical calculations of [ClSO₂NH₃]⁺·HF. As expected, in case of the protonated species three NH stretching vibrations are observed which occur in the range from 3171 cm⁻¹ to 2828 cm⁻¹ and are significantly red-shifted by approximately 200 cm⁻¹ compared to the neutral compound. In the IR spectra of **I** and **II** at 1726 cm⁻¹ a combination band of $\nu_5 + \nu_8$ is observed. At 1550 cm⁻¹ a NH deformation mode is detected in **I**. The antisymmetric SO₂ stretching mode is observed at around 1450 cm⁻¹. The symmetric SO₂ stretching mode is split due to Fermi resonance and occurs

at around 1215 cm⁻¹ and 1190 cm⁻¹, respectively. The SN stretching vibration occurs at around 485 cm⁻¹ and is red-shifted by 435 cm⁻¹ compared to the neutral compound. This remarkable shift can be explained by the significant elongation of the SN bond length. As expected for the almost ideal octahedral [GeF₆]²⁻ anion three Raman lines and two IR bands are observed. In case of the [AsF₆]⁻ more lines and bands than expected are detected, which can be explained by the distortion of the octahedral structure according to the findings in the crystal structure.

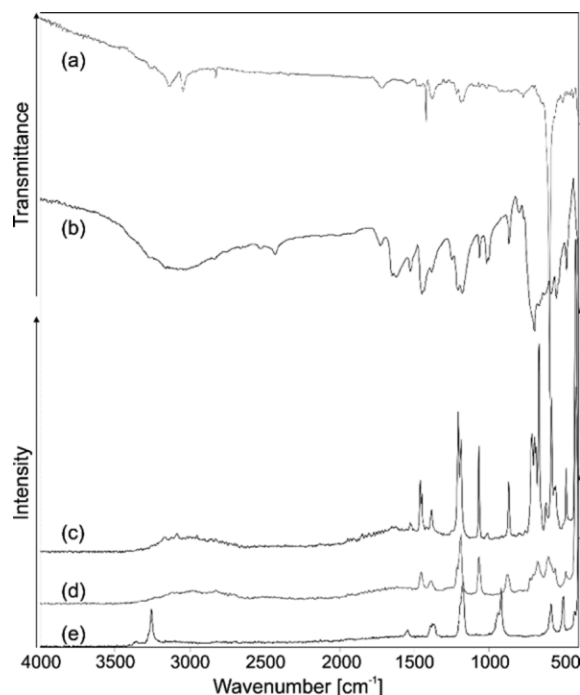


Figure 5. Low temperature vibrational spectra of ([ClSO₂NH₃]⁺)₂[GeF₆]²⁻: (a) IR spectrum, (d) Raman spectrum. [ClSO₂NH₃]⁺[AsF₆]⁻: (b) IR spectrum, (c) Raman spectrum. ClSO₂NH₂: (e) Raman spectrum.

Theoretical Calculations

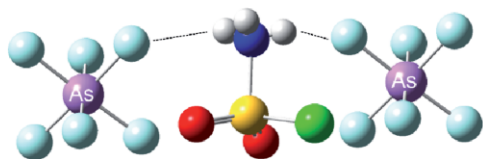
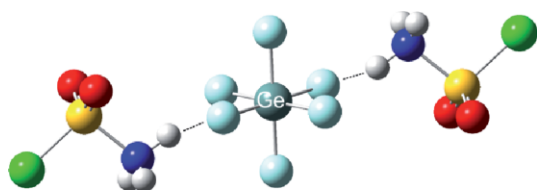
Quantum chemical calculations were carried out using the hybrid DFT method PBE1PBE employing the 6-311G++(3pd,3df) basis set. To support the vibrational spectroscopic investigations of the [ClSO₂NH₃]⁺ cation the frequencies were calculated in harmonic approximation. [ClSO₂NH₃]⁺ was calculated as free cation as well as HF adduct in the gas phase. Especially in case of the NH stretching vibrations the calculated frequencies of the HF adduct show a closer match to the observed frequencies summarized in Table 3. From Table 1 it can be assumed that the cationic structure is stronger influenced by [GeF₆]²⁻ than by [AsF₆]⁻ due to the closer match of the structural parameters for the calculated [ClSO₂NH₃]⁺ cation. This finding prompted us to a further theoretical investigation on the M06/aug-cc-pVTZ level of theory including all anions showing contacts to the cation. Therefore the units ([ClSO₂NH₃]⁺)₂[GeF₆]²⁻ and [ClSO₂NH₃]⁺[AsF₆]⁻ were calculated using the structural

Table 3. Observed vibrational frequencies /cm⁻¹ of ([ClSO₂NH₃)₂][GeF₆]²⁻, [ClSO₂NH₃][AsF₆]⁻ and calculated vibrational frequencies /cm⁻¹ of [ClSO₂NH₂]⁺·HF.

([ClSO ₂ NH ₃) ₂][GeF ₆] ²⁻		[ClSO ₂ NH ₃][AsF ₆] ⁻		[ClSO ₂ NH ₃] ⁺	[ClSO ₂ NH ₃] ⁺ ·HF	Assignment b)		
(a) IR	(d) Raman	(b) IR	(c) Raman	calcd. a)	calcd. a)			
3146 (m)			3171 (1)	3514 (145/22)	3519 (134/21)	v ₁₂	A''	v _{as} (NH ₂)
3048 (m)			3085 (4)	3492 (142/29)	3446 (134/48)	v ₁	A'	v _{iph} (NH ₃)
2828 (m)	2828 (5)	2828 (m)		3389 (138/93)	3163 (948/143)	v ₂	A'	v _{ooph} (NH ₃)
1726 (w)		1726 (w)				v _{5+v₈}		
1550 (w)				1612 (39/3)	1620 (30/2)	v ₁₃	A''	δ(NH ₂)
		1528 (m)	1528 (2)	1610 (35/3)	1608 (169/2)	v ₃	A'	δ(NH ₂)
1458 (w)	1455 (9)	1451 (m)	1460 (14)	1548 (165/7)	1541 (168/7)	v ₁₄	A''	v _{as} (SO ₂)
1426 (s)				1404 (162/0)	1450 (144/1)	v ₄	A'	δ(NH ₂)
1218 (w)	1215 (1)	1216 (m)	1207 (33)	1264 (122/21)	1262 (120/21)	v ₅	A'	v _s (SO ₂)
1193 (m)	1190 (27)	1184 (m)	1188 (10)					
1062 (vw)	1068 (17)	1066 (m)	1068 (24)	943(60/2)	1009 (39/2)	v ₆	A'	ρ(NH ₃)
1016 (w)			1012 (1)	936 (11/2)	973 (8/2)	v ₁₅	A''	τ(NH ₂)
562 (w)	560 (3)		562 (4)	596 (154/4)	618 (165/3)	v ₇	A'	δ(SO ₂)
				569 (90/10)	592 (87/13)	v ₈	A'	δ(ClSO)
485 (w)	486 (12)	484 (w)	484 (14)	448 (5/13)	469 (27/8)	v ₉	A'	v(SN)
	420 (100)		421 (100)	417 (2/7)	421 (1/9)	v ₁₀	A'	v(SCl)
438 (w)				351 (0/2)	361 (1/2)	v ₁₆	A''	δ(NSO)
				281 (6/2)	285 (27/2)	v ₁₇	A''	τ(SO ₂)
			198 (2)	233 (11/2)	273 (15/2)	v ₁₁	A'	δ(ClSN)
				162 (0/0)	162 (4/1)	v ₁₈	A''	δ(NH ₃)
			716 (14)					v[MF ₆] ⁻
596 (vs)	605 (15)	700 (s)	697 (9)					v[MF ₆] ⁻
			688 (4)					v[MF ₆] ⁻
		587 (m)	584 (33)					v[MF ₆] ⁻
		391 (m)	401 (5)					δ[MF ₆] ⁻
508 (w)	219 (2)		275 (6)					δ[MF ₆] ⁻
	126 (28)		248 (1)					δ[MF ₆] ⁻
								δ[MF ₆] ⁻

a) Calculated at the PBE1PBE/6-311G++(3pd,3df) level of theory. IR intensity in km·mol⁻¹ and Raman intensities in Å⁴·μ⁻¹. Abbreviations for IR intensities: v = very, s = strong, m = medium, w = weak. Raman activity is normalized, in which the most Raman active mode is normalized to be 100. b) M = Ge; As.

parameters observed in the crystal structures (Figure 6). A comparison of the calculated and the observed bond angles and bond lengths is given in Table 4. The quantum chemical calculations support the hypothesis that the cationic structure of [ClSO₂NH₃]⁺, especially the S–N bond, is remarkably influenced depending on the counterion.

**Figure 6.** Calculated units of ([ClSO₂NH₃)₂][GeF₆]²⁻ (top) and [ClSO₂NH₃][AsF₆]⁻ (bottom) on the M06/aug-cc-pVTZ level of theory.**Table 4.** Comparison of the observed and calculated bond lengths /Å and bond angles /° of ([ClSO₂NH₃)₂][GeF₆]²⁻ and [ClSO₂NH₃][AsF₆]⁻.

	([ClSO ₂ NH ₃) ₂][GeF ₆] ²⁻		[ClSO ₂ NH ₃][AsF ₆] ⁻	
	obsd.	calcd. a)	obsd.	calcd. a)
Bond length				
S1–O1	1.417(3)	1.421	1.406(2)	1.420
S1–N1	1.725(3)	1.733	1.765(3)	1.781
S1–Cl1	1.956(1)	2.023	1.945(1)	2.022
Bond angle				
O1–S1–O2	122.7(2)	124.4	123.6(1)	126.1
O1–S1–N1	107.2(2)	106.5	104.9(1)	107.5
O1–S1–Cl1	108.6(2)	109.1	111.0(1)	107.9
N1–S1–Cl1	99.6 (1)	97.9	100.3(1)	96.7

a) Calculated at the M06/aug-cc-pVTZ level of theory.

Conclusions

In the course of this study salts containing the [ClSO₂NH₃]⁺ cation were isolated for the first time using the two binary superacidic systems HF/GeF₄ and HF/AsF₅, respectively. ([ClSO₂NH₃)₂][GeF₆]²⁻ and [ClSO₂NH₃][AsF₆]⁻ are characterized by single-crystal X-ray structure analyses and low temperature vibrational spectroscopy supported by quantum chemical calculations. The protonation takes selectively place

at the nitrogen atom and leads in both cases to a significant elongation of the sulfur–nitrogen bond. It was found that depending on the counterion the sulfur–nitrogen bond is significantly different, 1.725(3) Å in **I** and 1.765(3) Å in **II**. Quantum chemical calculations involving all interacting anions confirm the significant influence of the counterions on the structure of the $[\text{ClSO}_2\text{NH}_3]^+$ cation.

Experimental Section

Caution! Avoid contact with any of these materials. HCl and HF are formed through hydrolysis of these compounds, respectively. HF burns skin and causes irreparable damage. Safety precautions should be taken when using and handling these materials.

Apparatus and Materials: All experimental work was carried out by using standard Schlenk techniques using a stainless-steel vacuum line. The reactions were performed in FEP/PFA reactors, which were closed with a stainless-steel valve. Data collections for **I** and **II** were performed with an Oxford Xcalibur3 diffractometer equipped with a Spellman generator (voltage 50 kV, current 40 mA) and a KappaCCD detector, operating with Mo- K_α radiation ($\lambda = 0.717 \text{ \AA}$). Data collection was performed at 173(2) K using the CrysAlisCCD software, the data reductions were carried out using CrysAlis RED software.^[16] The solution and refinement of the structure was performed with the programs SHELXL^[17] and SHELXS-97^[18] implemented in the WinGX software package^[19] and checked with the software PLATON.^[20] The absorption correction was achieved with the SCALE3 ABSPACK multi-scan method.^[21] Crystallographic data and structure refinement results are summarized in Table 5. Infrared spectra were recorded in

the range between 4000 cm^{-1} and 350 cm^{-1} at a temperature of $-196 \text{ }^\circ\text{C}$ with a Bruker Vertex 70V FTIR spectrometer. The Raman spectroscopic studies were carried out with a Bruker MultiRAM, which was equipped with a Nd:YAG laser ($\lambda = 1064 \text{ nm}$). The spectra were recorded in a range between 4000 cm^{-1} and 250 cm^{-1} . Quantum chemical calculations were carried out with the Gaussian 09 program package.^[22] All calculations were performed employing the hybrid method PBE1PBE and the base set 6-311++G(3df,3pd). ClSO_2NCO (Sigma Aldrich) was distilled several times prior to use. HCOOH was dried with B_2O_3 . GeF_4 and AsF_5 were synthesized from the elements and purified by fractionated distillation.

Synthesis of ClSO_2NH_2 : An amount of 3.59 g (25.3 mmol) ClSO_2NCO was stirred at $0 \text{ }^\circ\text{C}$ and dry HCOOH (1.16 g, 0.95 mL, 25.3 mmol) was added dropwise to the reaction vessel in a dry nitrogen atmosphere. A colorless solid was formed rapidly under gas formation.

Syntheses of $([\text{ClSO}_2\text{NH}_3]^+)_2[\text{GeF}_6]^{2-}$ (I**) and $[\text{ClSO}_2\text{NH}_3]^+[\text{AsF}_6]^-$ (**II**):** For the syntheses of **I** and **II** in the first step ClSO_2NH_2 was synthesized through the reaction of equimolar amounts (in a typical reaction each 1.0 mmol) of ClSO_2NCO and HCOOH were condensed in an FEP reactor and allowed to warm up to $0 \text{ }^\circ\text{C}$. The formed colorless solid was dried overnight in a dynamic vacuum. In the second step an excess of HF followed by 3 equiv. of GeF_4 (for **I**) or AsF_5 (for **II**) were condensed at $-196 \text{ }^\circ\text{C}$ into the FEP reaction vessel. The mixture was allowed to warm up to $-40 \text{ }^\circ\text{C}$ and was stored for 72 h at this temperature. Colorless crystals precipitated during this time. Excess GeF_4 and AsF_6^- , respectively, as well as HF were removed in dynamic vacuum at $-78 \text{ }^\circ\text{C}$ for a time period of 14 h.

Crystallographic data (excluding structure factors) for the structures in this paper have been deposited with the Cambridge Crystallographic

Table 5. Crystal data and structure refinement for $([\text{ClSO}_2\text{NH}_3]^+)_2[\text{GeF}_6]^{2-}$ and $[\text{ClSO}_2\text{NH}_3]^+[\text{AsF}_6]^-$.

	$([\text{ClSO}_2\text{NH}_3]^+)_2[\text{GeF}_6]^{2-}$	$[\text{ClSO}_2\text{NH}_3]^+[\text{AsF}_6]^-$	ClSO_2NH_2
M_r	419.68	305.46	115.54
T / K	173(3)	123(2)	173(2)
Crystal system	triclinic	monoclinic	orthorhombic
Space Group	$P\bar{1}$	$P2_1/n$	$Pmc2$
$a / \text{\AA}$	5.5686(4)	4.9653(3)	7.7652(6)
$b / \text{\AA}$	5.5718(5)	7.4256(4)	5.7998(4)
$c / \text{\AA}$	10.883(1)	19.3595(1)	8.7627(6)
$\alpha / ^\circ$	82.637(8)	90	90
$\beta / ^\circ$	86.425(7)	90.741(5)	90
$\gamma / ^\circ$	61.069(9)	90	90
$V / \text{\AA}^3$	293.09(4)	713.73(7)	394.64(5)
Z	1	4	4
$\rho_{\text{calcd}} / \text{g}\cdot\text{cm}^{-3}$	2.378	2.843	1.945
μ / mm^{-1}	3.508	5.507	1.313
$\lambda(\text{Mo-}K_\alpha) / \text{\AA}$	0.71073	0.71073	0.71073
$F(000)$	204	584	232
hkl range	$-6:6; -6:6; -13:10$	$-6:6; -10:10; -26:25$	$-6:10; -7:7; -11:9$
Refl. measured	2160	6331	1778
Refl. unique	1181	1920	871
R_{int}	0.0194	0.0337	0.0293
Parameters	91	121	63
$R(F)/wR(F^2)$ ^{a)} (all reflexions)	0.0290/0.0706	0.0325/0.0606	0.0334/ 0.0469
Weighting scheme ^{b)}	0.0251/0.5437	0.0221/0.1433	0.0121/0.0000
$S(\text{GoF})$ ^{c)}	1.096	1.093	1.020
Residual density $/e\cdot\text{\AA}^{-3}$	0.559/-0.576	0.416/-0.793	0.323/-0.271
Device type	Oxford XCalibur	Oxford XCalibur	Oxford XCalibur
Solution / refinement	SHELXS-97 [18] / SHELXL-97 [17]	SHELXS-97 [18] / SHELXL-97 [17]	SHELXS-97 [18] / SHELXL-97 [17]

a) $R_1 = \sum |F_o| - |F_c| / \sum |F_o|$. b) $wR_2 = [\sum (w(F_o^2 - F_c^2)^2) / \sum (w(F_o^2)^2)]^{1/2}$; $w = [\sigma_c^2(F_o^2) + (xP)^2 + yP]^{-1}$; $P = (F_o^2 + 2F_c^2) / 3$. c) $\text{GoF} = \{\sum [w(F_o^2 - F_c^2)^2] / (n - p)\}^{1/2}$ (n = number of reflexions; p = total number of parameters).

Data Centre, CCDC, 12 Union Road, Cambridge CB21EZ, UK. Copies of the data can be obtained free of charge on quoting the depository numbers CCDC-1574006 {for $[(\text{ClSO}_2\text{NH}_3)^+]_2[\text{GeF}_6]^{2-}$ }, CCDC-1574004 {for $[\text{ClSO}_2\text{NH}_3]^+[\text{AsF}_6]^-$ }, and CCDC-1574005 {for ClSO_2NH_2 } (Fax: +44-1223-336-033; E-Mail: deposit@ccdc.cam.ac.uk, <http://www.ccdc.cam.ac.uk>).

Acknowledgements

Financial support of this work by the Ludwig-Maximilian-University of Munich (LMU), by the Deutsche Forschungsgemeinschaft (DFG) and the F-Select GmbH is gratefully acknowledged.

Keywords: Protonation; Chlorosulfonamide; Superacid chemistry; Single-crystal structure; Vibrational spectroscopy

References

- [1] R. Graf, *Chem. Ber.* **1959**, *92*, 509–513.
- [2] W. Schneider, G. Kessler, H. A. Lehmann, *Z. Anorg. Allg. Chem.* **1968**, *356*, 239–243.
- [3] R. M. S. Álvarez, E. H. Cutín, H. G. Mack, C. O. D. Védova, *J. Mol. Struct.* **1998**, *440*, 213–219.
- [4] H. M. Badawi, *Spectrochim. Acta Part A* **2006**, *65*, 453–458.
- [5] F. M. Menger, L. Mandell, *J. Am. Chem. Soc.* **1967**, *89*, 4424–4426.
- [6] R. G. Laughlin, *J. Am. Chem. Soc.* **1967**, *89*, 4268–4271.
- [7] A. Bagnò, G. Scorrano, *J. Phys. Chem.* **1996**, *100*, 1545–1553.
- [8] B. A. Shainyan, N. N. Chipanina, L. P. Oznobikhina, *J. Phys. Org. Chem.* **2012**, *25*, 738–747.
- [9] D. Leitz, M. Hopfinger, K. Stierstorfer, J. Axhausen, A. Kornath, *Z. Anorg. Allg. Chem.* **2017**, *643*, 1202–1207.
- [10] T. Soltner, PhD Thesis **2011**.
- [11] M. Hopfinger, K. Lux, A. Kornath, *ChemPlusChem.* **2012**, *77*, 476–481.
- [12] R. Appel, G. Berger, *Chem. Ber.* **1958**, *91*, 1339–1341.
- [13] D. Mootz, A. Merschenz-Quack, *Acta Crystallogr., Sect. C* **1988**, *44*, 924–925.
- [14] R. Minkwitz, P. Garzarek, F. Neikes, A. Kornath, H. Preut, *Z. Anorg. Allg. Chem.* **1997**, *623*, 333–339.
- [15] E. Hansen, E. Limé, P.-O. Norrby, O. Wiest, *J. Phys. Chem.* **2016**, *A120*, 3677–3682.
- [16] CrysAlisRED, Version 1.171.35.11 (release 16–05–2011 CrysAlis 171.NET), Oxford Diffraction Ltd., UK, **2011**.
- [17] G. M. Sheldrick, *SHELXL-97*, Program for the Refinement of Crystal Structures, University of Göttingen, Germany, **1997**.
- [18] G. M. Sheldrick, *SHELXS-97*, Program for Crystal Structure Solution, University of Göttingen, Germany, **1997**.
- [19] L. Farrugia, *J. Appl. Crystallogr.* **1999**, *32*, 837–838.
- [20] A. L. Spek, *PLATON*, A Multipurpose Crystallographic Tool, U. Utrecht University, The Netherlands, 1999., **1999**.
- [21] SCALE3 ABSPACK, An Oxford Diffraction Program, O. Diffraction, Ltd., UK, **2005**.
- [22] H. B. Schlegel, G. W. Trucks, M. J. Frisch, G. E. Scuseria, M. A. Robb, J. R. Cheeseman, J. A. Montgomery, T. V. K. N. Kudin Jr., J. C. Burant, J. M. Millam, S. S. Iyengar, J. Tomasi, V. Barone, B. Mennucci, M. Cossi, G. Scalmani, N. Rega, G. A. Petersson, H. Nakatsuji, M. Hada, M. Ehara, K. Toyota, R. Fukuda, J. Hasegawa, M. Ishida, T. Nakajima, Y. Honda, O. Kitao, H. Nakai, M. Klene, X. Li, J. E. Knox, H. P. Hratchian, J. B. Cross, C. Adamo, J. Jaramillo, R. Gomperts, R. E. Stratmann, O. Yazyev, A. J. Austin, R. Cammi, C. Pomelli, J. W. Ochterski, P. Y. Ayala, K. Morokuma, G. A. Voth, P. Salvador, J. J. Dannenberg, V. G. Zakrzewski, S. Dapprich, A. D. Daniels, M. C. Strain, O. Farkas, D. K. Malick, A. D. Rabuck, K. Raghavachari, J. B. Foresman, J. V. Ortiz, Q. Cui, A. G. Baboul, S. Clifford, J. Cioslowski, B. B. Stefanov, G. Liu, A. Liashenko, P. Piskorz, I. Komaromi, R. L. Martin, D. J. Fox, T. Keith, M. A. Al-Laham, C. Y. Peng, A. Nanayakkara, M. Challacombe, P. M. W. Gill, B. Johnson, W. Chen, M. W. Wong, C. Gonzalez, J. A. Pople, Gaussian, Inc. **2003**, Pittsburgh PA.

Received: February 25, 2018

Published online: May 6, 2018

Crystal Structure and Vibrational Spectra of ClSO₂NHC(O)F

Dominik Leitz,^[a] Karin Stierstorfer,^[a] and Andreas Kornath*^[a]

Abstract. The reaction of chlorosulfonyl isocyanate (ClSO₂NCO) with anhydrous hydrogen fluoride (*a*HF) leads to the formation of ClSO₂NHC(O)F. The title compound with a melting point of −38 °C is characterized by vibrational spectroscopy and a single crystal structure

analysis. It crystallizes in the tetragonal space group *I*₄/*a* with 16 formula units per unit cell. *a* = 11.1115(2) Å, *c* = 16.5654(6) Å. The experimental data are supported by quantum-chemical calculations on the PBE1PBE/6-311G(3pd,3df) level of theory.

Introduction

Chlorosulfonyl isocyanate (CSI) is described to be probably the most reactive isocyanate compound,^[1] which was first synthesized by *Graf*.^[2] CSI is a widely used reagent for the synthesis of a large variety of organic compounds.^[1] At high temperatures CSI reacts with anhydrous hydrogen fluoride (*a*HF) forming FSO₂NCO,^[3] whereas at mild conditions organic isocyanates are known to react with hydrogen fluoride under the formation of fluorocarbamoyl derivatives in good yields.^[4] In this work we present the investigation of the behavior of CSI in *a*HF at ambient temperature, which has to the best of our knowledge not been reported in literature so far.

Results and Discussion

At room temperature the reaction of CSI with an excess of *a*HF leads to the formation of ClSO₂NHC(O)F according to the following Equation (1):



An excess of *a*HF was used since it serves as both, reagent and solvent. The two compounds were condensed into the reaction vessel and allowed to warm up to room temperature. A two-phase mixture was formed disappearing instantly after stirring. The excess of *a*HF was removed at −78 °C in dynamic vacuum leaving a solid, which melts at −38 °C. At room temperature ClSO₂NH(O)F is a colorless liquid and can easily be handled in an inert gas atmosphere.

Crystal Structure

ClSO₂NHC(O)F crystallizes in the tetragonal space group *I*₄/*a* with 16 formula units in the unit cell. In Figure 1 the asymmetric unit is shown. The bond lengths and bond angles are summarized in Table 1.

* Prof. Dr. A. Kornath
E-Mail: andreas.kornath@cup.uni-muenchen.de

[a] Department Chemie
Ludwig-Maximilians Universität München
Butenandtstr. 5–13(D)
81377 Munich, Germany

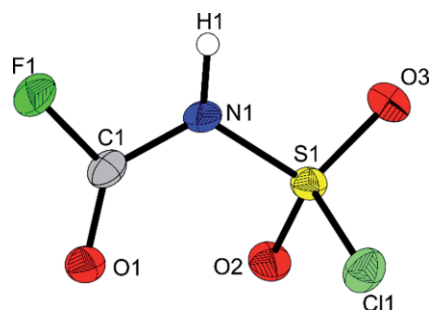


Figure 1. Asymmetric unit of ClSO₂NHC(O)F (thermal ellipsoids with 50% probability).

Table 1. Bond lengths /Å and angles /° of ClSO₂NHC(O)F.

Bond lengths /Å			
S1–Cl1	1.996(1)	N1–C1	1.359(2)
S1–O2	1.408(1)	C1–F1	1.324(2)
S1–O3	1.410(1)	C1–O1	1.182(2)
S1–N1	1.642(2)		
Bond angles /°			
O2–S1–O3	123.1(1)	N1–S1–Cl1	102.7(1)
O2–S1–N1	108.6(1)	C1–N1–S1	122.2(1)
O3–S1–N1	106.2(1)	O1–C1–F1	121.7(2)
O2–S1–Cl1	106.7(1)	O1–C1–N1	128.9(2)
O3–S1–Cl1	107.7(1)	F1–C1–N1	109.4(2)

The sulfur atom is coordinated in a distorted tetrahedral manner with the O2–S1–O3 bond angle of 123.1(1)° comparable to the corresponding bond angle in SO₂Cl₂.^[5] All other bond angles, including the sulfur atom are in the range slightly below the ideal tetrahedron angle of 109.5°. With exception of the atoms O2 and Cl1 all atoms are in a plane wherefore the sum of the bond angles around C1 and N1 is approximately 360°. The S–Cl bond length of 1.996(1) Å is slightly shorter than the S–Cl bond in SO₂Cl₂ [1.979(1) Å].^[5] The S–N bond of 1.642(2) Å is significantly shorter than reported for typical S–N bonds [1.74 Å].^[6] The shortened S–N bond can be explained by negative hyperconjugation, where electron density of the nitrogen lone pair is donated to the σ*(S–N) and σ*(S–O) orbitals.^[7] The S–O bonds of 1.408(1) Å and 1.410(1) Å are comparable to the S–O bonds in SO₂ClF.^[5] The

C–N bond of 1.359(2) Å is between a formal single and double bond.^[8] The bond lengths and angles of the fluorocarbonyl moiety are comparable to the corresponding values observed for H₂NCOF.^[9]

The ClSO₂NHC(O)F molecules form helices along the *c* axis are held together via medium strong N1(–H1)⋯O1 hydrogen bonds with donor-acceptor distances of 2.947(1) Å as shown in Figure 2.

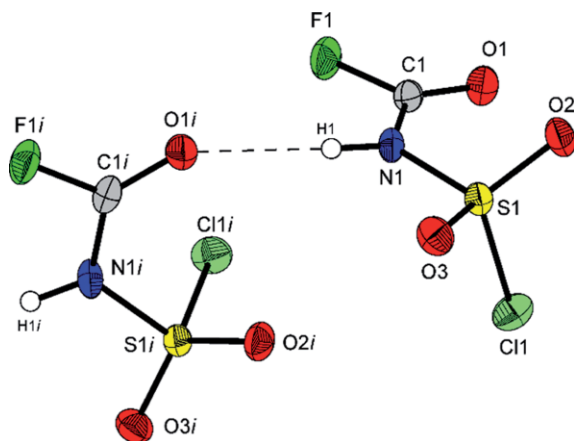


Figure 2. Contact of the ClSO₂NHC(O)F molecules (thermal ellipsoids with 50% probability).

Vibrational Spectroscopy

Figure 3 illustrates the vibrational spectra of CSI and ClSO₂NHC(O)F. The experimentally observed and quantum chemically calculated frequencies together with their assignments are summarized in Table 2. For ClSO₂NHC(O)F with C₁ symmetry 21 vibrational modes are expected. The NH stretching mode occurs at 3216 cm^{–1} (Ra) and 3215 cm^{–1} (IR). At 1805 cm^{–1} (Ra) and 1806 cm^{–1} (IR) the CO stretching mode is detected, whereas in CSI the CO vibration is part of the

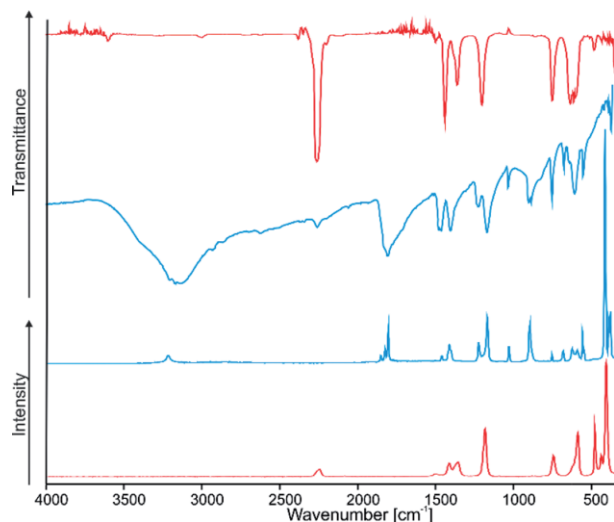


Figure 3. Vibrational spectra of ClSO₂NCO (red) and ClSO₂NHC(O)F (blue).

antisymmetric and symmetric NCO vibrations occurring at 2250 cm^{–1} and 1360 cm^{–1}.^[10] The SO₂ stretching modes occur at 1462 cm^{–1} (IR), 1461 cm^{–1} (Ra), and 1168 cm^{–1} (IR/Ra), but are blue-shifted by approximately 22 cm^{–1} and 31 cm^{–1}, respectively, compared to CSI.^[10] At 900 cm^{–1} (IR) and 897 cm^{–1} (Ra) the CF stretching vibration is detected. Besides the occurrence of the NH stretching, this can be considered as confirmation for the formation of ClSO₂NHC(O)F. The SCl stretching vibration is observed at 422 cm^{–1} (IR) and 415 cm^{–1} (Ra) and it is slightly blue-shifted compared to CSI.^[10]

Table 2. Experimental vibrational frequencies^{a)}/cm^{–1} of ClSO₂NHC(O)F and calculated species.

IR	Raman	Calcd. ^{b)} (IR/Raman)	Assignment
3206 (s)	3216 (3)	3626 (113/53)	v(NH)
1806 (m)	1805 (3)	1939 (626/38)	v(CO)
1462 (m)	1461 (14)	1501 (239/7)	v _{as} (SO ₂)
1401 (m)	1413 (8)	1389 (65/3)	δ(NH)
1223 (w)	1224 (9)	1321 (260/2)	v(CN)
1168 (m)	1169 (19)	1232 (230/19)	v _s (SO ₂)
1033 (w)	1030 (7)	1013 (116/1)	v(SN)
900 (m)	897 (17)	860 (49/8)	v(CF)
751 (m)	754 (4)	772 (36/0)	δ(NCO)
675 (w)	682 (5)	682 (7/3)	δ(OCF)
	624 (6)	614 (273/5)	δ(SO ₂)
606 (m)	592 (5)	570 (98/2)	ω(SO ₂)
552 (w)	558 (14)	543 (23/1)	δ(NH)
422 (w)	415 (100)	410 (4/16)	v(SCl)
		388 (22)	δ(NCO)
		378 (17)	ω(SO ₂)
		309 (18)	τ(SO ₂)
		300 (5)	δ(CISN)
		199 (11)	ρ(SO ₂)
		95 (29)	τ(CNF)
		64 (1/1)	τ(COF)

a) Abbreviations for IR intensities: v = very, s = strong, m = medium, w = weak. Raman activity is stated on a scale of 1 to 100. b) Calculated at the PBE1PBE/6-311G(3df,3dp) level of theory. IR intensity in km·mol^{–1} and Raman intensities in Å⁴·μ^{–1}.

Theoretical Calculations

As support for the experimental data of ClSO₂NHC(O)F a quantum chemical calculation on the PBE1PBE/6-311G(3pd,3df) level of theory was performed. Figure 4 shows a comparison of the experimental solid-state and calculated gas-phase structure of ClSO₂NHC(O)F containing the bond lengths.

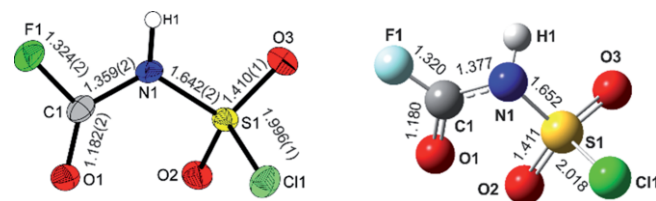


Figure 4. Comparison of the experimental (left) and the calculated (right) structure of ClSO₂NHC(O)F.

The calculated and experimentally observed geometric parameters are in satisfying agreement. As expected, the calculated bond lengths are slightly longer than the bond lengths in the solid state except for the C1–O1 bond length, which is slightly underestimated, whereas the C1–F1 is slightly overestimated, which can be explained by solid-state interactions.

Conclusions

This work shows that chlorosulfonyl isocyanate (CSI) selectively undergoes an HF addition at room temperature. The formed novel compound ClSO₂NHC(O)F is characterized by its single-crystal X-ray structure as well as low temperature vibrational spectra. Due to its multifunctionality, this molecule is a promising candidate as starting material for a large number of syntheses providing a high synthetic potential.

Experimental Section

Caution! The hydrolysis of the investigated compounds causes the formation of HF and HCl, respectively. Safety precautions should be taken while handling these compounds.

Apparatus and Materials: Chlorosulfonylisocyanate (99%, Sigma Aldrich) was triple distilled and anhydrous hydrogen fluoride (99%, Linde) was dried with fluorine for two weeks prior to use. All reactions during the course of this study were performed employing standard Schlenk technique using a stainless steel vacuum line. The reactions were performed in FEP/PFA reaction vessels, which were closed with stainless steel valves. Before starting the experiments both, stainless steel vacuum line and reaction vessels were dried with fluorine. Low temperature Raman spectra were recorded with a Bruker MultiRAM FT-Raman spectrometer equipped with a Nd:YAG laser ($\lambda = 1064$ nm) at -196 °C with a laser excitation up to 1000 mW in the range from 350 cm^{-1} to 4000 cm^{-1} . Low temperature IR measurements were performed with a Bruker Vertex-80V-FT-IR spectrometer. For the visualization of the spectra the software Bruker OPUS 6.5 was employed. The single-crystal structure X-ray analysis was carried out with an Oxford Xcalibur3 diffractometer equipped with a Spellman generator (50 kV, 40 mA, using Mo radiation ($\lambda = 0.7107$ Å)) and a Kappa CCD detector at a temperature of 173 K. For the data collection the CrysAlis CCD^[11] program and for the data reduction the program CrysAlis RED^[12] were employed. The programs SHELXS^[13] and SHELXL-97^[14] implemented in the WingGX^[15] software package were used for the solution and the refinement of the structure, which was finally checked with the PLATON software.^[16] The absorption correction was carried out by employing the SCALE3 APSPACK multi-scan method.^[17] For quantum-chemical calculations the Gaussian09 package^[18] was employed using the PBE1PBE density functional approach with the basis set 6-311G(3pd, 3df). Crystal data and structure refinement for ClSO₂NHC(O)F are listed in Table 3.

Crystallographic data (excluding structure factors) for the structure in this paper have been deposited with the Cambridge Crystallographic Data Centre, CCDC, 12 Union Road, Cambridge CB21EZ, UK. Copies of the data can be obtained free of charge on quoting the depository number CCDC-1586028 (Fax: +44-1223-336-033; E-Mail: deposit@ccdc.cam.ac.uk, http://www.ccdc.cam.ac.uk).

Synthesis of ClSO₂NHC(O)F: In a typical experiment ClSO₂NCO (125 mg, 1.00 mmol) followed by an excess of aHF (ca. 2 mL) were

Table 3. Crystal data and structure refinement for ClSO₂NHC(O)F.

	ClSO ₂ NHCOF
M_r	161.54
Crystal system	tetragonal
Space group	$I4_1/a$
a /Å	11.1115(2)
b /Å	11.1115(2)
c /Å	16.5654(6)
V /Å ³	2045.25(9)
Z	16
ρ_{calcd} /g·cm ⁻³	2.098
μ /mm ⁻¹	1.088
$\lambda(\text{Mo-K}\alpha)$ /Å	0.71073
$F(000)$	1280
T /K	173(2)
hkl range	$-13:13; -11:13; -17:20$
Reflections measured	1041
Reflections unique	929
R_{int}	0.0261
Parameters	74
$R(F)/wR(F^2)$ ^{a)} (all reflexions)	0.0279/0.0611
Weighting scheme ^{b)}	0.0270/1.4003
$S(\text{GoF})$ ^{c)}	1.098
Residual density /e·Å ⁻³	0.274 / -0.313
Device type	Oxford XCalibur
Solution / refinement	SHELXL-97 [14]

a) $R_1 = \frac{\sum |F_o| - |F_c|}{\sum |F_o|}$; b) $wR_2 = \frac{[\sum [w(F_o^2 - F_c^2)^2]]^{1/2}}{[\sum w(F_o^2)]^{1/2}}$; $w = [\sigma_c^2(F_o^2) + (\sigma_P)^2 + yP]^{-1}$; $P = (F_o^2 + 2F_c^2)/3$; c) $\text{GoF} = \{[\sum [w(F_o^2 - F_c^2)^2]/(n-p)]^{1/2}$ (n = number of reflexions; p = total number of parameters).

condensed in a reactor (FEP tube) at -196 °C. Afterwards, the mixture was allowed to warm up to room temperature. At ambient temperature a two-phase mixture was obtained, which disappears after stirring. The excess of aHF was removed within 14 h at -78 °C. A colorless crystalline solid remained, which melts at around -38 °C.

Acknowledgements

Financial support of this work by the Ludwig-Maximilian-University of Munich (LMU), the Deutsche Forschungsgemeinschaft (DFG) and the F-Select GmbH is gratefully acknowledged.

Keywords: Chlorosulfonyl isocyanate; HF addition; Sulfonyl-carbamate; Vibrational spectroscopy; Single crystal structure X-ray diffraction

References

- [1] W. A. Szabo, *Aldrichimica Acta* **1977**, *10*, 23–29.
- [2] R. Graf, *Chem. Ber.* **1956**, *89*, 1071–1079.
- [3] H. Ulrich, *Chem. Rev.* **1965**, *65*, 369–376.
- [4] a) G. D. Buckley, H. A. Piggott, A. J. E. Welch, *J. Chem. Soc.* **1945**, 864–865; b) G. A. Olah, J. T. Welch, Y. D. Vankar, M. Nojima, I. Kerekes, J. A. Olah, *J. Org. Chem.* **1979**, *44*, 3872–3881.
- [5] D. Mootz, A. Merschenz-Quack, *Acta Crystallogr., Sect. C* **1988**, *44*, 924–925.
- [6] R. Minkwitz, P. Garzarek, F. Neikes, A. Kornath, H. Preut, *Z. Anorg. Allg. Chem.* **1997**, *623*, 333–339.
- [7] E. Hansen, E. Limé, P.-O. Norrby, O. Wiest, *J. Phys. Chem. A* **2016**, *120*, 3677–3682.
- [8] F. H. Allen, O. Kennard, D. G. Watson, L. Brammer, A. G. Orpen, R. Taylor, *J. Chem. Soc.* **1987**, 1–19.

- [9] A. F. Baxter, K. O. Christe, R. Haiges, *Struct. Chem.* **2017**, *28*, 303–307.
- [10] a) R. M. S. Alvarez, E. H. Cutin, C. O. Della Védova, *Spectrochim. Acta Part A* **1995**, *51*, 555–561; b) J. R. Durig, L. Zhou, T. K. Gounev, G. A. Guirgis, *Spectrochim. Acta Part A* **1997**, *53*, 1581–1593.
- [11] *CrysAlisCCD*, Version 1.171.35.11 (release 16–05–2011 CrysAlis 171.NET), Oxford Diffraction Ltd, UK, **2001**.
- [12] *CrysAlisRED*, Version 1.171.35.11 (release 16–05–2011 CrysAlis 171.NET), Oxford Diffraction Ltd., UK, **2011**.
- [13] G. M. Sheldrick, *SHELXS-97*, Program for Crystal Structure Solution, University of Göttingen, Germany, **1997**.
- [14] G. M. Sheldrick, *SHELXL-97*, Program for the Refinement of Crystal Structures, University of Göttingen, Germany, **1997**.
- [15] L. Farrugia, *J. Appl. Crystallogr.* **1999**, *32*, 837–838.
- [16] A. L. Spek, *PLATON*, A Multipurpose Crystallographic Tool, U. Utrecht University, The Netherlands, **1999**.
- [17] SCALE3 ABSPACK, An Oxford Diffraction Program, O. Diffraction, Ltd., UK, **2005**.
- [18] M. J. Frisch, G. W. Trucks, H. B. Schlegel, G. E. Scuseria, M. A. Robb, J. R. Cheeseman, J. A. Montgomery Jr., T. Vreven, K. N. Kudin, J. C. Burant, J. M. Millam, S. S. Iyengar, J. Tomasi, V. Barone, B. Mennucci, M. Cossi, G. Scalmani, N. Rega, G. A. Petersson, H. Nakatsuji, M. Hada, M. Ehara, K. Toyota, R. Fukuda, J. Hasegawa, M. Ishida, T. Nakajima, Y. Honda, O. Kitao, H. Nakai, M. Klene, X. Li, J. E. Knox, H. P. Hratchian, J. B. Cross, C. Adamo, J. Jaramillo, R. Gomperts, R. E. Stratmann, O. Yazyev, A. J. Austin, R. Cammi, C. Pomelli, J. W. Ochterski, P. Y. Ayala, K. Morokuma, G. A. Voth, P. Salvador, J. J. Dannenberg, V. G. Zakrzewski, S. Dapprich, A. D. Daniels, M. C. Strain, O. Farkas, D. K. Malick, A. D. Rabuck, K. Raghavachari, J. B. Foresman, J. V. Ortiz, Q. Cui, A. G. Baboul, S. Clifford, J. Cioslowski, B. B. Stefanov, G. Liu, A. Liashenko, P. Piskorz, I. Komaromi, R. L. Martin, D. J. Fox, T. Keith, M. A. Al-Laham, C. Y. Peng, A. Nanayakkara, M. Challacombe, P. M. W. Gill, B. Johnson, W. Chen, M. W. Wong, C. Gonzalez, J. A. Pople, *Gaussian, Inc.* **2003**, Pittsburgh PA.

Received: March 8, 2018

Published online: April 17, 2018

CHEMISTRY

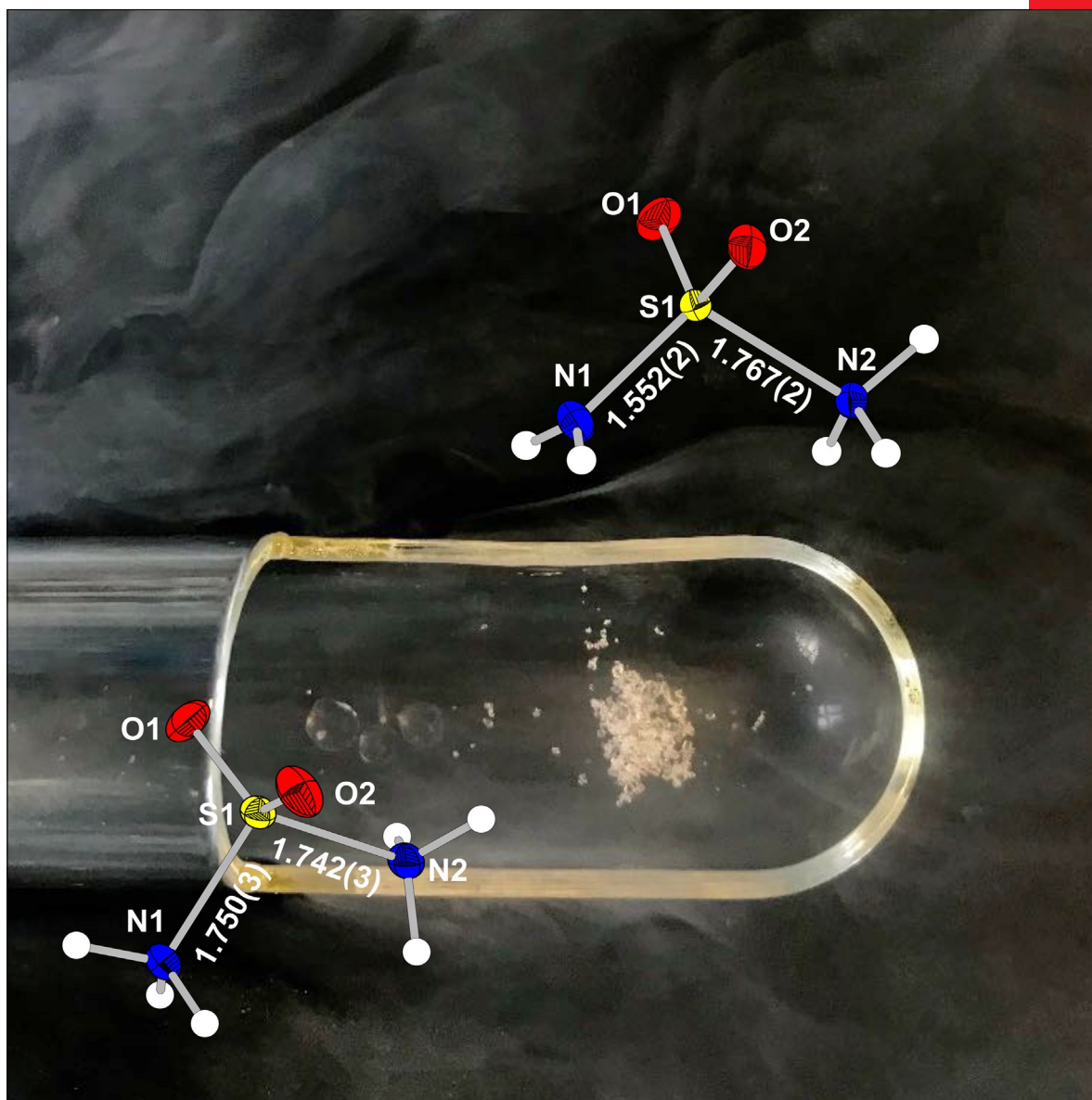
A European Journal

www.chemeurj.org

A Journal of



2018-24/59



Cover Feature:

A. J. Kornath et al.

Tuning the Anomeric Effect in Sulfamide with Superacids

Supported by



WILEY-VCH

The cover picture shows the structures of the mono- and diprotonated species of sulfamide, $[\text{H}_2\text{NSO}_2\text{NH}_3]^+$ and $[\text{H}_3\text{NSO}_2\text{NH}_3]^{2+}$, respectively. The isolation of salts containing these cations succeeded by the utilization of the superacidic systems HF/BF₃, XF/SbF₅ and XF/AsF₅ (X=H, D). In the background of the cover picture, a low-temperature device for single-crystal mounting loaded with a crystalline sample of $[\text{H}_2\text{NSO}_2\text{NH}_3]^+[\text{BF}_4]^-$ is shown. The structure analyses revealed remarkable changes, especially for the sulfur-nitrogen bond lengths. More information can be found in the Full Paper by A. J. Kornath et al. on page 15825.

Vibrational Spectroscopy

Tuning the Anomeric Effect in Sulfamide with Superacids

Dominik Leitz, Marie C. Bayer, Yvonne Morgenstern, Florian Zischka, and
Andreas J. Kornath*^[a]

Abstract: This study shows that the anomeric effect (negative hyperconjugation) that arises in sulfamide, as a result of the relatively short S–N bonds, can be tuned by the utilization of superacidic media. Sulfamide was reacted in binary superacidic systems XF/MF₅ (M = As, Sb; X = H, D) and HF/BF₃. The colorless salts formed, [X₂NSO₂NX₃]⁺[MF₆][−] and [H₂NSO₂NH₃]⁺[BF₄][−] were characterized by low-temperature vibrational spectroscopy. In the case of [H₂NSO₂NH₃]⁺[BF₄][−], a single crystal X-ray diffraction study was performed. The salt crystallizes in the monoclinic space group *P*2₁/*c* with

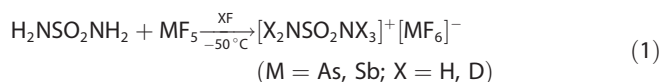
four formula units per unit cell. An exclusive *N,N'*-diprotonation was observed in the superacidic system HF/SbF₅ when using several equivalents of the Lewis acid. Low-temperature vibrational spectra as well as a single-crystal X-ray structure of [H₃NSO₂NH₃]²⁺·2[SbF₆][−]·2HF are reported. The salt crystallizes in the orthorhombic space group *Pna*2₁ with four formula units per unit cell. Upon mono- or diprotonation of sulfamide, remarkable structural changes of the sulfur–nitrogen bond lengths were observed. Herein, these changes are discussed together with quantum chemical calculations.

Introduction

Since the first synthesis of sulfamide by Regnault,^[1] research on this eponymous compound class has made major advances, driven especially by their biological activity.^[2–4] Among other properties, their inhibitory potential is of particular interest. Wiest et al. attributed this property to sulfamides' imitating a tetrahedral intermediate state.^[5] The authors reported quantum chemical studies on sulfamide giving a reason for its unique properties and rigidity.^[5] The latter is explained by an anomeric effect, whereby electron density from the nitrogen lone pairs is donated to the σ*(S–O) and σ*(S–N), providing 37 kJ mol^{−1} of stabilization energy.^[5] This result can also be considered as an explanation for the relatively short S–N bonds of 1.627(1) Å observed in the crystal structure of H₂NSO₂NH₂.^[6] Given that the anomeric effect is initiated by the donation of electron density of the nitrogen lone pairs, one could assume that this effect can be abolished by an *N*-protonation leading to the [H₂NSO₂NH₃]⁺ cation. This species has already been observed in highly acidic media by NMR spectroscopy under aqueous conditions.^[7] However, structural parameters are still unknown. Therefore, we were interested in isolating and structurally characterizing salts containing the [H₂NSO₂NH₃]⁺ cation. Herein, we report our investigations on sulfamide in binary superacidic systems.

Results and Discussion

Sulfamide was reacted in the superacidic solutions XF/MF₅ (X = D, H; M = As, Sb) and HF/BF₃ [Eqs. (1) and (2)]. In the case of an equimolar amount of the Lewis acids, salts containing the [H₂NSO₂NH₃]⁺ cation are formed. By employing an excess of the Lewis acids (BF₃, AsF₅, or SbF₅) with respect to sulfamide only in the case of SbF₅ was an *N,N'*-diprotonation achieved leading to the formation of [H₃NSO₂NH₃]²⁺·2[SbF₆][−] [Eq. (3)].



Anhydrous hydrogen fluoride (*a*HF) serves as reagent as well as a solvent. The excess was removed in a dynamic vacuum at −78 °C within 14 h. [X₂NSO₂NX₃]⁺[MF₆][−] (M = As, Sb; X = H, D) are hydrolysis-sensitive colorless salts and decompose above 30 °C. [H₂NSO₂NH₃]⁺[BF₄][−] is even stable towards moisture and showed no significant decomposition up to 60 °C.

Vibrational spectra of the [X₂NSO₂NX₃]⁺ salts

The low-temperature vibrational spectra are shown in Figure 1. Selected experimental vibrational frequencies of [X₂NSO₂NX₃]⁺[AsF₆][−] (X = H, D) and [H₂NSO₂NH₃]⁺[BF₄][−] and the calculated frequencies of [X₂NSO₂NX₃]⁺·5HF (X = H, D) are summarized in Table 1. The complete table is given in the Supporting Information (Table S1). For the [X₂NSO₂NX₃]⁺ cation with C_s symmetry, 24 vibrations are expected, showing both Raman and IR activi-

[a] D. Leitz, M. C. Bayer, Y. Morgenstern, F. Zischka, Prof. Dr. A. J. Kornath
Department Chemie
Ludwig-Maximilians-Universität München
Butenandtstr. 5–13(D), 81377 Munich (Germany)
E-mail: andreas.kornath@cup.uni-muenchen.de

Supporting information and the ORCID identification number(s) for the author(s) of this article can be found under:
<https://doi.org/10.1002/chem.201804009>

Table 1. Selected experimental vibrational frequencies (in cm^{-1}) of $[\text{H}_2\text{NSO}_2\text{NH}_3]^+[\text{AsF}_6]^-$, $[\text{H}_2\text{NSO}_2\text{NH}_3]^+[\text{BF}_4]^-$, and $[\text{D}_2\text{NSO}_2\text{ND}_3]^+[\text{AsF}_6]^-$ and calculated vibrational frequencies (in cm^{-1}) of $[\text{H}_2\text{NSO}_2\text{NH}_3]^+\cdot 5\text{HF}$ and $[\text{D}_2\text{NSO}_2\text{ND}_3]^+\cdot 5\text{HF}$.

$[\text{H}_2\text{NSO}_2\text{NH}_3]^+[\text{AsF}_6]^-$		$[\text{H}_2\text{NSO}_2\text{NH}_3]^+[\text{BF}_4]^-$		$[\text{H}_2\text{NSO}_2\text{NH}_3]^+\cdot 5\text{HF}$	$[\text{D}_2\text{NSO}_2\text{ND}_3]^+[\text{AsF}_6]^-$		$[\text{D}_2\text{NSO}_2\text{ND}_3]^+\cdot 5\text{HF}$	Assignment ^[b]		
IR	Raman	IR	Raman	calcd ^[a] (IR/Raman)	IR	Raman	calcd ^[a] (IR/Raman)			
3376 (m)	3384 (1)			3582 (650/69)	2545 (m)	2548 (8)	2662 (336/33)	ν_{15}	A''	$\nu_{\text{as}}(\text{NX}_2)$
3250 (s)	3294 (4)	3272 (w)	3285 (9)	3456 (449/173)	2473 (m)	2476 (6)	2518 (255/27)	ν_1	A'	$\nu_s(\text{NX}_2)$
3178 (m)	3185 (2)		3192 (4)	3407 (501/54)		2426 (11)	2497 (316/33)	ν_{16}	A''	$\nu_{\text{as}}(\text{NX}_3)$
			3156 (5)	3382 (588/65)		2408 (11)	2492 (264/79)	ν_2	A'	$\nu_s(\text{NX}_3)$
3154 (m)	3143 (4)		3116 (5)	3306 (422/126)	2388 (s)	2389 (8)	2362 (213/60)	ν_3	A'	$\nu_s(\text{NX}_3)$
1419 (m)	1417 (9)	1422 (m)	1415 (14)	1519 (238/4)	1419 (s)	1417 (6)	1513 (218/4)	ν_5	A'	$\nu_{\text{as}}(\text{SO}_2)$
1225 (m)	1227 (17)	1224 (m)	1223 (32)	1277 (177/3)	1252 (m)	1254 (4)	1295 (201/8)	ν_{19}	A''	$\nu_s(\text{SO}_2)$
981 (m)	976 (14)		972 (22)	988 (34/14)	947 (m)	950 (19)	955 (58/13)	ν_{20}	A''	$\nu(\text{S}(\text{NX}_2))$
	574 (16)			639 (197/6)	420 (s)	419 (5)	422 (4/10)	ν_{10}	A'	$\nu(\text{S}(\text{NX}_3))$
528 (m)	530 (18)		526 (20)	513 (33/2)	488 (s)	490 (21)	481 (25/2)	ν_{21}	A''	$\delta(\text{SO}_2)$

[a] Calculated at the PBE1PBE/6-311G++(3df,3dp) level of theory. IR intensity (in km mol^{-1}) and Raman intensity (in $\text{\AA}^4 \mu^{-1}$). Abbreviations for IR intensities: v = very, s = strong, m = medium, w = weak. Raman activity is stated to a scale of 1 to 100. [b] X = H, D.

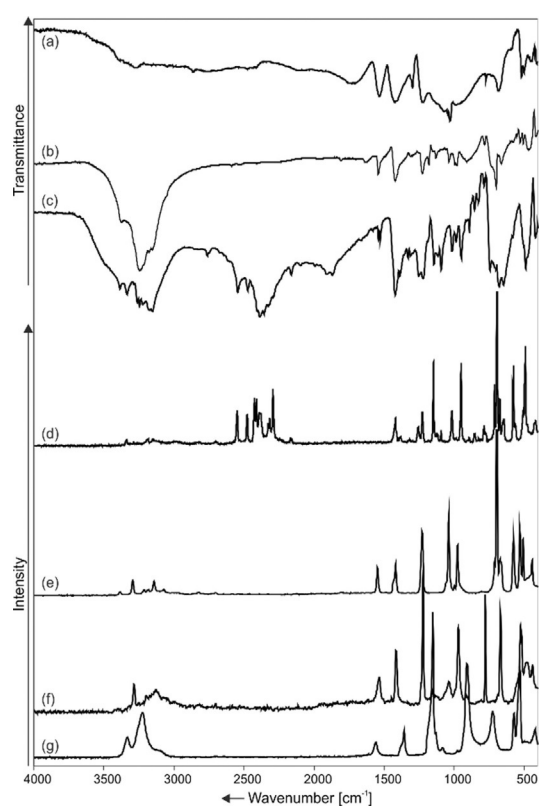


Figure 1. Low-temperature vibrational spectra of $[\text{H}_2\text{NSO}_2\text{NH}_3]^+[\text{BF}_4]^-$: a) IR spectrum, f) Raman spectrum; $[\text{H}_2\text{NSO}_2\text{NH}_3]^+[\text{AsF}_6]^-$: b) IR spectrum, e) Raman spectrum; $[\text{D}_2\text{NSO}_2\text{D}_3]^+[\text{AsF}_6]^-$: c) IR spectrum, d) Raman spectrum; and $\text{H}_2\text{NSO}_2\text{NH}_3$: g) Raman spectrum.

ty. For the vibrational assignment, the theoretical calculations for $[\text{X}_2\text{NSO}_2\text{NX}_3]^+\cdot 5\text{HF}$ (see the theoretical section below) were taken into account. The 24 internal vibrations of the $[\text{X}_2\text{NSO}_2\text{NX}_3]^+$ cation have been depicted by inspection of the Cartesian displacement coordinates of the vibrational modes.

The antisymmetric NH_2 stretching modes that occur at 3376 and 3384 cm^{-1} are blue-shifted by 40 cm^{-1} , whereas the symmetric NH_2 stretching modes in the range of 3294 to 3250 cm^{-1} and are blue-shifted by approximately 70 cm^{-1} com-

pared to the neutral compound.^[8] For the D-isotomeric species the corresponding ND_2 stretching modes are observed in the range of 2545 to 2476 cm^{-1} and are in fair agreement with the Teller–Redlich rule for an isotopic H/D shift.^[9]

Additionally, in the protonated species, NH_3 stretching modes are detected in the range of 3178 to 3192 cm^{-1} and are red-shifted by approximately 160 cm^{-1} compared to the amino stretching modes in $\text{H}_2\text{NSO}_2\text{NH}_2$.^[8] The SO_2 -stretching vibrations occur at around 1420 (antisymmetric) and 1230 cm^{-1} (symmetric) and they are blue-shifted by 60 cm^{-1} . At around 980 cm^{-1} , the $\text{S}-(\text{NH}_2)$ stretching mode is observed as blue-shifted by approximately 65 cm^{-1} compared to the average of the antisymmetric and symmetric stretching modes in the starting material.^[8] This is due to the shortening of the $\text{S}-(\text{NH}_2)$ bond caused by the protonation, whereas the $\text{S}-(\text{NH}_3)$ bond is elongated. Therefore, the related $\text{S}-\text{N}$ stretching mode observed at 574 cm^{-1} is red-shifted by approximately 335 cm^{-1} compared to the neutral compound.^[8] For the anions $[\text{BF}_4]^-$ and $[\text{AsF}_6]^-$ with ideal tetrahedral and octahedral symmetry, respectively, more vibrational modes are observed than expected which is due to solid-state effects causing a lower symmetry.

Crystal structure of $[\text{H}_2\text{NSO}_2\text{NH}_3]^+[\text{BF}_4]^-$

The salt crystallizes in the monoclinic space group $P2_1/c$ with four formula units per unit cell. Figure 2 shows an asymmetric unit. In Table 2 selected structural parameters are summarized. The sulfur atom is coordinated in a distorted tetrahedral manner. Compared to $\text{H}_2\text{NSO}_2\text{NH}_2$,^[6] the distortion of the tetrahedral coordination of the sulfur atom is increased: the $\text{N}1-\text{S}1-\text{N}2$ and the $\text{N}1-\text{S}1-\text{O}1$ bond angles of $105.8(1)$ and $102.6(1)^\circ$ are decreased by 5.6 and 3.6° , respectively, whereas the bond angles of $\text{N}2-\text{S}1-\text{O}1$ and $\text{O}1-\text{S}1-\text{O}2$ at $110.5(1)$ and $122.9(1)^\circ$ are increased by 4.4 and 4.0° , respectively.

The $\text{S}1-\text{N}1$ bond length of $1.767(2)\text{ \AA}$ is significantly elongated, whereas the $\text{S}1-\text{N}2$ bond length of $1.552(2)\text{ \AA}$ is significantly shortened compared to the neutral compound in which both $\text{S}-\text{N}$ bond lengths were observed to be $1.627(1)\text{ \AA}$.^[6] An explanation for this remarkable elongation is discussed in the theoretical section below. The $\text{S}-\text{O}$ bond lengths of $1.411(1)\text{ \AA}$

Table 2. Selected bond lengths (in Å) and angles (in °) of $\text{H}_2\text{NSO}_2\text{NH}_2$, $[\text{H}_2\text{NSO}_2\text{NH}_3]^+[\text{BF}_4]^-$, and $[\text{H}_3\text{NSO}_2\text{NH}_3]^{2+}2[\text{SbF}_6]^- \cdot 2\text{HF}$.

bond lengths [Å]	$\text{H}_2\text{NSO}_2\text{NH}_2$ ^[6]	$[\text{H}_2\text{NSO}_2\text{NH}_3]^+[\text{BF}_4]^-$	$[\text{H}_3\text{NSO}_2\text{NH}_3]^{2+}2[\text{SbF}_6]^- \cdot 2\text{HF}$
S1–N1	1.627(1)	1.767(2)	1.750(3)
S1–N2	1.627(1)	1.552(2)	1.742(3)
S1–O1	1.435(1)	1.411(1)	1.403(3)
S1–O2	1.435(1)	1.411(2)	1.398(3)
bond angles [°]			
N1–S1–N2	111.4(1)	105.8(1)	101.2(2)
N1–S1–O1	106.2(1)	102.6(1)	106.4(2)
N2–S1–O1	106.2(1)	110.5(1)	106.4(2)
O1–S1–O2	119.0(1)	122.9(1)	127.0(2)
donor–acceptor distances [Å]			
N1(–H1A)⋯F3 _{iv}	2.873(2)	N1(–H2B)⋯F3	3.030(2)
N1(–H1B)⋯F2 _{ii}	2.759(3)	N1(–H1B)⋯O2	2.860(2)
N2(–H2A)⋯F4 _v	3.076(3)	N1(–H2A)⋯O1	3.035(3)
N1(–H1C)⋯F2 _{iii}	3.060(3)	N1(–H1C)⋯O1	2.899(3)
N2(–H2B)⋯F1 _i	3.186(3)	–	–

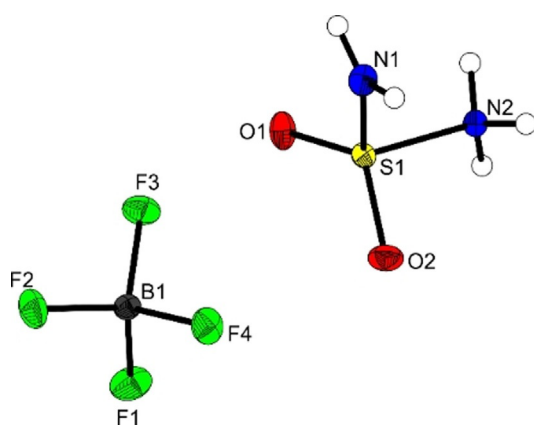


Figure 2. Asymmetric unit of $[\text{H}_2\text{NSO}_2\text{NH}_3]^+[\text{BF}_4]^-$ (thermal ellipsoids with 50% probability).

are slightly shorter than in $\text{H}_2\text{NSO}_2\text{NH}_2$. The B–F bond lengths in the $[\text{BF}_4]^-$ anion are in the range of 1.378(2) to 1.406(2) Å and are in a typical range for B–F bonds in $[\text{BF}_4]^-$ anions.^[10]

In the solid state, the cations and anions are linked by hydrogen bonds with N(–H)⋯F donor–acceptor distances in the range of 2.759(3) to 3.186(3) Å (Table 2) and can be classified as moderate hydrogen bonds.^[11] The cation–anion contacts that occur in $[\text{H}_2\text{NSO}_2\text{NH}_3]^+[\text{BF}_4]^-$ are shown in Figure S1 (Supporting Information). Furthermore, the cations are linked among each other by moderate hydrogen bonds with N(–H)⋯O donor–acceptor distances in the range of 2.860(2) to 3.035(3) Å forming zig–zag-like chains along the *b* axis (Figure S2, Supporting Information).

Vibrational spectra of $[\text{H}_3\text{NSO}_2\text{NH}_3]^{2+}2[\text{SbF}_6]^- \cdot 2\text{HF}$

The experimental and calculated vibrational frequencies are summarized together with their assignments in Table 3. Comparable to the isoelectronic species dimethylsulfone, $\text{H}_3\text{CSO}_2\text{CH}_3$, for the $[\text{H}_3\text{NSO}_2\text{NH}_3]^{2+}$ cation with an ideal C_{2v} sym-

metry, 27 vibrational modes are expected ($\Gamma_{\text{vib}} = 9A_1 + 5A_2 + 7B_1 + 6B_2$) whereby the A_2 modes are exclusively Raman-active. All other vibrational modes are both Raman- and IR-active. For the vibrational assignment, the frequencies of the calculated HF adduct $[\text{H}_3\text{NSO}_2\text{NH}_3]^{2+} \cdot 4\text{HF}$ were taken into account. The 27 internal vibrational modes of the $[\text{H}_3\text{NSO}_2\text{NH}_3]^{2+}$ cation have been depicted from the HF adduct by inspection of the Cartesian displacement coordinates of the vibrational modes

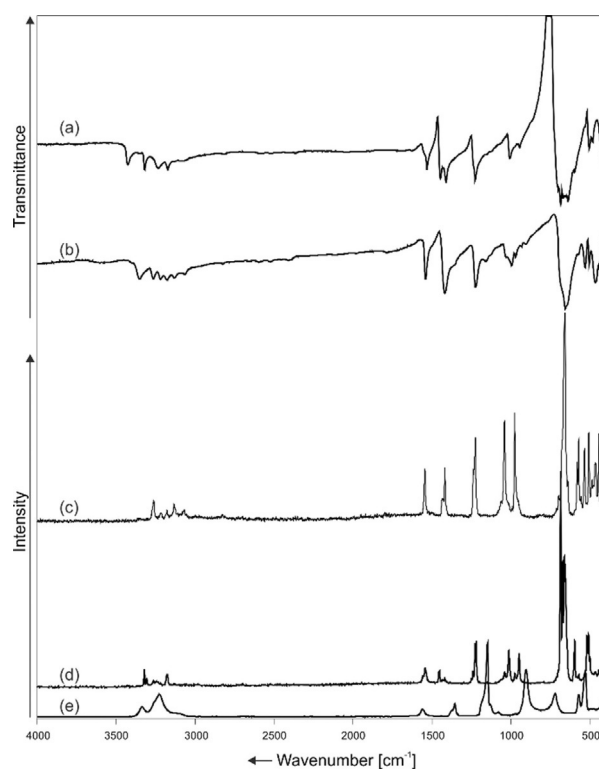


Figure 3. Low-temperature vibrational spectra of $[\text{H}_3\text{NSO}_2\text{NH}_3]^{2+}2[\text{SbF}_6]^- \cdot 2\text{HF}$: a) IR spectrum and d) Raman spectrum; $[\text{H}_2\text{NSO}_2\text{NH}_3]^+[\text{SbF}_6]^-$: b) IR spectrum and c) Raman spectrum; and $\text{H}_2\text{NSO}_2\text{NH}_2$: e) Raman spectrum.

Table 3. Experimental vibrational frequencies (in cm^{-1}) of $[\text{H}_3\text{NSO}_2\text{NH}_3]^{2+} \cdot 2[\text{SbF}_6]^- \cdot 2\text{HF}$ and calculated vibrational frequencies (in cm^{-1}) of $[\text{H}_3\text{NSO}_2\text{NH}_3]^{2+} \cdot 4\text{HF}$.

$[\text{H}_3\text{NSO}_2\text{NH}_3]^{2+} \cdot 2[\text{SbF}_6]^- \cdot 2\text{HF}$ IR	$[\text{H}_3\text{NSO}_2\text{NH}_3]^{2+} \cdot 2[\text{SbF}_6]^- \cdot 2\text{HF}$ Raman	$[\text{H}_3\text{NSO}_2\text{NH}_3]^{2+} \cdot 4\text{HF}$ calcd ^[a]	Assignment
3424 (m)	–	3358 (650/56)	$\nu_{15} \text{B}_1 \nu_{\text{as}}(\text{NH}_2)$
3318 (m)	3320 (3)	3343 (118/28)	$\nu_{10} \text{A}_2 \nu_{\text{s}}(\text{NH}_2)$
–	3304 (3)	3275 (460/107)	$\nu_1 \text{A}_1 \nu_{\text{s}}(\text{NH}_3)$
–	3262 (2)	3254 (72/6)	$\nu_{21} \text{B}_1 \nu_{\text{as}}(\text{NH}_3)$
3231 (m)	–	3215 (16/176)	$\nu_2 \text{A}_1 \nu_{\text{s}}(\text{NH}_3)$
3172 (m)	3176 (4)	2878 (2020/51)	$\nu_{22} \text{B}_2 \nu_{\text{as}}(\text{NH}_3)$
–	1544 (6)	1623 (35/1)	$\nu_{16} \text{B}_1 \delta(\text{NH}_3)$
–	–	1619 (41/3)	$\nu_{11} \text{A}_2 \delta(\text{NH}_2)$
–	1532 (m)	1594 (18/1)	$\nu_3 \text{A}_1 \delta(\text{NH}_3)$
1447 (m)	1452 (5)	1594 (2/13)	$\nu_{23} \text{B}_2 \delta(\text{NH}_3)$
1412 (m)	1420 (3)	1586 (238/3)	$\nu_{17} \text{B}_1 \nu_{\text{as}}(\text{SO}_2)$
–	–	1450 (65/12)	$\nu_4 \text{A}_1 \delta(\text{NH}_3)$
–	–	1480 (552/2)	$\nu_{24} \text{B}_2 \delta(\text{NH}_3)$
1227 (m)	1228 (16)	1270 (13/16)	$\nu_5 \text{A}_1 \nu_{\text{s}}(\text{SO}_2)$
–	1221 (17)	1123 (25/2)	$\nu_6 \text{A}_1 \rho(\text{NH}_3)$
–	–	1096 (41/1)	$\nu_{18} \text{B}_1 \delta(\text{NH}_3)$
–	1042 (4)	1052 (195/0)	$\nu_{25} \text{B}_2 \rho(\text{NH}_3)$
–	–	1038 (0/1)	$\nu_{12} \text{A}_2 \tau(\text{NH}_3)$
506 (w)	509 (17)	654 (48/7)	$\nu_{26} \text{B}_2 \nu_{\text{as}}(\text{SN}_2)$
485 (w)	502 (9)	632 (35/13)	$\nu_7 \text{A}_1 \delta(\text{SO}_2)$
420 (w)	414 (4)	478 (13/7)	$\nu_8 \text{A}_1 \nu_{\text{s}}(\text{SN}_2)$
–	352 (10)	385 (6/8)	$\nu_{27} \text{B}_2 \delta(\text{SO}_2)$
–	337 (10)	323 (8/2)	$\nu_{19} \text{B}_1 \delta(\text{SN}_2)$
–	321 (8)	264 (0/3)	$\nu_{13} \text{A}_2 \delta(\text{SN}_2)$
–	297 (21)	215 (23/3)	$\nu_9 \text{A}_1 \delta(\text{SN}_2)$
–	–	141 (2/0)	$\nu_{20} \text{B}_1 \omega(\text{NH}_3)$
–	–	107 (0/0)	$\nu_{14} \text{A}_2 \delta(\text{NH}_2)$
686 (m)	686 (100)	–	$[\text{SbF}_6]^-$
–	676 (47)	–	$[\text{SbF}_6]^-$
–	664 (48)	–	$[\text{SbF}_6]^-$
639 (m)	–	–	$[\text{SbF}_6]^-$
–	597 (16)	–	$[\text{SbF}_6]^-$

[a] Calculated at the PBE1PBE/6–311G++(3df,3dp) level of theory. IR intensity in km mol^{-1} and Raman intensities in $\text{\AA}^4 \mu^{-1}$. Abbreviations for IR intensities: v=very, s=strong, m=medium, w=weak. Raman activity is stated on a scale of 1 to 100.

(X=H, D). The experimentally observed low-temperature vibrational spectra are shown in Figure 3. The antisymmetric NH_2 stretching mode occurs at 3424 cm^{-1} and is blue-shifted by 161 cm^{-1} compared to the $[\text{H}_2\text{NSO}_2\text{NH}_3]^+$ cation. At 3318 (IR) and 3320 (Ra) , respectively, the symmetric NH_2 stretching modes are detected and are blue-shifted by 102 cm^{-1} compared to the *N*-monoprotonated species. Compared to the $[\text{H}_2\text{NSO}_2\text{NH}_3]^+$ cation, additionally, NH_3 stretching modes at 3231 (IR) and 3262 (Ra) are observed. The SO_2 stretching modes occur at 1412 (IR) and 1420 (Ra) and stay approximately unchanged compared to the $[\text{H}_2\text{NSO}_2\text{NH}_3]^+$ species. The *N,N'*-diprotonation causes a significant elongation of both S–N bonds as discussed in the crystallographic section below. Therefore, the $\nu_{\text{as}}(\text{SN})$ and $\nu_{\text{s}}(\text{SN})$ modes are observed at 509 (Ra) and 506 (IR) and at 420 (IR) and 414 (Ra) , respectively, and are enormously red-shifted by approximately 409 and 490 cm^{-1} , respectively, compared to sulfamide.^[8]

Crystal structure of $[\text{H}_3\text{NSO}_2\text{NH}_3]^{2+} \cdot 2[\text{SbF}_6]^- \cdot 2\text{HF}$

The salt of diprotonated sulfamide crystallizes in the orthorhombic space group $Pna2_1$ with four formula units per unit

cell (Figure 4). Selected bond lengths and angles are summarized in Table 2.

In the $[\text{H}_3\text{NSO}_2\text{NH}_3]^{2+}$ cation the sulfur atom is coordinated in a strongly distorted tetrahedral manner. The O1–S1–O2 bond angle of $127.0(2)^\circ$ is increased by 4.1° , whereas the N1–

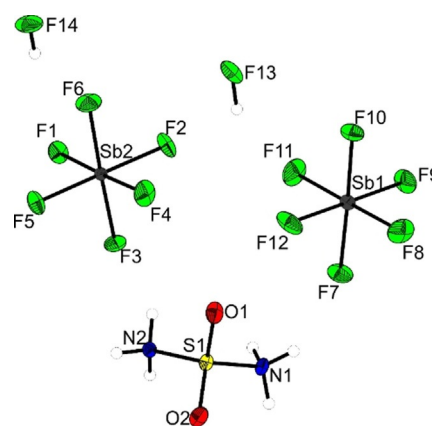


Figure 4. Asymmetric unit of $[\text{H}_3\text{NSO}_2\text{NH}_3]^{2+} \cdot 2[\text{SbF}_6]^- \cdot 2\text{HF}$ (thermal ellipsoids with 50% probability).

S1–N2 bond angle of 101.2(2)° is decreased by 4.6° compared to the monoprotonated species. The N–S–O bond angles of 106.4(2)° are comparable to the neutral compound. The S–N bond lengths of 1.750(3) and 1.742(3) Å, respectively, are significantly elongated, whereas the S–O bond lengths of 1.403(3) and 1.398(3) Å are significantly shortened compared to H₂NSO₂NH₂.

The cations, anions, and HF molecules form a 3D network linked by hydrogen bonds. Figure S3 (Supporting Information) shows the coordination sphere of the [H₃NSO₂NH₃]²⁺ cation. The donor–acceptor distances are summarized in Table S2 (Supporting Information). According to Jeffrey's classification, the hydrogen bonds F13(–H13)…F2 (2.482(3) Å) and F14(–H14)…F6 (2.457(3) Å) can be described as strong whereas all other hydrogen bonds can be assigned as medium strong.^[11]

Theoretical calculations

Structural gas-phase optimizations of [H₂NSO₂NH₃]⁺ and [H₃NSO₂NH₃]²⁺ were performed by employing the PBE1PBE/6–311G++(3pd,3df) level of theory. As already reported, the closest match with experimentally observed structures of protonated species is achieved by addition of HF molecules to the naked cations.^[12] Therefore, the HF adducts [H₂NSO₂NH₃]⁺·5HF and [H₃NSO₂NH₃]²⁺·4HF were calculated with the aim to simulate hydrogen bonding in the solid state. Compared with the structural parameters of the naked cations, the corresponding HF adducts show remarkably smaller discrepancies to the experimentally observed ones. (Tables S3 and S4, Supporting Information). In Figure 5, a comparison of the calculated and experimentally observed cationic structures is shown. For clarification in the case of the calculated structures, the added HF molecules are omitted. For the complete figure see the Supporting Information (Figure S4).

In agreement with the values observed in the crystal structure, the *N*-monoprotonation of H₂NSO₂NH₂ leads to a significant elongation of the S–N bond on the NH₃ site next to a significant shortening of the S–N bond on the amino site. This

finding prompted us to perform a calculation of the rotational barriers around the S–(NH₂) bond in H₂NSO₂NH₂ compared to [H₂NSO₂NH₃]⁺ (Figure S5, Supporting Information). We found that the rotational barrier around the S–(NH₂) bond in [H₂NSO₂NH₃]⁺ (76 kJ mol^{–1}) is increased by approximately three times compared to the neutral compound (26 kJ mol^{–1}). Wiest and co-workers reported a similar value for the barrier of rotation around the S–N bond in the neutral compound.^[5] This remarkable increase of the rotational barrier can be considered as a measure for the reinforcement of the anomeric effect.

Conclusions

Sulfamide was investigated in the superacidic solutions HF/SbF₅, HF/AsF₅, and HF/BF₃. In the case of an equimolar ratio of the Lewis acids with respect to sulfamide an *N*-monoprotonation was observed, which leads to a significant elongation of the S1–N1 bond, whereas the S1–N2 bond is significantly shortened as observed in the crystal structure of [H₂NSO₂NH₃]⁺ [BF₄][–]. This remarkable effect can be explained by elimination or reinforcement, respectively, of the anomeric effect due to protonation. The reinforcement of the anomeric effect was indicated by the calculation of the barrier of rotation around the S–N bond showing a three-fold increase of energy compared to the neutral compound.

[H₂NSO₂NH₃]⁺[BF₄][–] has a remarkable thermal stability of up to 60 °C. An *N,N'*-diprotonation was merely achieved through the utilization of HF/SbF₅ by employing several equivalents of the Lewis acid with respect to sulfamide. For [H₃NSO₂NH₃]²⁺·2[SbF₆][–]·2HF a single-crystal structure was obtained showing that both S–N bonds are remarkably elongated in comparison to the neutral compound.

Experimental Section

Caution! The hydrolysis of AsF₅, SbF₅, BF₃ and the reported salts might form HF, which burns skin and causes irreparable damage. Avoid contact with any of these compounds. Safety precautions should be taken when using and handling these materials.

Apparatus and materials

All reactions were carried out on a stainless-steel vacuum line. The reactions were performed by using FEP-reactors with PFA-adaptors. Prior synthetic work on the stainless-steel vacuum line, it was dried using fluorine. Excess fluorine was afterwards removed in dynamic vacuum and quenched through Sodalime. All reactions under an inert gas were performed using nitrogen (Air Liquide) that was dried over OrangeGel and Sicapent. SbF₅ was handled in a Duran glass line by using Young valves. Low-temperature Raman spectroscopic investigations were performed on a Bruker® MultiRAMII FT-Raman spectrometer equipped with a Nd:YAG-laser (λ = 1064 nm). The spectra were evaluated with the software OPUS 6.5 of Bruker®. IR spectra were recorded on a Bruker® Vertex-80V-FTIR spectrometer. For the evaluation of the IR spectra, the same software as for Raman spectra was used. Single-crystal X-ray structural analyses were performed on an Oxford XCalibur3 diffractometer equipped with a Spellman generator (50 kV, 40 mA, Mo_{Kα} radiation λ = 0.7107 Å) and a Kappa CCD-detector. The measurements were per-

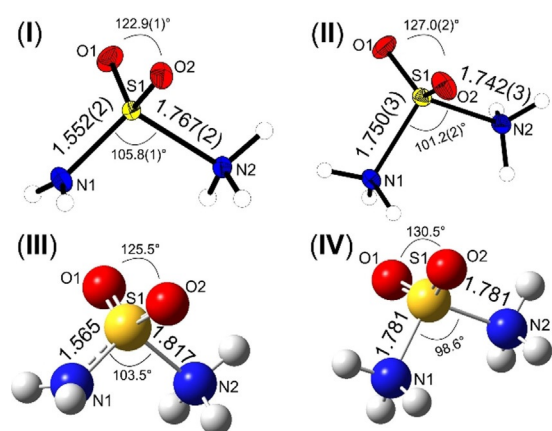


Figure 5. Comparison of the calculated and experimental cationic structures of [H₂NSO₂NH₃]⁺ (I) and (III) and [H₃NSO₂NH₃]²⁺ (II) and (IV). For clarification, the HF molecules in structures (III) and (IV) are omitted.

formed at 173 K. The program CrysAlisCCD^[13] and for its reduction CrysAlisRED^[14] were employed for the data collection. The structures were solved utilizing SHELXS-97^[15] and SHELXL-97^[16] of the WINGX software package.^[17] The structures were checked using the software PLATON.^[18] The absorption correction was performed using the SCALE3 ABSPACK multiscan method.^[19] Crystal data and structure refinements for the reported single-crystal structures in this study are summarized in Table S5 (Supporting Information). Quantum chemical calculations were performed using the software package Gaussian 09.^[20] The theoretical calculations were performed on the PBE1PBE/6-311G++(3df,3pd) level of theory.

Syntheses of $[X_2NSO_2NX_3]^+[MF_6]^-$ (M = As, Sb; X = H, D) and $[H_2NSO_2NH_3]^+[BF_4]^-$

In a typical experiment, Lewis acid AsF₅, SbF₅ or BF₃ (1 mmol) was condensed in an FEP reactor vessel followed by anhydrous hydrogen fluoride (aHF) (1 mL) or deuterium fluoride (dDF) at -196 °C. Afterwards, sulfamide (1 mmol) was loaded on the frozen mixture under a nitrogen atmosphere. The reaction mixture was warmed up to -40 °C at which the reaction takes place. Excess solvent was removed within 14 h at -78 °C in a dynamic vacuum. In these experiments, colorless crystalline solids were formed. In case of $[H_2NSO_2NH_3]^+[BF_4]^-$, the crystals were suitable to perform a single-crystal X-ray diffraction study.

Synthesis of $[H_3NSO_2NH_3]^{2+}2[SbF_6]^{-}2HF^{-}$

The diprotonated species as a $[SbF_6]^-$ salt was achieved by condensing SbF₅ (433 mg, 2.0 mmol, 2.0 equiv) in an FEP-reactor vessel followed by HF (1 mL) at -196 °C. This mixture was allowed to warm up to 0 °C and was mixed rigorously to ensure the formation of the superacid. Afterwards, the mixture was frozen at -196 °C again. Then, H₂NSO₂NH₂ (96 mg, 1.0 mmol, 1.0 equiv) was given to the frozen mixture under an inert gas atmosphere. The mixture was then warmed up to -50 °C and mixed until a colorless solution was obtained that was stored for 72 h at this temperature. Colorless crystals were grown.

Supporting Information Summary

The Supporting Information contains the complete table of experimental and calculated vibrational frequencies and their assignment (Table S1), an illustration of the cation-anion contacts in $[H_2NSO_2NH_3]^+[BF_4]^-$ (Figure S1), a crystal packing of $[H_2NSO_2NH_3]^+[BF_4]^-$ (Figure S2), the contacts around the $[H_3NSO_2NH_3]^{2+}$ cation in $[H_3NSO_2NH_3]^{2+}2[SbF_6]^{-}2HF^{-}$ (Figure S3), a comparison of the bond lengths and angles between the experimentally observed $[H_2NSO_2NH_3]^+$ and quantum chemically calculated species $[H_2NSO_2NH_3]^+$ and $[H_2NSO_2NH_3]^+ \cdot 5HF$ (Table S3), a comparison of the bond lengths and angles between the experimentally observed $[H_3NSO_2NH_3]^{2+}$ and quantum chemically calculated species $[H_3NSO_2NH_3]^{2+}$ and $[H_3NSO_2NH_3]^{2+} \cdot 4HF$ (Table S4), an illustration of the calculated HF adducts $[H_2NSO_2NH_3]^+ \cdot 5HF$ and $[H_3NSO_2NH_3]^{2+} \cdot 4HF$ (Figure S4), a scan of the barrier of rotation around the S-(NH₂) bond (Figure S5), and a data refinement for $[H_2NSO_2NH_3]^+[BF_4]^-$ and $[H_3NSO_2NH_3]^{2+}2[SbF_6]^{-}2HF$ (Table S5)

Acknowledgements

The authors of this work gratefully acknowledge financial support by the Deutsche Forschungsgemeinschaft (DFG), the

Ludwig-Maximilians-Universität (LMU) München, and the F-Select GmbH. We are grateful to Dr. R. Bröchler for the construction of the low-temperature device for single-crystal mounting.

Conflict of interest

The authors declare no conflict of interest.

Keywords: anomeric effect • X-ray structure analysis • sulfamide • superacid chemistry • vibrational spectroscopy

- [1] V. H. Regnault, *Ann. Chim. Phys.* **1838**, 170–180.
- [2] H. He, J. Feng, J. He, Q. Xia, Y. Ren, F. Wang, H. Peng, H. He, L. Feng, *RSC Adv.* **2016**, *6*, 4310–4320.
- [3] J.-Y. Winum, A. Scozzafava, J.-L. Montero, C. T. Supuran, *Med. Res. Rev.* **2006**, *26*, 767–792.
- [4] F. Abbate, C. T. Supuran, A. Scozzafava, P. Orioli, M. T. Stubbs, G. Klebe, *J. Med. Chem.* **2002**, *45*, 3583–3587.
- [5] E. Hansen, E. Limé, P.-O. Norrby, O. Wiest, *J. Phys. Chem.* **2016**, *120*, 3677–3682.
- [6] F. Belaj, C. Kratky, E. Nachbaur, A. Popitsch, *Monatsh. Chem.* **1987**, *118*, 427–433.
- [7] M. Garrett, T. Tao, W. L. Jolly, *J. Phys. Chem.* **1964**, *68*, 824–826.
- [8] I. W. Herrick, E. L. Wagner, *Spectrochim. Acta* **1965**, *21*, 1569–1577.
- [9] J. Weidlein, U. Müller, K. Dehnicke, *Schwingungsspektroskopie, Vol. 2nd ed.*, Georg Thieme Verlag, Stuttgart, Germany, **1988**.
- [10] M. Finze, E. Bernhardt, H. Willner, C. W. Lehmann, F. Aubke, *Inorg. Chem.* **2005**, *44*, 4206–4214.
- [11] G. A. Jeffrey in *An Introduction to Hydrogen Bonding*, Oxford University Press, Oxford, **1997**, pp. 1–303.
- [12] T. Soltner, N. R. Goetz, A. Kornath, *Eur. J. Inorg. Chem.* **2011**, 3076–3081.
- [13] CrysAlisCCD, Version 1.171.35.11 (release 16-05-2011 CrysAlis 171.NET), Oxford Diffraction Ltd, UK, **2001**.
- [14] CrysAlisRED, Version 1.171.35.11 (release 16-05-2011 CrysAlis 171.NET), Oxford Diffraction Ltd., UK, **2011**.
- [15] G. M. Sheldrick, SHELXS-97, Program for Crystal Structure Solution, University of Göttingen, Germany, **1997**.
- [16] G. M. Sheldrick, SHELXL-97, Program for the Refinement of Crystal Structures, University of Göttingen, Germany, **1997**.
- [17] L. Farrugia, *J. Appl. Crystallogr.* **1999**, *32*, 837–838.
- [18] A. L. Spek in *PLATON, A Multipurpose Crystallographic Tool*, U. Utrecht University, The Netherlands, **1999**.
- [19] SCALE3 ABSPACK, An Oxford Diffraction Program, O. Diffraction, Ltd., UK, **2005**.
- [20] Gaussian 09, Revision A.1, M. J. Frisch, G. W. Trucks, H. B. Schlegel, G. E. Scuseria, M. A. Robb, J. R. Cheeseman, G. Scalmani, V. Barone, B. Menonucci, G. A. Petersson, H. Nakatsuji, M. Caricato, X. Li, H. P. Hratchian, A. F. Izmaylov, J. Bloino, G. Zheng, J. L. Sonnenberg, M. Hada, M. Ehara, K. Toyota, R. Fukuda, J. Hasegawa, M. Ishida, T. Nakajima, Y. Honda, O. Kitao, H. Nakai, T. Vreven, J. A. Montgomery, Jr., J. E. Peralta, F. Ogliaro, M. Bearpark, J. J. Heyd, E. Brothers, K. N. Kudin, V. N. Staroverov, R. Kobayashi, J. Normand, K. Raghavachari, A. Rendell, J. C. Burant, S. S. Iyengar, J. Tomasi, M. Cossi, N. Rega, J. M. Millam, M. Klene, J. E. Knox, J. B. Cross, V. Bakken, C. Adamo, J. Jaramillo, R. Gomperts, R. E. Stratmann, O. Yazyev, A. J. Austin, R. Cammi, C. Pomelli, J. W. Ochterski, R. L. Martin, K. Morokuma, V. G. Zakrzewski, G. A. Voth, P. Salvador, J. J. Dannenberg, S. Dapprich, A. D. Daniels, O. Farkas, J. B. Foresman, J. V. Ortiz, J. Cioslowski, and D. J. Fox, Gaussian, Inc., Wallingford CT, **2009**.

Manuscript received: August 5, 2018

Revised manuscript received: September 4, 2018

Accepted manuscript online: September 9, 2018

Version of record online: October 17, 2018

CHEMISTRY

A **European** Journal

Supporting Information

Tuning the Anomeric Effect in Sulfamide with Superacids

Dominik Leitz, Marie C. Bayer, Yvonne Morgenstern, Florian Zischka, and
Andreas J. Kornath^{*[a]}

chem_201804009_sm_miscellaneous_information.pdf

Table S1. Experimental vibrational frequencies (in cm^{-1}) of $[\text{H}_2\text{NSO}_2\text{NH}_3]^+[\text{AsF}_6]^-$, $[\text{H}_2\text{NSO}_2\text{NH}_3]^+[\text{BF}_4]^-$ and $[\text{D}_2\text{NSO}_2\text{ND}_3]^+[\text{AsF}_6]^-$ and calculated vibrational frequencies (in cm^{-1}) of $[\text{H}_2\text{NSO}_2\text{NH}_3]^+ \cdot 5 \text{ HF}$ and $[\text{D}_2\text{NSO}_2\text{ND}_3]^+ \cdot 5 \text{ HF}$.

$[\text{H}_2\text{NSO}_2\text{NH}_3]^+[\text{AsF}_6]^-$		$[\text{H}_2\text{NSO}_2\text{NH}_3]^+[\text{BF}_4]^-$		$[\text{H}_2\text{NSO}_2\text{NH}_3]^+ \cdot 5 \text{ HF}$	$\text{D}_2\text{NSO}_2\text{ND}_3]^+[\text{AsF}_6]^-$		$[\text{D}_2\text{NSO}_2\text{ND}_3]^+ \cdot 5 \text{ HF}$		Assignment	
IR	Raman	IR	Raman	calc. ^[a] (IR/Raman)	IR	Raman	calc. ^[a] (IR/Raman)		[b]	
3376 (m)	3384 (1)			3582 (650/69)	2545 (m)	2548 (8)	2662 (336/33)	ν_{15}	A''	$\nu_{\text{as}}(\text{NX}_2)$
3250 (s)	3294 (4)	3272 (w)	3285 (9)	3456 (449/173)	2473 (m)	2476 (6)	2518 (255/27)	ν_1	A'	$\nu_{\text{s}}(\text{NX}_2)$
3178 (m)	3185 (2)		3192 (4)	3407 (501/54)		2426 (11)	2497 (316/33)	ν_{16}	A''	$\nu_{\text{as}}(\text{NX}_3)$
			3156 (5)	3382 (588/65)		2408 (11)	2492 (264/79)	ν_2	A'	$\nu_{\text{s}}(\text{NX}_3)$
3154 (m)	3143 (4)		3116 (5)	3306 (422/126)	2388 (s)	2389 (8)	2362 (213/60)	ν_3	A'	$\nu_{\text{s}}(\text{NX}_3)$
				1650 (28/2)	1221 (m)	1227 (7)	1189 (12/2)	ν_{17}	A''	$\delta(\text{NX}_3)$
1539 (m)	1545 (8)	1532 (7)	1532 (m)	1639(12/2)	1143 (m)	1146 (18)	1174 (18/1)	ν_4	A'	$\delta(\text{NX}_3)$
	1431 (4)			1585 (57/1)	1091 (m)	1092 (4)	1167 (15/1)	ν_{18}	A''	$\delta(\text{NX}_2)$
1419 (m)	1417 (9)	1422 (m)	1415 (14)	1519 (238/4)	1419 (s)	1417 (6)	1513 (218/4)	ν_5	A'	$\nu_{\text{as}}(\text{SO}_2)$
1310 (w)		1296 (w)	1237 (7)	1463 (113/0)	1013 (m)	1016 (7)	1067 (102/1)	ν_6	A'	$\delta(\text{NX}_3)$
1225 (m)	1227 (17)	1224 (m)	1223 (32)	1277 (177/3)	1252 (m)	1254 (4)	1295 (201/8)	ν_{19}	A''	$\nu_{\text{s}}(\text{SO}_2)$
907 (m)			914 (30)	1055 (60/9)	700 (w)	711 (14)	707 (2/2)	ν_7	A'	$\delta(\text{NX}_3)$
1038 (m)	1038 (22)	1028 (m)	1044 (7)	1081 (1/2)	853 (w)	857 (3)	841 (3/2)	ν_8	A'	$\delta(\text{NX}_2)$
			935 (100)	1011 (3/1)	785 (w)	786 (5)	715 (10/3)	ν_9	A'	$\delta(\text{NX}_2)$
981 (m)	976 (14)		972 (22)	988 (34/14)	947 (m)	950 (19)	955 (58/14)	ν_{20}	A''	$\nu(\text{S}(\text{NX}_2))$
	574 (16)			639 (197/6)	420 (s)	419 (5)	422 (4/10)	ν_{10}	A'	$\nu(\text{S}(\text{NX}_3))$
528 (m)	530 (18)		526 (20)	513 (33/2)	488 (s)	490 (21)	481 (25/2)	ν_{21}	A''	$\delta(\text{SO}_2)$
507 (m)	507 (16)	500 (w)		487 (124/4)		375 (13)	384 (1/1)	ν_{11}	A'	$\delta(\text{NX}_2)$
	441 (10)		471 (9)	471 (58/8)		369 (19)	329 (1/0)	ν_{12}	A'	$\rho(\text{NX}_2)$
415 (w)			411 (15)	414 (109/4)		305 (9)	320 (94/0)	ν_{13}	A'	$\rho(\text{NX}_2)$
	346 (16)		353 (21)	394 (1/1)			276 (7/1)	ν_{22}	A''	$\omega(\text{NX}_2)$
	317 (12)		339 (19)	310 (8/2)		490 (21)	481 (7/1)	ν_{23}	A''	$\tau(\text{SO}_2)$
	263 (2)			265 (0/2)			246 (0/2)	ν_{14}	A'	$\delta(\text{NSN})$
			162 (6)	150 (0/0)			108 (0/0)	ν_{24}	A''	$\delta(\text{NX}_3)$
688 (m)	688 (100)					694 (100)				$[\text{AsF}_6]^-$
660 (m)					677 (m)	672 (11)				$[\text{AsF}_6]^-$
	647 (16)				646 (m)	643 (6)				$[\text{AsF}_6]^-$
	591 (10)									$[\text{AsF}_6]^-$
		772 (w)	775 (46)							$[\text{BF}_4]^-$
		684 (m)	671 (25)							$[\text{BF}_4]^-$
		518 (w)	518 (16)							$[\text{BF}_4]^-$
		452 (m)								$[\text{BF}_4]^-$
		423 (m)								$[\text{BF}_4]^-$

[a] Calculated at the PBE1PBE/6-311G++(3df,3dp) level of theory. IR intensity in km/mol and Raman intensity in $\text{\AA}^4/\mu$. Abbreviations for IR intensities: ν = very, s = strong, m = medium, w = weak. $X = \text{H, D}$. Raman activity is stated to a scale of 1 to 100. [b] $X = \text{H, D}$.

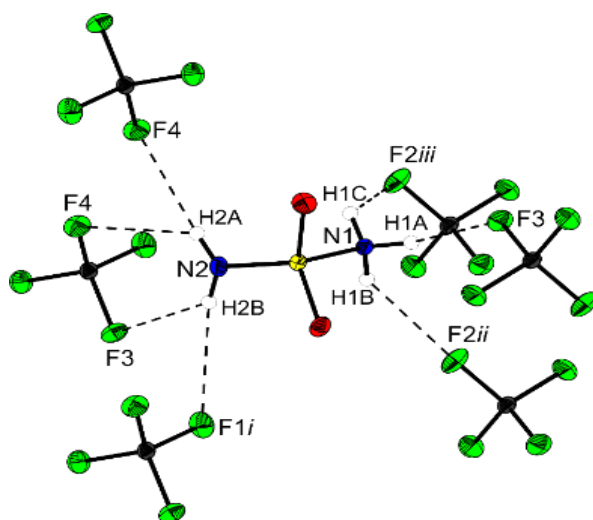


Figure S1. Cation-anion contacts (represented by dashed lines) in $[\text{H}_2\text{NSO}_2\text{NH}_3]^+[\text{BF}_4]^-$ (thermal ellipsoids with 50% probability). Symmetry codes: $i = -1+x, y, z$; $ii = -1+x, 2.5-y, 0.5+z$, $iii = x, 2.5-y, -0.5+z$, $iv = 1-x, -0.5+y, 0.5-z$, $v = 2-x, 2y, 1-z$.

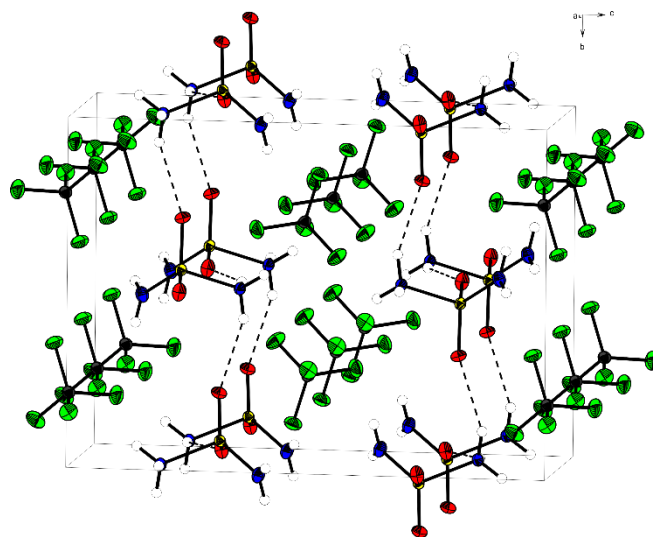


Figure S2. Crystal packing of $[\text{H}_2\text{NSO}_2\text{NH}_3]^+[\text{BF}_4]^-$. Intercationic contacts are represented as dashed lines. View along the a -axis.

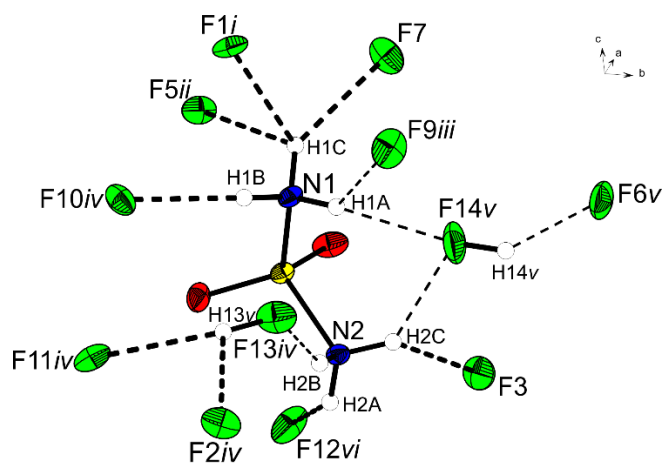


Figure S3. Contacts of the $[\text{H}_3\text{NSO}_2\text{NH}_3]^{2+}$ cation in $[\text{H}_3\text{NSO}_2\text{NH}_3]^{2+}[\text{SbF}_6]^- \cdot 2\text{HF}$ (thermal ellipsoids with 50% probability). Symmetry codes: $i = 0.5-x, -0.5+y, 0.5+z$; $ii = -x, -y, 0.5+z$; $iii = 1-x, -y, -0.5+z$; $iv = 0.5-x, -0.5+y, -0.5+z$; $v = 0.5+x, 0.5-y, z$; $vi = -x, -y, -0.5+z$.

Table S2. Donor acceptor distances (in Å) and angles (in deg) of $[\text{H}_3\text{NSO}_2\text{NH}_3]^{2+}2[\text{SbF}_6]^{-} \cdot 2\text{HF}$.

Donor acceptor distances [Å]			
N1(-H1C)⋯F1	2.702(3)	N1(-H1A)⋯F9	2.833(4)
N1(-H1C)⋯F5	2.789(2)	N1(-H1B)⋯F10	2.846(4)
N1(-H1C)⋯F7	2.929(4)	N1(-H1C)⋯F14	2.731(4)
N2(-H2C)⋯F3	2.686(4)	N2(-H2B)⋯F13	2.673(4)
N2(-H2A)⋯F12	2.720(4)	N2(-H2C)⋯F14	2.653(4)
F13(-H13)⋯F2	2.482(3)	F14(-H14)⋯F6	2.457(3)
F13(-H13)⋯F11	3.060(4)		

Table S3. Selected bond lengths (in Å) and angles (in deg) of $[\text{H}_2\text{NSO}_2\text{NH}_3]^+$, $[\text{H}_2\text{NSO}_2\text{NH}_3]^+ \cdot 5 \text{HF}$ and $[\text{H}_2\text{NSO}_2\text{NH}_3]^+[\text{BF}_4]^-$.

	Bond lengths [Å]		
	$[\text{H}_2\text{NSO}_2\text{NH}_3]^+$ (calc.) ^[a]	$[\text{H}_2\text{NSO}_2\text{NH}_3]^+ \cdot 5 \text{HF}$ (calc.) ^[a]	$[\text{H}_2\text{NSO}_2\text{NH}_3]^+[\text{BF}_4]^-$ (exp.)
S1-N1	1.871	1.816	1.767(2)
S1-N2	1.578	1.564	1.552(2)
S1-O1	1.406	1.413	1.411(1)
S1-O2	1.406	1.413	1.411(2)
Bond angles [°]			
N1-S1-N2	101.0	103.1	105.8(1)
N1-S1-O1	99.8	101.1	102.6(1)
N2-S1-O1	111.4	111.1	110.5(1)
O1-S1-O2	127.8	125.5	122.9(1)

[a] calculated on the PBE1PBE/6-311G++(3pd, 3df) level of theory.

Table S4. Selected bond lengths (in Å) and angles (in deg) of $[\text{H}_3\text{NSO}_2\text{NH}_3]^+$, $[\text{H}_3\text{NSO}_2\text{NH}_3]^+ \cdot 4 \text{HF}$ and $[\text{H}_3\text{NSO}_2\text{NH}_3]^{2+}([\text{SbF}_6]^-)_2 \cdot 2\text{HF}$.

	Bond lengths [Å]		
	$[\text{H}_3\text{NSO}_2\text{NH}_3]^+$ (calc.) ^[a]	$[\text{H}_3\text{NSO}_2\text{NH}_3]^+ \cdot 4 \text{HF}$ (calc.) ^[a]	$[\text{H}_3\text{NSO}_2\text{NH}_3]^{2+}([\text{SbF}_6]^-)_2 \cdot 2\text{HF}$ (exp.)
S1-N1	1.893	1.780	1.750(3)
S1-N2	1.893	1.780	1.742(3)
S1-O1	1.416	1.402	1.403(3)
S1-O2	1.416	1.402	1.398(3)
Bond angles [°]			
N1-S1-N2	101.8	98.6	101.2(2)
N1-S1-O1	104.3	105.4	106.4(2)
N2-S1-O1	104.3	106.2	106.4(2)
O1-S1-O2	133.8	130.5	127.0(2)

[a] calculated on the PBE1PBE/6-311G++(3pd, 3df) level of theory.

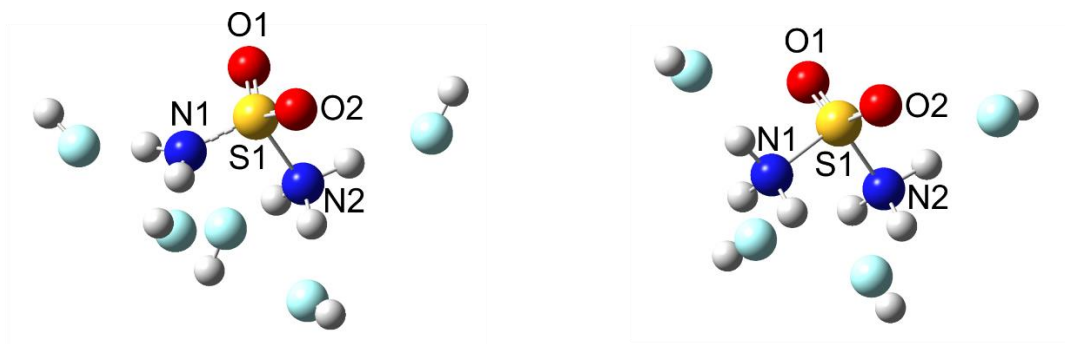


Figure S4. Calculated HF-adducts $[\text{H}_2\text{NSO}_2\text{NH}_3]^+ \cdot 5 \text{ HF}$ (left) and $[\text{H}_3\text{NSO}_2\text{NH}_3]^{2+} \cdot 4 \text{ HF}$ (right) on the PBE1PBE/6-311G++(3df, 3pd) level of theory.

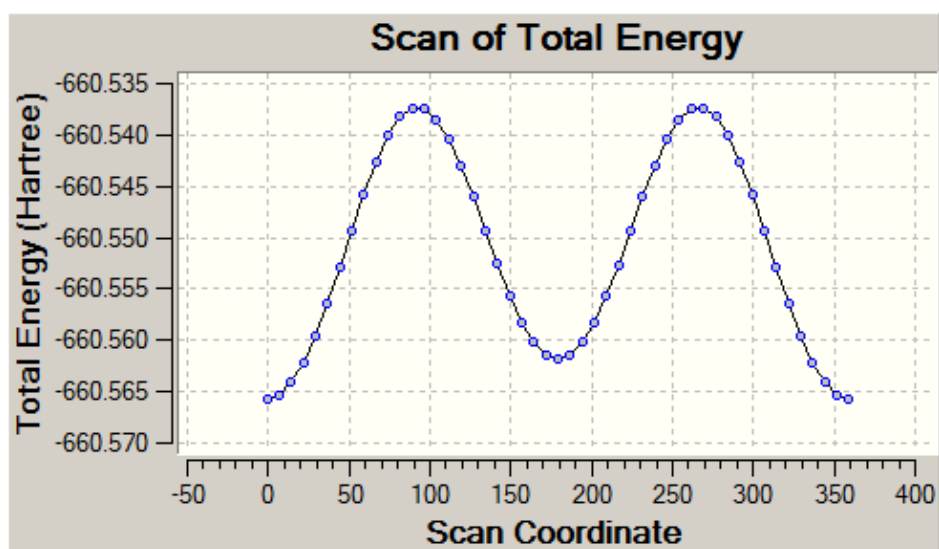


Figure S5. Scan of the barrier of rotation around the S-(NH₂) bond. 50 steps à 6°.

Table S5. Crystal data and structure refinement for $[\text{H}_2\text{NSO}_2\text{NH}_3]^+[\text{BF}_4]^-$ and $[\text{H}_3\text{NSO}_2\text{NH}_3]^{2+}([\text{SbF}_6]^-)_2 \cdot 2\text{HF}$

Empirical formula	$[\text{H}_2\text{NSO}_2\text{NH}_3]^+[\text{BF}_4]^-$	$[\text{H}_3\text{NSO}_2\text{NH}_3]^{2+}([\text{SbF}_6]^-)_2 \cdot 2\text{HF}$
M_r	183.93	609.66
Crystal system	monoclinic	orthorhombic
Space Group	$P2_1/c$	$Pna2_1$
a [Å]	4.700(5)	10.3270(5)
b [Å]	9.469(5)	14.9540(6)
c [Å]	12.972(5)	9.0250(3)
α [°]	90	90
β [°]	91.300(5)	90
γ [°]	90	90
V[Å ³]	577.2(7)	1393.73(10)
Z	4	4
ρ_{calcd} , [gcm ⁻³]	2.117	2.905
μ [mm ⁻¹]	0.590	4.191
F(000)	368	1128
T[K]	173(2)	173(2)
λ (Mo-K α) [Å]	0.71073	0.71073
<i>hkl</i> range	-6:6; -7:12; -17:17	-8:14; -22:17; -13:13
refl. measured	5160	5644
refl. unique	1550	3704
R_{int}	0.0304	0.0186
parameters	111	201
R(F)/wR(F ²) ^a	0.0396/0.0708	0.0218/0.0494
weighting	0.0268/0.1933	0.0254/0
S(GoF) ^c	1.086	1.029
residual density	0.290/-0.436	0.705/-1.297
device type	Oxford XCalibur	Oxford XCalibur
solution/refinem	SHELXS-97 ^[15]	SHELXS-97 ^[15]
CCDC	1827448	1827451

Selenourea

Preparation and Structure of Protonated Selenourea

Dominik Leitz,^[a] Alan Virmani,^[a] Yvonne Morgenstern,^[a] Florian Zischka,^[a] and
Andreas J. Kornath*^[a]

Abstract: Selenourea was investigated in the binary superacidic media XF/MF_5 ($X = H, D; M = As, Sb$). The protonation selectively takes place at the selenium atom leading to the corresponding salts $[(X_2N)_2CSeX]^+[MF_6]^-$. The characterization of the colorless salts was performed by low temperature vibrational spectroscopy. In the case of $[(H_2N)_2CSeH]^+[SbF_6]^-$ a sin-

gle-crystal X-ray structure analysis is reported. The observed $Se\cdots F$ interaction in the solid state is discussed in context of σ -hole interactions. Selenourea undergoes structural changes due to the protonation which are discussed together with quantum-chemical calculations.

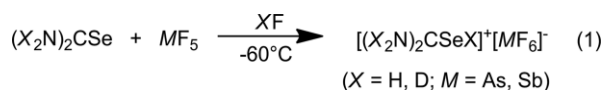
Introduction

The protonation site of urea and thiourea was controversially discussed in literature. In 1959 *Spinner* investigated the reaction of urea and thiourea with HCl in non-aqueous solvents. On the basis of vibrational spectra he concluded the formation of the $[H_2NC(X)NH_3]^+$ cation ($X = O, S$).^[1] Whereas two years later *Janssen*^[2] as well as *Kutzelnigg*^[3] unanimously reported that the protonation of urea and thiourea takes place at the chalcogen atom. A first indication for the correctness of this finding was given in the crystal structure of urea phosphate. However, the results were not conclusive.^[4] *Feil* et al. carried out single-crystal structure analyses of urea-^[5] and thiourea^[6] nitrate confirming the occurrence of chalcogen protonations. In 1963 *Birchall* and *Gillespie* reported an NMR spectroscopic study of thiourea in fluorosulfuric acid.^[7] In these strong acidic media they reported indications for an *N,S*-diprotonation. *Olah* et al. revisited this investigation finding indications that only in presence of SbF_5 an *N,S*-diprotonation takes place.^[8] *Olah* and *Christe* confirmed the existence of the $[H_2NC(SH)NH_3]^{2+}$ cation by Raman spectroscopy using the superacidic system HF/AsF_5 .^[9] Later, in a previous work at our group, urea and thiourea were investigated in the superacidic solutions HF/MF_5 ($M = As, Sb$). In this study it was shown that dependent on the molar ratio, salts of the type $[(H_2N)_2C(XH)]^+[MF_6]^-$ or $[H_2NC(XH)NH_3]^{2+}2[MF_6]^-$ are observed.^[10]

The basicity of selenourea is rarely described in literature. In a theoretical study *Kaur* et al. reported that a protonation at the Se atom is more favorable than an *N*-protonation.^[11] Experimental studies have not been reported so far. This prompted us to investigate selenourea in the binary superacidic systems HF/MF_5 ($M = As, Sb$) with the aim to investigate its basicity.

Results and Discussion

In the binary superacidic systems XF/MF_5 ($X = H, D; M = As, Sb$) selenourea reacts under the formation of the corresponding salts $[(X_2N)_2CSeX]^+[MF_6]^-$ according to Equation (1).



The reactions were carried out at $-60^\circ C$. The formed colorless salts are moisture-sensitive and stable below $-40^\circ C$. In the case of the utilization of several equivalents of Lewis acids with respect to selenourea no *Se,N*-diprotonation was detected.

Vibrational Spectroscopy

The salts $[(X_2N)_2CSeX]^+[MF_6]^-$ ($X = H, D; M = As, Sb$) were characterized by low temperature vibrational spectroscopy. The corresponding experimental IR and Raman spectra (blue) are shown together with their calculated spectra (orange) in Figure 1. In Table 1 selected experimentally observed and quantum chemically calculated frequencies are summarized together with their assignment. The complete Tables (Tables S1–S3) are provided in the Supporting Information. The protonation causes a lowering of the symmetry from C_{2v} to C_1 . Therefore, in case of the $[(X_2N)_2SeX]^+$ cation 21 fundamental vibrations are expected showing both Raman and IR activity. The stretching vibrations of the amino groups are detected in the range from 3378 cm^{-1} to 3375 cm^{-1} (antisymmetric) and from 3268 cm^{-1} to 3264 cm^{-1} (symmetric). In the case of the *d*-isotopomeric species a broad IR band in the range of 3425 to 3350 cm^{-1} is observed which is due to an incomplete H/D exchange. The corresponding ND_2 vibrations of the *d*-isotopomers occur in the range from 2607 cm^{-1} to 2595 cm^{-1} (antisymmetric) and from 2519 cm^{-1} to 2466 cm^{-1} (symmetric). The NX_2 stretching modes are slightly blue-shifted compared to $(X_2N)_2CSe$.^[12,13]

[a] Department of Chemistry, Ludwig-Maximilians Universität München, Butenandtstr. 5-13, 81377 Munich, Germany
E-mail: andreas.kornath@cup.uni-muenchen.de
<http://www.org.chemie.uni-muenchen.de/ac/kornath/>

Supporting information and ORCID(s) from the author(s) for this article are available on the WWW under <https://doi.org/10.1002/ejic.201800933>.

Table 1. Experimental vibrational frequencies [cm^{-1}] of $[(\text{H}_2\text{N})_2\text{CSeH}]^+[\text{AsF}_6]^-$, $(\text{H}_2\text{N})_2\text{CSe}$, $[(\text{D}_2\text{N})_2\text{CSeD}]^+[\text{AsF}_6]^-$ and $(\text{D}_2\text{N})_2\text{CSe}$ as well as calculated vibrational frequencies [cm^{-1}] of $[(\text{H}_2\text{N})_2\text{CSeH}]^+$, $(\text{H}_2\text{N})_2\text{CSe}$, $[(\text{D}_2\text{N})_2\text{CSeD}]^+$ and $(\text{D}_2\text{N})_2\text{CSe}$.

$[(\text{H}_2\text{N})_2\text{CSeH}]^+[\text{AsF}_6]^-$ IR/Raman	$[(\text{H}_2\text{N})_2\text{CSeH}]^+$ calcd. ^[a]	$(\text{H}_2\text{N})_2\text{CSe}$ IR/Raman	$(\text{H}_2\text{N})_2\text{CSe}$ calcd. ^[a]	$[(\text{D}_2\text{N})_2\text{CSeD}]^+[\text{AsF}_6]^-$ IR/Raman	$[(\text{D}_2\text{N})_2\text{CSeD}]^+$ calcd. ^[a]	$(\text{D}_2\text{N})_2\text{CSe}$ IR/Raman	$(\text{D}_2\text{N})_2\text{CSe}$ calcd. ^[a]	Assignment (b)
	3601		3610	2607/ 2609	2667	2537	2667	$\nu_{\text{as}}(\text{NX}_2)$
3425*	3592	3258/3277	3608	2595	2661	2501	2663	$\nu_{\text{as}}(\text{NX}_2)$
3378	3481		3473	2526/ 2519	2520	2380	2508	$\nu_{\text{s}}(\text{NX}_2)$
3270/3268	3471	3148	3465	2466	2510	2338/2344	2500	$\nu_{\text{s}}(\text{NX}_2)$
2342/2350	2310	–	–	1686/1692	1644	–	–	$\nu(\text{SeX})$
1708/1708	1642	1605/1609	1568	1595	1587	1356	1438	$\nu_{\text{as}}(\text{CN}_2)$
1419/1418	1383	1400/1400	1343	1401/1404	1374	1293	1321	$\nu_{\text{s}}(\text{CN}_2)$
633	617	640	637	544/546	535	555/563	571	$\nu(\text{CSe})(\text{NX}_2)$

[a] Calculated at the PBE/PBE/6-311G++(3df,3dp) level of theory. IR intensities and Raman scattering activities are provided in Supporting Information (Tables S1–S3). [b] X = H, D. *observed in the IR spectra of $[(\text{D}_2\text{N})_2\text{CSeD}]^+[\text{AsF}_6]^-$.

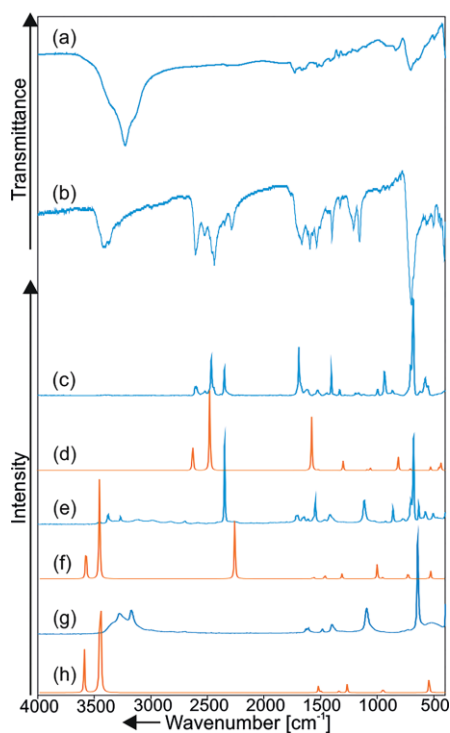


Figure 1. (a) IR spectrum (exp.) of $[(\text{H}_2\text{N})_2\text{CSeH}]^+[\text{AsF}_6]^-$, (b) IR spectrum (exp.) of $[(\text{D}_2\text{N})_2\text{CSeD}]^+[\text{AsF}_6]^-$, (c) Raman spectrum of $[(\text{D}_2\text{N})_2\text{CSeD}]^+[\text{AsF}_6]^-$ (exp.), (d) Raman spectrum of $[(\text{D}_2\text{N})_2\text{CSeD}]^+$ (calcd.), (e) Raman spectrum of $[(\text{H}_2\text{N})_2\text{CSeH}]^+[\text{AsF}_6]^-$ (exp.), (f) Raman spectrum of $[(\text{H}_2\text{N})_2\text{CSeH}]^+$ (calcd.), (g) Raman spectrum of $(\text{H}_2\text{N})_2\text{CSe}$ (exp.), (h) Raman spectrum of $(\text{H}_2\text{N})_2\text{CSe}$.

The most meaningful vibrational mode for the successful protonation of selenourea is the SeH stretching vibration at around 2350 cm^{-1} . In case of the *d*-isotopomere the corresponding SeD stretching vibration occurs at 1692 cm^{-1} and is in fair agreement with the Teller-Redlich rule for an H/D isotopic effect.^[14] The antisymmetric and symmetric CN_2 stretching vibrations are observed at around 1710 cm^{-1} and 1420 cm^{-1} , respectively. The CSe stretching vibration is detected at 633 cm^{-1} $\{[(\text{H}_2\text{N})_2\text{CSeH}]^+\}$ and $544(\text{IR})/546(\text{Ra})\text{ cm}^{-1}$ $\{[(\text{D}_2\text{N})_2\text{CSeD}]^+\}$ respectively, and is slightly red-shifted compared to $(\text{H}_2\text{N})_2\text{CSe}$ [640 cm^{-1}] and $(\text{D}_2\text{N})_2\text{CSe}$ [$555(\text{IR})/563(\text{Ra})\text{ cm}^{-1}$] which is consistent with the elongation of the C–Se bond due to the Se-protonation (see crystallographic section below). The values for the CSe stretching vibrations in case of the starting

material are in fair agreement to previous studies.^[12,13] For the $[\text{MF}_6]^-$ anions with octahedral symmetry more vibrations than expected are observed which can be explained by a lower symmetry caused by donor–acceptor interactions in the solid state.

Crystal Structure of $[(\text{H}_2\text{N})_2\text{CSeH}]^+[\text{SbF}_6]^-$

After slow removal of the solvent HF within 72 h at $-60\text{ }^\circ\text{C}$ colorless single-crystals suitable for a single-crystal X-ray diffraction study were obtained. $[(\text{H}_2\text{N})_2\text{CSeH}]^+[\text{SbF}_6]^-$ crystallizes in the triclinic space group $P\bar{1}$ with two formula units per unit cell. In Figure 2 an asymmetric unit is shown. Bond lengths and bond angles are summarized together with the parameters of selenourea^[15] in Table 2.

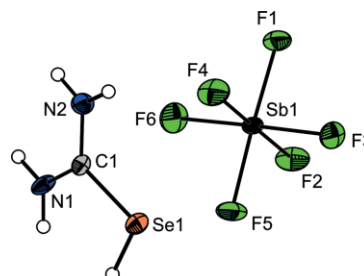


Figure 2. Asymmetric unit of $[(\text{H}_2\text{N})_2\text{CSeH}]^+[\text{SbF}_6]^-$ (thermal ellipsoids with 50 % probability).

The selenourea skeleton of the cation is nearly planar (sum of the bond angles around the C atom approximately 360°). The C1–Se1 bond of $1.900(1)\text{ \AA}$ is elongated compared to the starting material [$1.873(6)\text{ \AA}$].^[15] The two C–N bonds of $1.303(7)$ and $1.306(7)\text{ \AA}$ as well as the bond angles around the C1 atom stay approximately constant compared to the ones observed in selenourea.^[15] The Sb–F bonds of the slightly distorted octahedral $[\text{SbF}_6]^-$ anion are in the range between $1.859(4)$ and $1.876(3)\text{ \AA}$ which is typical for Sb–F bonds in $[\text{SbF}_6]^-$ anions.^[16–18]

In the solid state the cations and anions are linked via weak N(H)⋯F donor–acceptor interactions in the range between $2.887(6)\text{ \AA}$ and $3.318(6)\text{ \AA}$. Furthermore a Se⋯F contact with a donor–acceptor distance of $2.90(1)\text{ \AA}$ which is below the sum of the van der Waals radii [3.30 \AA]^[19] is observed. (Figure 3) A comparable Se⋯F contact distance [2.74 \AA] was observed in the crystal structure of $[\text{SeF}_3]^+[\text{Nb}_2\text{F}_{11}]^-$.^[20]

Table 2. Bond lengths (Å) and bond angles (°) of $(\text{H}_2\text{N})_2\text{CSe}^{15}$, $[(\text{H}_2\text{N})_2\text{CSeH}]^+[\text{SbF}_6]^-$ and the calculated $[(\text{H}_2\text{N})_2\text{CSeH}]^{+[\text{a}]}$.

	$(\text{H}_2\text{N})_2\text{CSe}^{15}$	$[(\text{H}_2\text{N})_2\text{CSeH}]^+[\text{SbF}_6]^-$	$[(\text{H}_2\text{N})_2\text{CSeH}]^{+[\text{a}]}$
Bond lengths (Å)			
C1–N1	1.322(7)	1.303(7)	1.328
C1–N2	1.322(7)	1.306(7)	1.329
C1–Se1	1.873(6)	1.900(1)	1.899
Se1–H3			1.462
Bond angles (°)			
N1–C1–N2	118.6(4)	121.8(5)	121.0
N1–C1–Se1	120.7(5)	121.6(6)	122.0
N2–C1–Se1	120.7(5)	116.6(4)	117.0
C1–Se1–H3			93.0
Donor–acceptor distances (Å)			
N1–(H1A)⋯F5		2.942(5)	
N1–(H1B)⋯F2		2.938(6)	
Se1⋯F1		2.90(1)	
N2–(H2A)⋯F3		3.223(5)	
N2–(H2A)⋯F5		3.318(6)	
N2–(H2B)⋯F3		2.887(6)	
Donor–acceptor angle (°)			
C1–Se1⋯F1		164.2(2)	

[a] Calculated on the PBEPBE/6-311G++(3pd,3df) level of theory.

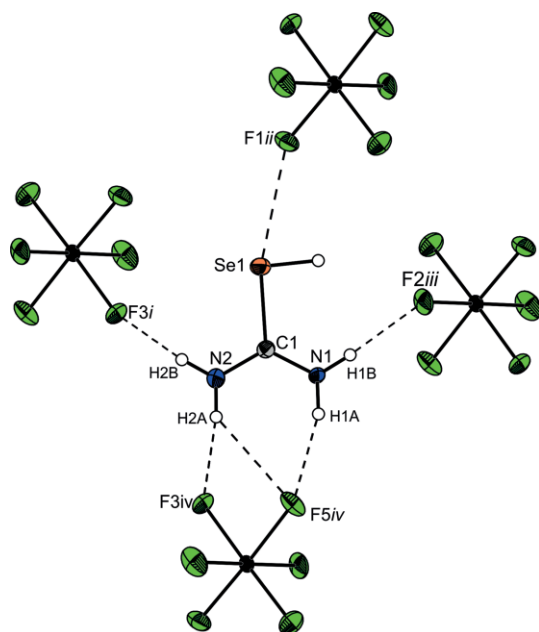


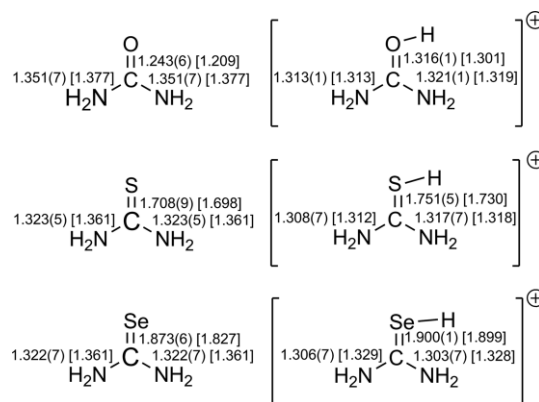
Figure 3. Cation-anion contacts in $[(\text{H}_2\text{N})_2\text{CSeH}]^+[\text{SbF}_6]^-$ (thermal ellipsoids with 50 % probability). Donor-acceptor interactions are represented as dashed lines. Symmetry codes: *i*: 1 - *x*, 2 - *y*, 1 - *z*; *ii*: *x*, 1 + *y*, *z*; *iii*: 1 - *x*, 2 - *y*, -*z*; *iv*: 1 + *x*, *y*, *z*.

Theoretical Section

The quantum chemical calculations were carried out on the PBEPBE/6-331G++(3df, 3pd) level of theory. For the support of the vibrational assignment gas-phase optimizations of $[(\text{H}_2\text{N})_2\text{CSeH}]^+$ and $[(\text{D}_2\text{N})_2\text{SeD}]^+$ and the corresponding starting material were carried out.

The experimentally observed N–H stretching vibrations are notably overestimated by the calculation which can be explained by the occurrence of the above mentioned N(H)⋯F donor–acceptor interactions in the solid state.

A comparison of experimentally and quantum chemically calculated structures of urea, thiourea and selenourea and their monoprotonated species are shown in Scheme 1. The protonation of urea leads to a significant elongation of the CO bond length and to a shortening of the CN bonds which is due to a lower resonance stabilization compared to the neutral compound.^[10] This effect is considerably weaker in the order thiourea^[10] and selenourea, where the protonation displays a decreasing influence on the bond lengths.



Scheme 1. Comparison of the experimentally observed and quantum chemically calculated structures of urea,^[21] thiourea,^[22] and selenourea as well as their monoprotonated species $\{[(\text{H}_2\text{N})_2\text{COH}]^+,^{[10]}$ $[(\text{H}_2\text{N})_2\text{CSH}]^{+[10]}$ and $[(\text{H}_2\text{N})_2\text{CSeH}]^+\}$. Calculated values in parentheses.

As stated in the crystallographic section, the observed Se⋯F distance is below the sum of the van der Waals radii. The most prominent representatives of such kind of interactions are those between halogen atoms, known as halogen bond.^[23] These

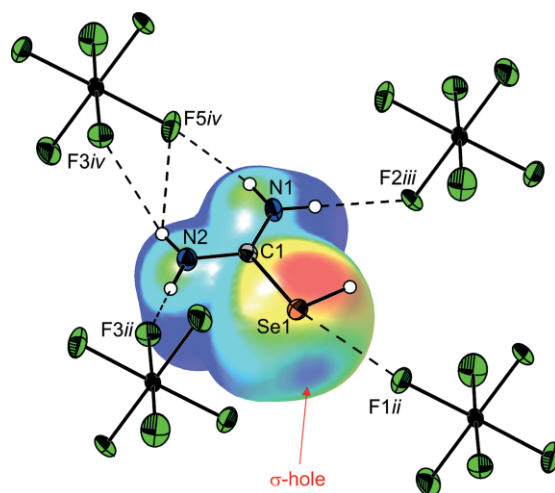


Figure 4. Cation-anion contacts in $[(\text{H}_2\text{N})_2\text{CSeH}]^+[\text{SbF}_6]^-$ (thermal ellipsoids with 50 % probability). Donor-acceptor interactions are represented as dashed lines. In the background of the cation an electrostatic potential (ESP) map is superimposed as a color scale ranging from 0.145 a.u. (red) and 0.210 a.u. (blue); isoval. = 0.001. Symmetry codes: *i*: 1 - *x*, 2 - *y*, 1 - *z*; *ii*: *x*, 1 + *y*, *z*; *iii*: 1 - *x*, 2 - *y*, -*z*; *iv*: 1 + *x*, *y*, *z*.

highly directed interactions are based on inhomogeneous charge distributions on the scope of the atoms leading to so-called σ -holes in the extension of the covalent bond.^[24] The concept of σ -hole bonds can also be expanded to divalent group VI atoms.^[25] This prompted us to perform a calculation of the electrostatic potential map (ESP) of the protonated selenourea. In accordance with the σ -hole concept we found a positive local maximum (0.170 a.u.) located approximately on the extension of the C–Se bond. The gas-phase optimization of the $[(\text{H}_2\text{N})_2\text{CSeH}]^+$ cation and its electrostatic potential (ESP) map are shown in Figure 4.

Conclusions

In this work the reaction behavior of selenourea in the binary superacidic systems XF/MF_5 ($X = \text{H}, \text{D}$; $M = \text{As}, \text{Sb}$) is reported. The reactions employing a selenourea to Lewis acid ratio of 1:1 leads to salts of the type $[(X_2\text{N})_2\text{CSeX}]^+[\text{MF}_6]^-$ which were characterized by low temperature vibrational spectroscopy and in the case of $[(\text{H}_2\text{N})_2\text{CSeH}]^+[\text{SbF}_6]^-$ by a single-crystal X-ray diffraction for the first time. In case of the utilization of several equivalents of Lewis acids with respect to selenourea a Se, N -diprotation was not detected.

Experimental Section

Caution! The hydrolysis of the investigated compounds cause the formation of HF. Safety precautions should be taken while handling these compounds.

Apparatus and Materials: In the course of this study all reactions were performed in FEP/PFA reactors equipped with stainless steel valves using standard Schlenk techniques at a stainless-steel vacuum line. The reactors and the stainless-steel vacuum line were dried with fluorine prior to use. The obtained compounds were characterized by single-crystal X-ray diffraction, low temperature IR and Raman spectroscopy as well as quantum chemical calculations. For the single-crystal X-ray diffraction study, which was performed at a temperature of 123(2) K, an Oxford Xcalibur3 diffractometer equipped with a Spellman generator (50 kV, 40 mA), Mo- K_α radiation ($\lambda = 0.7107 \text{ \AA}$) and a KappaCCD detector was used. For the data collection the CrysAlis CCD software^[26] and for its reduction the CrysAlis RED software^[27] was employed. The solution and refinement was carried out with the programs SHELXS-97^[28] and SHELXL-97^[29] implemented in the WinGX software package^[30] and finally validated with the PLATON software.^[31] The Scale 3 ABSPACK multi scan method^[32] was utilized for the absorption correction. In Table S2 (Supporting Information) crystal data and structure refinement for $[(\text{H}_2\text{N})_2\text{CSeH}]^+[\text{SbF}_6]^-$ are summarized. Low temperature IR spectroscopic investigations were performed in the range between 350 and 4000 cm^{-1} with a Bruker Vertex-80V FTIR spectrometer using a cooled cell where small amounts of the samples were placed on a CsBr single-crystal plate. Low temperature Raman measurements were carried out with a Bruker MultiRAM FT-Raman spectrometer equipped with a Nd:YAG laser (maximum excitation 1000 mW/wavelength $\lambda = 1064 \text{ nm}$) in the range between 250 and 4000 cm^{-1} . For quantum-chemical calculations the Gaussian09 package^[33] was employed using the PBE1PBE density functional approach with the basis set 6-311G++(3pd, 3df). The starting material Selenourea (abcr) was used as received. SbF_5 (Merck) was triple distilled prior to use. AsF_5 was synthesized from the elements and

purified by several condensations. HF (Linde) was dried with fluorine for several weeks in a stainless steel pressure cylinder prior to use. DF was synthesized from dried CaF_2 and D_2SO_4 .

CCDC 1831457 {for $[(\text{H}_2\text{N})_2\text{CSeH}]^+[\text{SbF}_6]^-$ contains the supplementary crystallographic data for this paper) contains the supplementary crystallographic data for this paper. These data can be obtained free of charge from The Cambridge Crystallographic Data Centre.

Synthesis of $[(X_2\text{N})_2\text{CSeX}]^+[\text{AsF}_6]^-$ ($X = \text{H}, \text{D}$): 50 mg (0.41 mmol, 1 equiv.) Selenourea was placed into a reactor (FEP tube) under dry nitrogen atmosphere. Then a large excess (ca. 1 mL) of anhydrous hydrogen fluoride or anhydrous deuterium fluoride was condensed at $-196 \text{ }^\circ\text{C}$ into the reactor followed by 70 mg (0.41 mmol, 1 equiv.) of arsenic pentafluoride. The reaction mixture then was warmed up to $-60 \text{ }^\circ\text{C}$ for a time period of 10 min and afterwards cooled down to $-78 \text{ }^\circ\text{C}$. At this temperature excess anhydrous hydrogen fluoride or anhydrous deuterium fluoride was removed in dynamic vacuum for a time period of 14 h. A colorless precipitate was formed.

Synthesis of $[(X_2\text{N})_2\text{CSeX}]^+[\text{SbF}_6]^-$ ($X = \text{H}, \text{D}$): 100 mg (0.46 mmol, 1 equiv.) antimony pentafluoride followed by an excess (ca. 1 mL) of anhydrous hydrogen fluoride or anhydrous deuterium fluoride were condensed at $-196 \text{ }^\circ\text{C}$ into a reactor (FEP tube). Afterwards 57 mg (0.46 mmol, 1 equiv.) selenourea was added under a dry nitrogen atmosphere. The reaction mixture was then warmed up to $-60 \text{ }^\circ\text{C}$ for 10 min. Then the colorless solution was cooled down to $-78 \text{ }^\circ\text{C}$ where the excess of HF or DF was removed in dynamic vacuum for a time period of 14 h. A colorless precipitate was formed. For the growth of single-crystals the reaction mixture was stored for several weeks at $-60 \text{ }^\circ\text{C}$ and then the solvent was carefully removed.

Supporting Information (see footnote on the first page of this article): The Supporting Information contains the complete Table of the experimentally observed vibrational frequencies (in cm^{-1}) of $[\text{H}_2\text{NC}(\text{SeH})\text{NH}_2]^+[\text{AsF}_6]^-$, $[\text{D}_2\text{NC}(\text{SeD})\text{ND}_2]^+[\text{AsF}_6]^-$ and $[\text{H}_2\text{NC}(\text{SeH})\text{NH}_2]^+[\text{SbF}_6]^-$ and calculated vibrational frequencies (in cm^{-1}) of $[\text{H}_2\text{NC}(\text{SeH})\text{NH}_2]^+$ and $[\text{D}_2\text{NC}(\text{SeD})\text{ND}_2]^+$ (Table S1) as well as the crystal data and structure refinement for $[(\text{H}_2\text{N})_2\text{CSeH}]^+[\text{SbF}_6]^-$ (Table S2).

Acknowledgments

The authors gratefully acknowledge the financial support of the Deutsche Forschungsgemeinschaft (DFG), the Ludwig-Maximilians-Universität (LMU) München, and the F-Select GmbH.

Keywords: Selenourea · Superacidic systems · Selenium · Fluorine · Electrostatic interactions · Structure elucidation

- [1] E. Spinner, *Spectroch. Acta* **1959**, *15*, 95–109.
- [2] M. J. Janssen, *Spectrochim. Acta* **1961**, *17*, 475–485.
- [3] W. Kutzelnigg, R. Mecke, *Spectrochim. Acta* **1961**, *17*, 530–544.
- [4] R. V. G. Sundera-Rao, J. W. Turley, R. Pepinsky, *Acta Crystallogr.* **1957**, *10*, 435–436.
- [5] S. Harkema, D. Feil, *Acta Crystallogr., Sect. B* **1969**, *25*, 589–591.
- [6] D. Feil, W. Song Loong, *Acta Crystallogr., Sect. B* **1968**, *24*, 1334–1339.
- [7] T. Birchall, R. J. Gillespie, *Can. J. Chem.* **1963**, *41*, 2642–2650.
- [8] G. A. Olah, A. Burrichter, G. Rasul, K. O. Christe, G. K. S. Prakash, *J. Am. Chem. Soc.* **1997**, *119*, 4345–4352.
- [9] G. A. Olah, G. K. S. Prakash, G. Rasul, *J. Phys. Chem. C* **2008**, *112*, 7895–7899.
- [10] J. Axhausen, Dissertation **2013**, LMU Munich.

- [11] D. Kaur, P. Sharma, R. P. Kaur, M. Kaur, P. V. Bharatam, *J. Mol. Struct.* **2007**, *805*, 119–125.
- [12] D. Hadži, J. Kidrič, Ž. V. Knežević, B. Barlič, *Spectroch.* **1976**, *A32*, 693–704.
- [13] A. C. Dhayagude, N. Maiti, A. K. Debnath, S. S. Joshi, S. Kapoor, *RSC Adv.* **2016**, *6*, 17405–17414.
- [14] J. Weidlein, U. Müller, K. Dehnicke, *Schwingungsspektroskopie, Vol. 2nd ed.*, Georg Thieme Verlag, Stuttgart, Germany, **1988**.
- [15] Z. Luo, Z. Dauter, *PLoS ONE* **2017**, *12*, e0171740.
- [16] R. Seelbinder, N. R. Goetz, J. Weber, R. Minkwitz, A. J. Kornath, *Chem. Eur. J.* **2010**, *16*, 1026–1032.
- [17] Z. Mazej, E. Goresnik, *Z. Kristallogr.* **2017**, *232*, 339–347.
- [18] J. F. Lehmann, S. Riedel, G. J. Schrobilgen, *Inorg. Chem.* **2008**, *47*, 8343–8356.
- [19] A. Bondi, *J. Phys. Chem.* **1964**, *68*, 441–451.
- [20] A. J. Edwards, G. R. Jones, *J. Chem. Soc. A* **1969**, 2858–2861.
- [21] J. E. Worsham, H. A. Levy, S. W. Peterson, *Acta Crystallogr.* **1957**, *10*, 319–323.
- [22] A. Vijay, D. N. Sathyanarayana, *Spectrochim. Acta* **1993**, *A49*, 1565–1574.
- [23] P. Metrangolo, G. Resnati, *Halogen Bonding: Fundamentals and Applications*, Springer-Verlag, **2007**.
- [24] J. Halli, G. Manolikakes, *Nachr. Chem.* **2016**, *64*, 131–134.
- [25] J. S. Murray, P. Lane, T. Clark, P. Politzer, *J. Mol. Model.* **2007**, *13*, 1033–1038.
- [26] *CrysAlisCCD*, Version 1.171.35.11 (release 16–05–2011 CrysAlis 171.NET), Oxford Diffraction Ltd, UK, **2011**.
- [27] *CrysAlisRED*, Version 1.171.35.11 (release 16–05–2011 CrysAlis 171.NET), Oxford Diffraction Ltd., UK, **2011**.
- [28] G. M. Sheldrick, *SHELXS-97*, Program for Crystal Structure Solution, University of Göttingen, Germany, **1997**.
- [29] G. M. Sheldrick, *SHELXL-97*, Program for the Refinement of Crystal Structures, University of Göttingen, Germany, **1997**.
- [30] L. Farrugia, *J. Appl. Crystallogr.* **1999**, *32*, 837–838.
- [31] A. L. Spek, *PLATON*, A Multipurpose Crystallographic Tool, U. Utrecht University, The Netherlands, 1999. **1999**.
- [32] *SCALE3 ABSPACK*, An Oxford Diffraction Program, O. Diffraction, Ltd., UK, **2005**.
- [33] M. J. Frisch, G. W. Trucks, H. B. Schlegel, G. E. Scuseria, M. A. Robb, J. R. Cheeseman, G. Scalmani, V. Barone, B. Mennucci, G. A. Petersson, H. Nakatsuji, M. Caricato, X. Li, H. P. Hratchian, A. F. Izmaylov, J. Bloino, G. Zheng, J. L. Sonnenberg, M. Hada, M. Ehara, K. Toyota, R. Fukuda, J. Hasegawa, M. Ishida, T. Nakajima, Y. Honda, O. Kitao, H. Nakai, T. Vreven, J. A. Montgomery Jr., J. E. Peralta, F. Ogliaro, M. Bearpark, J. J. Heyd, E. Brothers, K. N. Kudin, V. N. Staroverov, R. Kobayashi, J. Normand, K. Raghavachari, A. Rendell, J. C. Burant, S. S. Iyengar, J. Tomasi, M. Cossi, N. Rega, J. M. Millam, M. Klene, J. E. Knox, J. B. Cross, V. Bakken, C. Adamo, J. Jaramillo, R. Gomperts, R. E. Stratmann, O. Yazyev, A. J. Austin, R. Cammi, C. Pomelli, J. W. Ochterski, R. L. Martin, K. Morokuma, V. G. Zakrzewski, G. A. Voth, P. Salvador, J. J. Dannenberg, S. Dapprich, A. D. Daniels, Ö. Farkas, J. B. Foresman, J. V. Ortiz, J. Cioslowski, D. J. Fox, *Gaussian 09, Revision A.1*, Gaussian, Inc., Wallingford CT, **2009**.

Received: August 2, 2018



Supporting Information

Preparation and Structure of Protonated Selenourea

Dominik Leitz, Alan Virmani, Yvonne Morgenstern, Florian Zischka, and
Andreas J. Kornath*

[ejic201800933-sup-0001-SupMat.pdf](#)

Table S1. Experimental vibrational frequencies [cm^{-1}] of $[(\text{H}_2\text{N})_2\text{CSeH}]^+[\text{AsF}_6]^-$, $(\text{H}_2\text{N})_2\text{CSe}$, $[(\text{D}_2\text{N})_2\text{CSeD}]^+[\text{AsF}_6]^-$ and $(\text{D}_2\text{N})_2\text{CSe}$ as well as calculated vibrational frequencies [cm^{-1}] of $[(\text{H}_2\text{N})_2\text{CSeH}]^+$, $(\text{H}_2\text{N})_2\text{CSe}$, $[(\text{D}_2\text{N})_2\text{CSeD}]^+$ and $(\text{D}_2\text{N})_2\text{CSe}$.

$[(\text{H}_2\text{N})_2\text{CSeH}]^+[\text{AsF}_6]^-$	$[(\text{H}_2\text{N})_2\text{CSeH}]^+$	$(\text{H}_2\text{N})_2\text{CSe}$	$(\text{H}_2\text{N})_2\text{CSe}$	$[(\text{D}_2\text{N})_2\text{CSeD}]^+[\text{AsF}_6]^-$	$[(\text{D}_2\text{N})_2\text{CSeD}]^+$	$(\text{D}_2\text{N})_2\text{CSe}$	$(\text{D}_2\text{N})_2\text{CSe}$	Assignment
IR / Raman	calcd. ^[a]	IR / Raman	calcd. ^[a]	IR / Raman	calcd. ^[a]	IR / Raman	calcd. ^[a]	[b]
	3601		3610	2607/ 2609	2667	2537	2667	$\nu_{\text{as}}(\text{NX}_2)$
3425*	3592	3258 / 3277	3608	2595	2661	2501	2663	$\nu_{\text{as}}(\text{NX}_2)$
3378	3481	3172	3473	2526/ 2519	2520	2380	2508	$\nu_s(\text{NX}_2)$
3270 / 3268	3471	3148	3465	2466	2510	2338 / 2344	2500	$\nu_s(\text{NX}_2)$
2342 / 2350	2310	–	–	1686 / 1692	1644	–	–	$\nu(\text{SeX})$
1708 / 1708	1642	1605 / 1609	1568	1595	1587	1354 / 1356	1438	$\nu_{\text{as}}(\text{CN}_2)$
1636 / 1647	1626	1629	1590	1209 / 1192	1168	1186	1142	$\delta(\text{NX}_2)$
1541 / 1549	1531	1483	1413		1141	/ 1140	1109	$\delta(\text{NX}_2)$
1419 / 1418	1383	1400 / 1400	1343	1401 / 1404	1374		1321	$\nu_s(\text{CN}_2)$
1116	1079	1087	1040		902	910 / 916	875	$\delta(\text{NX}_2)$
959	1031	1041 / 1041	1030	794	799	814 / 822	797	$\delta(\text{NX}_2)$
859 / 860	812	–	–	594	623		–	$\delta(\text{CSeX})$
	647		592		551		407	$\delta(\text{CN}_2)$
633	617	640	637	544 / 546	535	552 / 563	571	$\nu(\text{CSe})$
507 / 502	503	520	553	458	391		407	$\delta(\text{CN}_2)$
	482	342	342		365		262	$\delta(\text{NX}_2)$
	447	387 / 390	461	350	352	/ 359	356	$\delta(\text{NX}_2)$
385 / 380	423	237	292		301		216	$\tau(\text{NX}_2)$
336	363		382	307	331	/ 316	338	$\delta(\text{CN}_2)$
	307		326		272	/ 236	297	$\delta(\text{NCSe})$
	167	–	–		121	–	–	$\delta(\text{CSeX})$
699	–	–	–	699	–	–	–	$[\text{AsF}_6]^-$
680	–	–	–	680	–	–	–	$[\text{AsF}_6]^-$
576	–	–	–	575	–	–	–	$[\text{AsF}_6]^-$
395	–	–	–	375	–	–	–	$[\text{AsF}_6]^-$
363	–	–	–	370	–	–	–	$[\text{AsF}_6]^-$

[a] Calculated at the PBE/6-311G++(3df,3dp) level of theory. IR intensity in [km/mol] and Raman scattering activities in [$\text{\AA}^4/\mu$]. Abbreviations for IR intensities: ν = very, s = strong, m = medium, w = weak. Experimental Raman scattering activity is stated to a scale of 1 to 100. [b] $X = \text{H}, \text{D}$. *observed in the IR spectra of $[(\text{D}_2\text{N})_2\text{CSeD}]^+[\text{AsF}_6]^-$.

Table S2. Experimental vibrational frequencies [cm^{-1}] of $[(\text{H}_2\text{N})_2\text{CSeH}]^+[\text{AsF}_6]^-$, and $[(\text{H}_2\text{N})_2\text{CSeH}]^+[\text{SbF}_6]^-$, $[(\text{D}_2\text{N})_2\text{CSeD}]^+[\text{AsF}_6]^-$ and calculated vibrational frequencies [cm^{-1}] of $[(\text{H}_2\text{N})_2\text{CSeH}]^+$ and $[(\text{D}_2\text{N})_2\text{CSeD}]^+$.

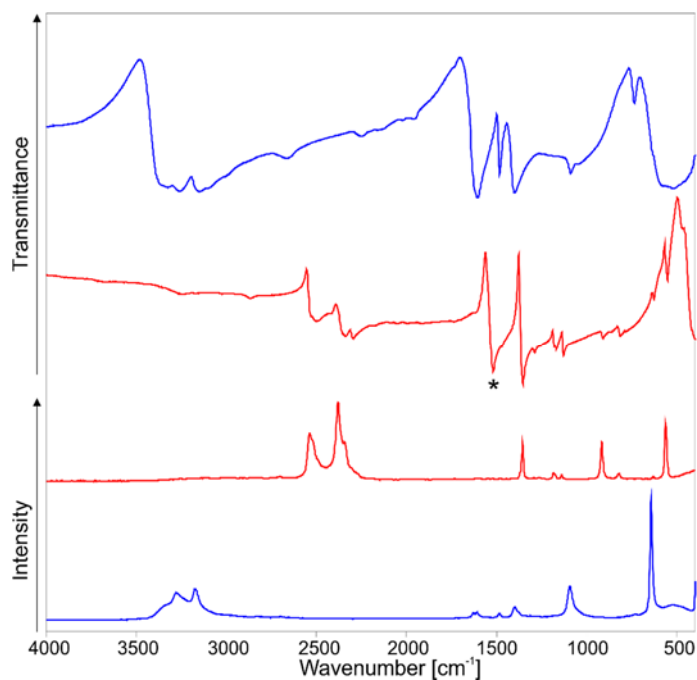
$[(\text{H}_2\text{N})_2\text{CSeH}]^+[\text{AsF}_6]^-$		$[(\text{H}_2\text{N})_2\text{CSeH}]^+[\text{SbF}_6]^-$		$[(\text{H}_2\text{N})_2\text{CSeH}]^+$	$[(\text{D}_2\text{N})_2\text{CSeD}]^+[\text{AsF}_6]^-$		$[(\text{D}_2\text{N})_2\text{CSeD}]^+$	Assignment
IR	Raman	IR	Raman	calc. ^[a] (IR/Raman)	IR	Raman	calc. ^[a] (IR/Raman)	[b]
				3601 (91/41)		2609 (12)	2667 (55/31)	$\nu_{\text{as}}(\text{NX}_2)$
3425 (s)*				3592(98/39)	2607 (m)	2595 (12)	2661 (47/13)	$\nu_{\text{as}}(\text{NX}_2)$
	3378 (9)		3375 (3)	3481 (124/233)	2526 (m)	2519 (4)	2520 (77/99)	$\nu_{\text{s}}(\text{NX}_2)$
3270 (s)	3268 (5)		3264 (2)	3471 (183/29)		2466 (34)	2510 (157/11)	$\nu_{\text{s}}(\text{NX}_2)$
2342 (w)	2350 (85)	2341 (w)	2346 (31)	2310 (3/11)	1686 (m)	1692 (48)	1644 (2/54)	$\nu(\text{SeX})$
1708 (m)	1708 (15)	1709 (m)	1709 (20)	1642 (343/1)	1595 (w)		1587 (231/1)	$\nu_{\text{as}}(\text{CN}_2)$
1636 (m)	1647 (3)	1648 (m)	1644 (2)	1626 (72/2)	1209 (m)	1192 (3)	1168 (6/1)	$\delta(\text{NX}_2)$
1541 (w)	1549 (11)	1547 (m)	1550 (5)	1531 (0/6)	1157 (m)	1164 (3)	1141 (33/2)	$\delta(\text{NX}_2)$
1419 (w)	1418 (10)	1405 (m)	1411 (8)	1383 (133/7)	1401 (m)	1404 (30)	1374 (169/9)	$\nu_{\text{s}}(\text{CN}_2)$
	1116 (18)	1116 (w)	1117 (8)	1079 (1/18)			902 (2/15)	$\delta(\text{NX}_2)$
	959 (4)	947 (m)	953 (2)	1031 (3/2)	794 (vw)		799 (1/2)	$\delta(\text{NX}_2)$
859 (vs)	860 (14)	858 (m)	859 (5)	812 (12/9)	594 (vw)		623 (2/3)	$\delta(\text{CSeX})$
				647 (3/0)			551 (4/3)	$\delta(\text{CN}_2)$
	633 (21)	633 (s)		617 (7/9)	544 (vw)	546 (8)	535 (8/7)	$\nu(\text{CSe})$
				503 (122/0)	458 (vw)		391 (31/0)	$\delta(\text{CN}_2)$
				482 (227/1)			365 (136/0)	$\delta(\text{NX}_2)$
507 (5)	502 (m)	506 (s)		447 (8/0)			352 (9/0)	$\delta(\text{NX}_2)$
		494 (2)		423 (5/2)		307 (5)	301 (2/2)	$\tau(\text{NX}_2)$
385 (s)	380 (28)	387 (s)	387 (15)	363 (4/5)		350 (14)	331 (5/3)	$\delta(\text{CN}_2)$
	336 (10)			307 (3/1)			272 (40/1)	$\delta(\text{NCSe})$
				167 (11/1)			121 (5/0)	$\delta(\text{CSeX})$
699 (m)			648 (64)		699 (vw)			$[\text{MF}_6]^-$
	680 (78)		571 (6)			680 (81)		$[\text{MF}_6]^-$
	576 (7)		279 (36)			575 (12)		$[\text{MF}_6]^-$
395 (vs)					395 (vs)			$[\text{MF}_6]^-$
	369 (40)					370 (40)		$[\text{MF}_6]^-$

[a] Calculated at the PBEPBE/6-311G++(3df,3dp) level of theory. IR intensity in [km/mol] and Raman scattering activities in [$\text{\AA}^4/\mu$]. Abbreviations for IR intensities: v = very, s = strong, m = medium, w = weak. Experimental Raman scattering activity is stated to a scale of 1 to 100. [b] X = H, D. *observed in the IR spectra of $[(\text{D}_2\text{N})_2\text{CSeD}]^+[\text{AsF}_6]^-$.

Table S3. Experimental and calculated vibrational frequencies (in cm^{-1}) of $(\text{H}_2\text{N})_2\text{CSe}$ and $(\text{D}_2\text{N})_2\text{CSe}$.

$(\text{H}_2\text{N})_2\text{CSe}$		$(\text{H}_2\text{N})_2\text{CSe}$	$(\text{D}_2\text{N})_2\text{CSe}$		$(\text{D}_2\text{N})_2\text{CSe}$	Assignment
IR	Raman	calcd. ^[a]	IR	Raman	calcd. ^[a]	[b]
		3610 (17/106)		2538 (42)	2667 (10/71)	$\nu_{\text{as}}(\text{NX}_2)$
3258 (s)	3277 (9)	3608 (58/47)	2501 (m)		2663 (29/31)	$\nu_{\text{as}}(\text{NX}_2)$
	3172 (26)	3474 (4/561)		2380 (91)	2508 (9/275)	$\nu_{\text{s}}(\text{NX}_2)$
3148 (s)		3465 (22/176)	2338	2344 (2)	2500 (33/82)	$\nu_{\text{s}}(\text{NX}_2)$
	1629 (1)	1590 (67/15)		1186 (7)	1142 (28/3)	$\delta(\text{NX}_2)$
1605 (m)	1609 (5)	1568 (236/3)	1356 (s)	1356 (44)	1438 (225/1)	$\nu_{\text{as}}(\text{CN}_2)$
1483 (m)		1413 (46/5)		1140 (4)	1109 (23/3)	$\delta(\text{NX}_2)$
1400 (m)	1400 (8)	1343 (244/16)	1293 (w)		1321 (328/12)	$\nu_{\text{s}}(\text{CN}_2)$
1087 (m)		1040 (47/3)	914 (w)	916 (44)	875 (8/8)	$\delta(\text{NX}_2)$
1041 (m)	1041 (3)	1030 (19/5)	814 (w)	822 (7)	797 (7/3)	$\delta(\text{NX}_2)$
	643 (100)	637 (6/27)	555 (m)	563 (63)	571 (5/22)	$\nu(\text{CSe})$
		592 (18/0)			571 (2/1)	$\delta(\text{CN}_2)$
520 (w)		553 (28/0)	384 (m)		407 (28/0)	$\delta(\text{CN}_2)$
		461 (10/1)		316 (3)	356 (16/1)	$\delta(\text{NX}_2)$
387 (m)	390 (88)	382 (10/4)			338 (0/3)	$\delta(\text{CN}_2)$
		342 (296/1)			262 (149/0)	$\delta(\text{NX}_2)$
		326 (3/0)		236 (65)	297 (12/0)	$\delta(\text{NCSe})$
	237 (11)	292 (107/2)			216 (57/1)	$\tau(\text{NX}_2)$

[a] Calculated at the PBE/6-311G++(3df,3dp) level of theory. IR intensity in $[\text{km}/\text{mol}]$ and Raman scattering activities in $[\text{\AA}^4/\mu]$. Abbreviations for IR intensities: ν = very, s = strong, m = medium, w = weak. Experimental Raman scattering activity is stated to a scale of 1 to 100. [b] $X = \text{H}, \text{D}$. *observed in the IR spectra of $[(\text{D}_2\text{N})_2\text{CSeD}]^+[\text{AsF}_6]^-$.

**Figure S1.** Vibrational spectra of $(\text{H}_2\text{N})_2\text{CSe}$ (blue) and $(\text{D}_2\text{N})_2\text{CSe}$ (red). * $\delta(\text{NH}_2)$ mode due to an incomplete H/D exchange.

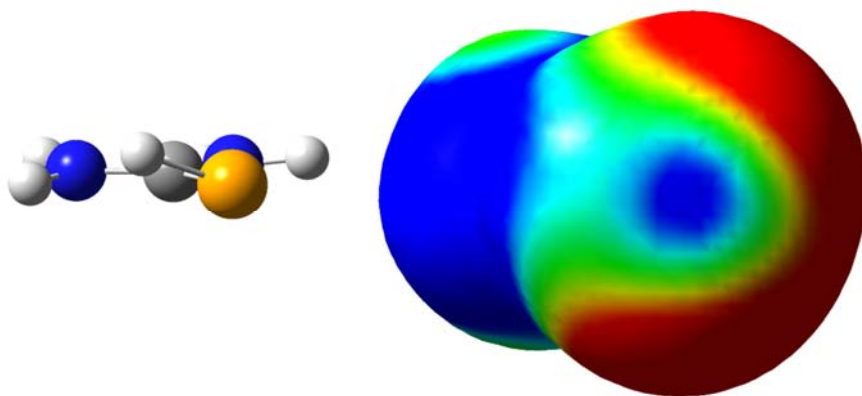


Figure S2. Quantum chemically calculated structure of the $[(\text{H}_2\text{N})_2\text{CSeH}]^+$ cation (left) and its electrostatic potential (ESP) map (right). Color scale ranging from 0.140 a.u. (red) and 0.0170 a.u. (blue); isoval. = 0.001.

Table S4. Crystal data and structure refinement for $[(\text{H}_2\text{N})_2\text{CSeH}]^+[\text{SbF}_6]^-$.

Empirical formula	$[(\text{H}_2\text{N})_2\text{CSeH}]^+[\text{SbF}_6]^-$
M_r	359.79
Crystal system	triclinic
Space Group	$P\bar{1}$
a [Å]	5.7372(6)
b [Å]	8.1135(7)
c [Å]	9.1404(9)
V [Å ³]	409.89(7)
Z	2
ρ_{calcd} , [gcm ⁻³]	2.915
μ [mm ⁻¹]	7.852
$\lambda_{\text{MoK}\alpha}$ [Å]	0.71073
$F(000)$	328
T [K]	123(2)
hkl range	-6:7; -10:9; -11:10
refl. measured	3072
refl. unique	1667
R_{int}	0.0365
parameters	104
$R(F)/wR(F^2)^a$	0.0401/0.0669
weighting scheme ^{b)}	0.0186
$S(\text{GoF})^c$	1.004
residual density [eÅ ⁻³]	1.027/-1.372
device type	Oxford XCalibur
solution/refinement	SHELXL-97 ^[14]
CCDC	1831457

a) $R_1 = \sum ||F_o| - |F_c|| / \sum |F_o|$; b) $wR_2 = [\sum [w(F_o^2 - F_c^2)^2] / \sum [w(F_o^2)]]^{1/2}$;
 $w = [\sigma_o^2(F_o^2) + (xP)^2 + yP]^{-1}$; $P = (F_o^2 + 2F_c^2) / 3$ c)
 $\text{GoF} = \{\sum [w(F_o^2 - F_c^2)^2] / (n-p)\}^{1/2}$ (n = number of reflexions;
 p = total number of parameters).

Supercacids

Structural Investigation of Thiourea Dioxide in Supercacids

Dominik Leitz,^[a] Alexander Nitzer,^[a] Yvonne Morgenstern,^[a] Florian Zischka,^[a] and Andreas J. Kornath*^[a]

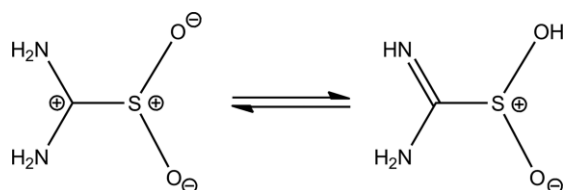
Dedicated to Professor Ingo-Peter Lorenz on the occasion of his 75th birthday

Abstract: In this study a vibrational spectroscopic investigation of thiourea dioxide [(H₂N)₂CSO₂] in the superacidic systems XF/MF₅ (X = H, D; M = As, Sb) as well as HF/GeF₄ is presented. The formed salts [(X₂N)₂CS(OX)₂]²⁺2[MF₆]⁻ are characterized by low temperature vibrational spectroscopy. In the case of

2[(H₂N)₂CS(OH)₂]²⁺[Ge₄F₂₀]⁴⁻·4HF a single-crystal X-ray structure is reported. The salt crystallizes in the triclinic space group P $\bar{1}$ with one formula unit per unit cell. The results are discussed together with quantum-chemical calculations at the PBE1PBE/6-311G++(3df, 3pd) level of theory.

Introduction

Thiourea dioxide (TDO), (H₂N)₂CSO₂, is a widely used bleaching agent in textile industry.^[1,2] In 1910 it was first synthesized by *Barnett* through the oxidation of thiourea with hydrogen peroxide.^[3] *Krug* mentioned in another study that an origin of its reducing power is due to the occurrence of two tautomeric forms (H₂N)₂CSO₂ (TDO) and H₂NC(NH)CSO(OH) (formamidine sulfinic acid/FSA).^[4] (Scheme 1).



Scheme 1. Tautomerism of thiourea dioxide (TDO) (left) and formamidine sulfinic acid (FSA) (right).

In aqueous alkaline solution (pK_a ≈ 9.5) TDO was reported to decompose under the formation of hydrogen sulfoxylate, [HSO₂]⁻, to which its reducing properties are attributed.^[1]

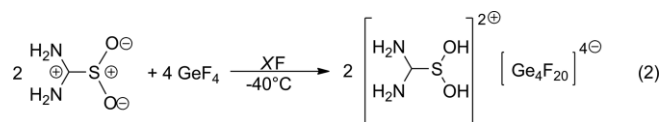
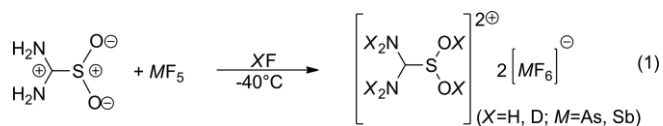
Sullivan and *Hargreaves* reported the crystal structure of the title compound for the first time, concluding that the structure in the solid state is in fact the TDO form with two equally long C–N bonds, but an unusually long C–S bond.^[5] This finding was confirmed by two additional crystallographic and theoretical studies.^[6,7] Based on thermochemical data and quantum chemical calculations *Denk* et al. described TDO as a Lewis acid-base complex of diaminocarbene and SO₂.^[8] *Kis* et al. performed a theoretical study in order to elucidate the structure of TDO.^[9]

The authors concluded that at least *in vacuo* H₂NC(NH)CSO(OH) (FSA) appears to be the slightly more stable tautomer. However, TDO is stabilized by a supramolecular arrangement and in aqueous solution FSA is the more stable tautomer. As a further study *Hawkes* et al. investigated the title compound in the solid-state as well as in solutions with different pH values by Fourier transform infrared (FT-IR) spectroscopy, finding no proton on the SO₂ moiety under any conditions and therefore concluded the group to be a sulfinate.^[10]

Despite being a well characterized compound, so far no data of a protonated TDO were reported. This prompted us to carry out a study of the title compound in binary superacidic systems with the aim to isolate and structurally characterize salts containing a protonated TDO species.

Results and Discussion

Thiourea dioxide (TDO) was reacted in the binary superacidic systems XF/MF₅ (X = H, D; M = As, Sb) and HF/GeF₄ using two equivalents of the Lewis acid, as presented in Equation (1) and Equation (2). In the first step the corresponding superacidic solutions were homogenized at –20 °C and afterwards frozen at –196 °C. Then TDO was added to the frozen mixture and warmed up to –40 °C, where the protonation reaction took place.



[a] Department Chemie, Ludwig-Maximilians-Universität München, Butenandtstr. 5–13, 81377 Munich, Germany
E-mail: andreas.kornath@cup.uni-muenchen.de

Supporting information and ORCID(s) from the author(s) for this article are available on the WWW under <https://doi.org/10.1002/ejic.201801298>.

Attempts to prepare salts containing the *O*-monoprotonated species led to mixtures containing both, the *O,O'*-diprotonated species and the starting material.

Vibrational Spectroscopy

The low temperature vibrational spectra of $[(\text{H}_2\text{N})_2\text{CS}(\text{OH})_2]^{2+} \cdot 2[\text{SbF}_6]^-$, $[(\text{H}_2\text{N})_2\text{CS}(\text{OD})_2]^{2+} \cdot 2[\text{AsF}_6]^-$ and $(\text{H}_2\text{N})_2\text{CSO}_2$ are shown in Figure 1. Selected observed frequencies of the protonated species are summarized together with the quantum chemical calculated frequencies of $[(\text{X}_2\text{N})_2\text{CS}(\text{OX})_2]^{2+}$ ($X = \text{H}, \text{D}$) and their

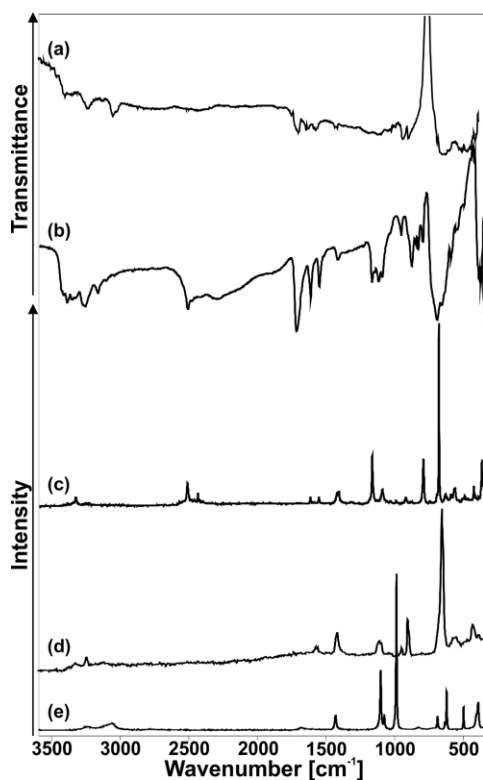


Figure 1. Low-temperature vibrational spectra of $[(\text{H}_2\text{N})_2\text{CS}(\text{OH})_2]^{2+} \cdot 2[\text{SbF}_6]^-$: (a) IR spectrum, (d) Raman spectrum; $[(\text{H}_2\text{N})_2\text{CS}(\text{OD})_2]^{2+} \cdot 2[\text{AsF}_6]^-$: (b) IR spectrum, (c) Raman spectrum; $(\text{H}_2\text{N})_2\text{CSO}_2$: (e) Raman spectrum.

Table 1. Selected experimental vibrational frequencies [cm^{-1}] of $[(\text{H}_2\text{N})_2\text{CS}(\text{OH})_2]^{2+} \cdot 2[\text{AsF}_6]^-$, and $[(\text{H}_2\text{N})_2\text{CS}(\text{OH})_2]^{2+} \cdot 2[\text{SbF}_6]^-$, $[(\text{D}_2\text{N})_2\text{CS}(\text{OD})_2]^{2+} \cdot 2[\text{AsF}_6]^-$ and calculated vibrational frequencies [cm^{-1}] of $[(\text{H}_2\text{N})_2\text{CS}(\text{OH})_2]^{2+}$ and $[(\text{D}_2\text{N})_2\text{CS}(\text{OD})_2]^{2+}$.

$[(\text{H}_2\text{N})_2\text{CS}(\text{OH})_2]^{2+} \cdot 2[\text{AsF}_6]^-$		$[(\text{H}_2\text{N})_2\text{CS}(\text{OH})_2]^{2+} \cdot 2[\text{SbF}_6]^-$		$[(\text{H}_2\text{N})_2\text{CS}(\text{OH})_2]^{2+}$	$[(\text{D}_2\text{N})_2\text{CS}(\text{OD})_2]^{2+} \cdot 2[\text{AsF}_6]^-$		$[(\text{D}_2\text{N})_2\text{CS}(\text{OD})_2]^{2+}$	Assignment [b]
IR	Raman	IR	Raman	calcd. ^[a] (IR/Raman)	IR	Raman	calcd. ^[a] (IR/Raman)	
3401 (m)		3411 (w)		3633 (543/121)			2683 (152/20)	ν_{17} A' $\nu_{\text{S}}(\text{OX})$
3397 (w)		3400 (w)		3619 (497/51)	2576 (m)	2578 (1)	2675 (61/8)	ν_{17} A'' $\nu_{\text{S}}(\text{OX})$
3333 (w)	3333 (3)	3337 (w)		3618 (218/37)	2517 (m)	2520 (12)	2648 (289/57)	ν_{22} A' $\nu_{\text{S}}(\text{NX}_2)$
				3613 (68/5)	2448 (w)	2444 (5)	2636 (231/21)	ν_{18} A'' $\nu_{\text{S}}(\text{NX}_2)$
3231 (s)	3237 (2)	3249 (m)	3240 (3)	3515 (297/171)			2551 (143/76)	ν_{32} A' $\nu_{\text{S}}(\text{NX}_2)$
3118 (s)				3491 (393/19)			2528 (307/7)	ν_{19} A'' $\nu_{\text{S}}(\text{NX}_2)$
1727 (s)		1714 (s)		1792 (375/0)	1720 (m)	1706 (1)	1766 (253/1)	ν_{20} A'' $\nu_{\text{S}}(\text{CN}_2)$
1431 (w)	1427 (14)	1421 (w)	1424 (15)	1433 (29/13)	1423 (w)	1404 (41)	1431 (43/10)	ν_{25} A' $\nu_{\text{S}}(\text{CN}_2)$
968 (vw)	953 (2)	945 (w)		965 (231/2)	961 (m)	966 (9)	976 (119/4)	ν_{24} A'' $\nu_{\text{S}}(\text{SO}_2)$
908 (vw)	905 (9)	904 (w)	908 (13)	915 (79/13)			913 (94/13)	ν_{8} A' $\nu_{\text{S}}(\text{SO}_2)$
630 (w)				645 (4/0)		573 (23)	560 (17/6)	ν_{25} A'' $\nu(\text{SC})$

[a] Calculated at the PBE1PBE/6-11G++(3df,3pd) level of theory. IR intensity in [km/mol] and Raman scattering activities in [$\text{\AA}^4/\mu$]. Abbreviations for IR intensities: ν = very, s = strong, m = medium, w = weak. Experimental Raman scattering activity is stated to a scale of 1 to 100. [b] $X = \text{H}, \text{D}$; $M = \text{As}, \text{Sb}$.

assignments in Table 1. The complete table (Table S1) as well as the assignment of the starting material (Table S2) are provided in the Supporting Information. For the $[(\text{X}_2\text{N})_2\text{CS}(\text{OX})_2]^{2+}$ cation with C_s symmetry 30 fundamental vibrational modes are expected, showing both IR and Raman activity ($\Gamma_{\text{vib}} = 16 A' + 14 A''$). A confirmation of the *O,O'*-diprotonation is the occurrence of the OH stretching vibration at around 3400 cm^{-1} and in the case of the *D*-isotopomeric species at around 2577 cm^{-1} , which is in fair agreement with the Teller-Redlich rule for an H/D isotopomeric effect.^[11] The stretching modes of the amino groups are observed at around 3335 and 3240 cm^{-1} and are slightly blue-shifted compared to the starting material. Due to the *O,O'*-diprotonation the S–O stretching vibrations are observed at around 950 cm^{-1} (antisymmetric) and 905 cm^{-1} (symmetric) and are red-shifted by approximately 160 and 120 cm^{-1} compared to $(\text{H}_2\text{N})_2\text{CSO}_2$. The C–S stretching vibration is detected at 630 cm^{-1} and is blue-shifted by approximately 10 cm^{-1} , which is consistent with the shortening of the S–C bond due to the protonation (see crystallographic section below). For the octahedral anions $[\text{AsF}_6]^-$ and $[\text{SbF}_6]^-$, respectively, more vibrations are observed than expected, which is due to solid-state effects causing a lower symmetry.

Crystal Structure of $2[(\text{H}_2\text{N})_2\text{CS}(\text{OH})_2]^{2+} \cdot [\text{Ge}_4\text{F}_{20}]^{4-} \cdot 4 \text{HF}$

The salt crystallizes in the triclinic space group $P\bar{1}$ with one formula unit per unit cell. In Figure 2 a formula unit is shown. Crystal data and structure refinement are provided in the Supporting Information (Table S3). Selected bond lengths, bond angles, torsion angles and donor–acceptor distances are summarized in Table 2. The $[(\text{H}_2\text{N})_2\text{CS}(\text{OH})_2]^{2+}$ cation consists of a nearly planar thiourea group. The sulfur atom is coordinated in a trigonal-pyramidal manner. The torsion angles (see Table 2) indicate a slight deviation from the C_s symmetry which can be explained by the influence of $\text{O}(-\text{H}) \cdots \text{F}$ donor–acceptor interactions (H-bonding). The C–S bond of $1.827(3) \text{ \AA}$ is significantly shorter than in the neutral compound [$1.867(7) \text{ \AA}$].^[7] An explanation for the shortening of the C–S bond is provided in the theoretical section below. Due to the protonation, the S–O bond lengths of $1.543(2)$ and $1.557(2) \text{ \AA}$ are significantly elon-

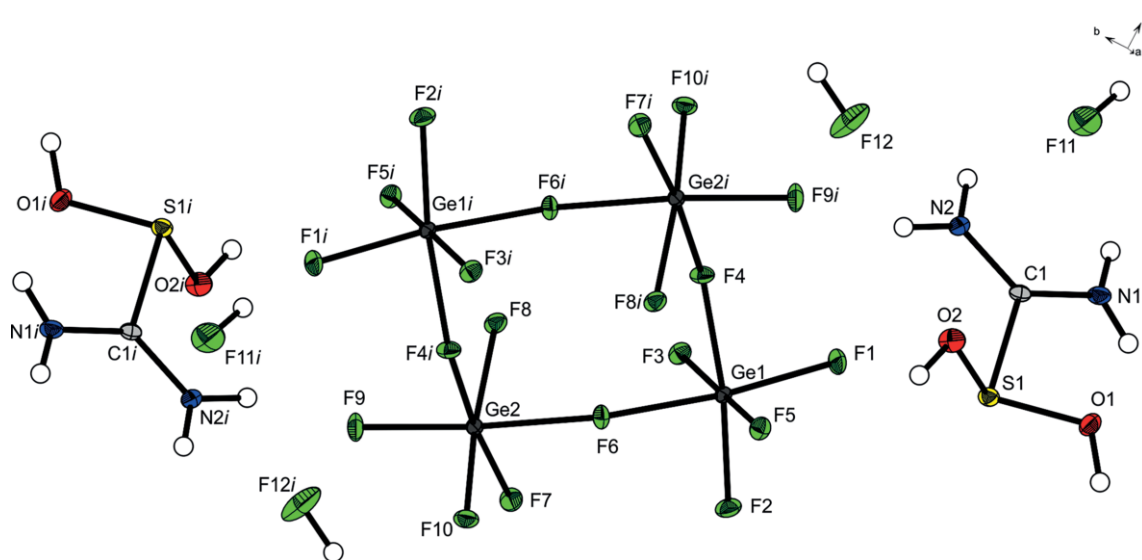


Figure 2. Formula unit of $2[(\text{H}_2\text{N})_2\text{CS}(\text{OH})_2]^{2+}[\text{Ge}_4\text{F}_{20}]^{4-} \cdot 4\text{HF}$ (thermal ellipsoids with 50 % probability). Symmetry code: $i: -x, 1 - y, 1 - z$.

gated compared to the starting material. The C=N bond lengths of 1.294(3) and 1.302(3) Å stay approximately unchanged compared to $(\text{H}_2\text{N})_2\text{CSO}_2$ and thus a protonation at the *N*-positions can be excluded.^[7] The $[\text{Ge}_4\text{F}_{20}]^{4-}$ anion consists of $[\text{GeF}_5]^-$ units forming tetramers with the *Niggli* formula $\infty[\text{GeF}_{2/2}\text{F}_{4/1}]^-$. The germanium atoms are coordinated in a distorted octahedral manner by six fluorine atoms, where two of these atoms are μ -bridging to other germanium atoms with Ge– μ F–Ge bond

angles of 142.3(1) and 146.6(1) Å, leading to a corrugated tetrameric structure. This structural motif is also found in the compounds RuF_5 ,^[12] RhF_5 ^[13] and PtF_5 .^[14] whereas in case of NbF_5 ,^[15] TaF_5 ^[15] and MoF_5 ^[16] the *M*– μ F–*M* angles are observed to be around 180°. The Ge– μ F bond lengths are in the range of 1.866(2) and 1.942(2) Å, thus being significantly longer than the bond lengths between germanium and terminal fluorine atoms [1.731(2)–1.779(2) Å]. The geometric parameters of the $[\text{Ge}_4\text{F}_{20}]^{4-}$ anion are summarized in the Supporting Information (Figure S3 and Table S4). In the solid state, the cations, the anions as well as the co-crystallized HF molecules are linked by medium strong donor–acceptor interactions in the range from 2.549(3) to 2.998(3) Å forming a three-dimensional network. The contacts around the $[(\text{H}_2\text{N})_2\text{CS}(\text{OH})_2]^{2+}$ cation are depicted in Figure 3.

Table 2. Selected bond lengths [Å] and bond angles [°] of $(\text{H}_2\text{N})_2\text{CSO}_2$ (I)^[7] $2[(\text{H}_2\text{N})_2\text{CS}(\text{OH})_2]^{2+}[\text{Ge}_4\text{F}_{20}]^{4-} \cdot 4\text{HF}$ (II) and the calculated $[(\text{H}_2\text{N})_2\text{CS}(\text{OH})_2]^{2+}$ (III) as well as donor–acceptor distances in (III).

	(I)	(II)	(III) ^[a]
Bond lengths [Å]			
C1–N1	1.296(5)	1.294(3)	1.298
C1–N2	1.296(5)	1.302(3)	1.298
S1–C1	1.867(7)	1.827(3)	1.843
S1–O1	1.496(6)	1.543(2)	1.557
S1–O2	1.496(6)	1.557(2)	1.557
Bond angles [°]			
N1–C1–N2	125.2(6)	126.9(2)	127.9
N1–C1–S1	117.2(4)	116.5(2)	115.9
O1–S1–C1	100.4(2)	94.9(1)	95.5
O1–S1–O2	111.1(2)	106.9(1)	107.3
Torsion angles [°]			
O1–S1–C1–N1	35.8(4)	29.6(2)	38.5
O2–S1–C1–N1	150.3(4)	137.0(2)	146.6
O1–S1–C1–N2	–150.3(4)	–152.4(2)	–146.6
O2–S1–C1–N2	–35.8(4)	–45.0(2)	–38.5
Donor–acceptor distances [Å]			
N1(–H1A)⋯F11	2.809(3)	N2(–H1A)⋯F12	2.822(3)
N1(–H1A)⋯F12	2.886(3)	N2(–H1A)⋯F11	2.998(3)
N1(–H1B)⋯F7	2.972(3)	N2(–H1B)⋯F9	2.838(3)
F11(–H11)⋯F1	2.554(2)	O1(–H1)⋯F3	2.492(3)
F12(–H12)⋯F10	2.549(3)	O1(–H1)⋯F8	2.912(3)
O2(–H2)⋯F5	2.521(2)		

[a] Calculated at the PBE1PBE/6-311G++(3df,3pd) level of theory.

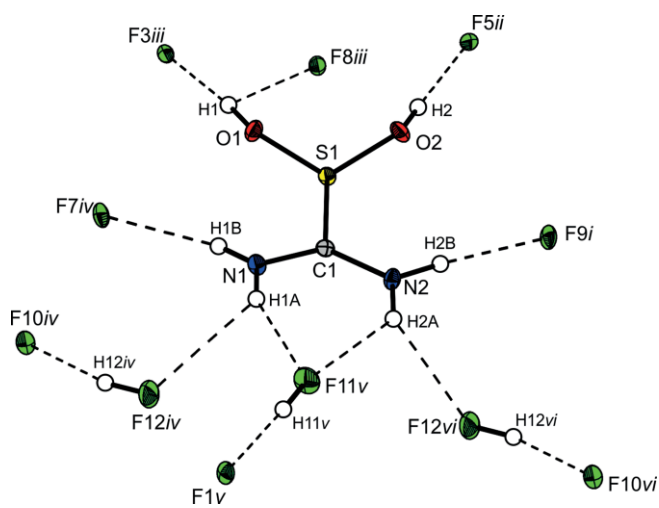


Figure 3. Contacts around the $[(\text{H}_2\text{N})_2\text{CS}(\text{OH})_2]^{2+}$ cation (thermal ellipsoids with 50 % probability). Symmetry codes: $i: -x, 1 - y, 1 - z$; $ii: -x, -y, 1 - z$; $iii: x, -1 + y, z$; $iv: 1 - x, -y, 1 - z$; $v: 1 - x, -y, 2 - z$; $vi: x, y, 1 + z$.

Theoretical Calculations

Gas-phase optimizations of $[(X_2N)_2CS(OX)_2]^{2+}$ ($X = H, D$) and $(H_2N)_2CSO_2$ were carried out at the PBE1PBE/6-311G++(3df, 3pd) level of theory. This method was chosen for a better comparability with our previous studies on the basicity of the sulfone moiety. The calculated geometric parameters are in satisfying agreement to the ones observed in the crystal structure. In case of the vibrational frequencies the OH and NH stretching vibrations are overestimated by approximately 200 cm^{-1} , which can be explained by the influence of H-bonding in the solid-state. As observed in the single-crystal X-ray structure the O,O' -diprotonation causes a significant shortening of the C–S bond. This finding prompted us to perform further theoretical investigations in order to get an insight into the nature of the bond. In the case of the starting material we found that the $\sigma_{(C-S)}^*$ is occupied by 0.267 e and the p-orbitals of the oxygen atoms are occupied by 1.779 e. Therefore, we conclude that electron-density of the $p_{(O)}$ -orbitals is donated into the $\sigma_{(C-S)}^*$ causing a weakening of this bond since these orbitals are overlapping. Due to the O,O' -diprotonation the overlap of the oxygen $p_{(O)}$ -orbitals with the $\sigma_{(C-S)}^*$ is nearly abolished. In case of the $[(H_2N)_2CS(OH)_2]^{2+}$ cation the $\sigma_{(C-S)}^*$ is considerably lower occupied [0.105 e]. In Figure 4 a comparison of the calculated starting material and its O,O' -diprotonated species together with the relevant orbitals are shown.

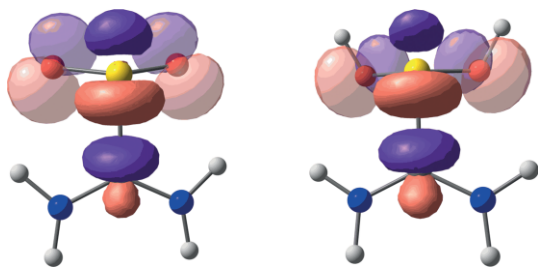


Figure 4. Calculated TDO (left) and its O,O' -diprotonated species (right) with illustrated $\sigma_{(C-S)}^*$ and $p_{(O)}$ orbitals.

In case of the starting material and the O,O' -diprotonated species the donation of sulfur lone-pairs ($n_{(S)}$) to the $\sigma_{(C-S)}^*$ can be considered as low since the occupancy of $n_{(S)}$ is 1.959 e (starting material) and 1.977 e (O,O' -diprotonated species). This becomes evident when considering the overlap of the corresponding orbitals (see Supporting Information, Figure S1 and S2).

Conclusions

In the course of this study thiourea dioxide (TDO) was investigated in the superacidic media XF/MF_5 ($X = H, D; M = As, Sb$). The observed colorless salts, containing the $[(X_2N)_2CS(OH)_2]^{2+}$ cation, were characterized by low-temperature vibrational spectroscopy. The assignments were supported by quantum-chemical calculations at the PBE1PBE/6-311G++(3pd, 3df) level of theory. For $2[(H_2N)_2CS(OH)_2]^{2+}[Ge_4F_{20}]^{4-}\cdot 4HF$ a crystal structure is described. In addition, a salt containing the $[Ge_4F_{20}]^{4-}$ anion is reported for the first time. Due to the O,O' -diprotonation, the

remarkably long C–S bond is significantly shortened. In the case of the starting material, this unusual bond length can be explained by a notable occupation of the $\sigma_{(C-S)}^*$ orbital, which is nearly abolished by the O,O' -diprotonation, leading to a shortening of the C–S bond.

Experimental Section

Caution! The hydrolysis of the investigated compounds causes the formation of HF/DF. Safety precautions should be taken while handling these compounds.

Apparatus and Materials: Anhydrous hydrogen fluoride (99 %, Linde) was dried with fluorine for two weeks prior to use. All reactions during the course of this study were performed employing standard Schlenk techniques using a stainless-steel vacuum line. The reactions were performed in FEP/PFA reaction vessels, which were closed with stainless-steel valves. Before starting the experiments, the stainless-steel vacuum line and the reaction vessels were dried with fluorine. Low temperature Raman spectra were recorded with a Bruker MultiRAM FT-Raman spectrometer equipped with a Nd:YAG laser ($\lambda = 1064\text{ nm}$) at $-196\text{ }^\circ\text{C}$ with a laser excitation of up to 350 mW in the range from 350 to 4000 cm^{-1} . Low temperature IR measurements were performed with a Bruker Vertex-80V-FT-IR spectrometer. For the visualization of the spectra the software Bruker OPUS 6.5 was employed. The single-crystal structure X-ray analysis was carried out with an Oxford Xcalibur3 diffractometer equipped with a Spellman generator (50 kV, 40 mA), using Mo radiation ($\lambda = 0.7107\text{ \AA}$) and a Kappa CCD detector at a temperature of 173 K. For data collection the CrysAlis CCD^[17] program was employed and for data reduction the program CrysAlis RED^[18] The programs SHELXS^[19] and SHELXL-97^[20] implemented in the WingGX^[21] software package were used for structure solution, as well as refinement and checked with the PLATON software.^[22] The absorption correction was carried out using the SCALE3 APSACK multi-scan method.^[23] For quantum-chemical calculations the Gaussian09 package^[24] was employed, together with the PBE1PBE density functional approach and the basis set 6-311G++(3pd, 3df). Crystal data and structure refinement for $2[(H_2N)_2CS(OH)_2]^{2+}[Ge_4F_{20}]^{4-}\cdot 4HF$ are listed in the Supporting Information (Table S2).

CCDC 1869464 {for $2[(H_2N)_2CS(OH)_2]^{2+}[Ge_4F_{20}]^{4-}\cdot 4HF$ } contains the supplementary crystallographic data for this paper. These data can be obtained free of charge from The Cambridge Crystallographic Data Centre.

Synthesis of $[(X_2N)_2CS(OX)_2]^{2+}2[MF_6]^-$ ($M = Sb, As; X = H, D$) and $2[(H_2N)_2CS(OH)_2]^{2+}[Ge_4F_{20}]^{4-}$: In a typical experiment SbF_5 (434 mg, 2 mmol, 2 eq.), AsF_5 (340 mg, 2 mmol, 2 eq.) or GeF_4 (446 mg, 3 mmol, 3 eq.) were condensed in a reactor (FEP tube) followed by an excess of aHF or aDF (ca. 1 mL) at $-196\text{ }^\circ\text{C}$. After allowing the compounds to mix, $(H_2N)_2CSO_2$ (108 mg, 1 mmol, 1 eq.) was added under N_2 atmosphere to the again frozen mixture. Afterwards, the mixture was warmed up to $-60\text{ }^\circ\text{C}$, then further to room temperature. Excess of aHF or aDF was removed within 14 h at $-78\text{ }^\circ\text{C}$. Colorless crystals of the above-mentioned species were received.

Acknowledgments

This project received funding from the LMU Munich and the Deutsche Forschungsgemeinschaft (DFG). Further support by the F-Select GmbH is gratefully acknowledged.

Keywords: Thiourea dioxide · Protonation · Superacid chemistry · Germanium · Structure elucidation

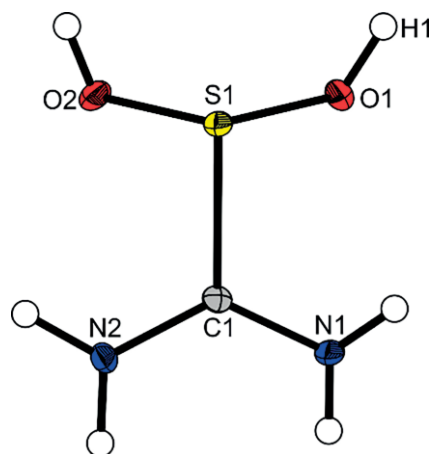
- [1] S. V. Makarov, *Russ. Chem. Rev.* **2001**, *70*, 885–895.
 [2] T. S. Jagodzinski, *Chem. Rev.* **2003**, *103*, 197–227.
 [3] E. de Barry Barnett, *J. Chem. Soc.* **1910**, *97*, 63–65.
 [4] P. Krug, *J. Soc. Dyers Colour.* **1953**, *69*, 606–611.
 [5] R. A. L. Sullivan, A. Hargreaves, *Acta Crystallogr.* **1962**, *15*, 675–682.
 [6] Y. Wang, N. L. Chang, C. T. Pai, *Inorg. Chem.* **1990**, *29*, 3256–3259.
 [7] J. S. Song, E. H. Kim, S. K. Kang, S. S. Yun, I. H. Suh, S. S. Choi, S. Lee, W. P. Jensen, *Bull. Korean Chem. Soc.* **1996**, *17*, 201–205.
 [8] M. K. Denk, K. Hatano, A. J. Lough, *Eur. J. Inorg. Chem.* **2003**, *2003*, 224–231.
 [9] Z. Kis, S. V. Makarov, R. Silaghi-Dumitrescu, *J. Sulfur Chem.* **2010**, *31*, 27–39.
 [10] D. Lewis, J. Mama, J. Hawkes, *Appl. Spectrosc.* **2014**, *68*, 1327–1332.
 [11] J. Weidlein, U. Müller, K. Dehnicke, *Schwingungsspektroskopie, Vol. 2nd ed.*, Georg Thieme Verlag, Stuttgart, Germany, **1988**.
 [12] W. J. Casteel, A. P. Wilkinson, H. Borrmann, R. E. Serfass, N. Bartlett, *Inorg. Chem.* **1992**, *31*, 3124–3131.
 [13] B. K. Morrell, A. Zalkin, A. Tressaud, N. Bartlett, *Inorg. Chem.* **1973**, *12*, 2640–2644.
 [14] B. G. Mueller, M. Serafin, *ChemInform* **1992**, *23*.
 [15] A. J. Edwards, *J. Chem. Soc.* **1964**, 3714–3718.
 [16] R. E. Stene, B. Scheibe, C. Pietzonka, A. J. Karttunen, W. Petry, F. Kraus, *J. Fluorine Chem.* **2018**, *211*, 171–179.
 [17] *CrysAlisCCD*, Version 1.171.35.11 (release 16–05–2011 CrysAlis 171.NET), Oxford Diffraction Ltd, UK, **2011**.
 [18] *CrysAlisRED*, Version 1.171.35.11 (release 16–05–2011 CrysAlis 171.NET), Oxford Diffraction Ltd., UK, **2011**.
 [19] G. M. Sheldrick, *SHELXS-97*, Program for Crystal Structure Solution, University of Göttingen, Germany, **1997**.
 [20] G. M. Sheldrick, *SHELXL-97*, Program for the Refinement of Crystal Structures, University of Göttingen, Germany, **1997**.
 [21] L. Farrugia, *J. Appl. Crystallogr.* **1999**, *32*, 837–838.
 [22] A. L. Spek, *PLATON*, A Multipurpose Crystallographic Tool, U. Utrecht University, The Netherlands, **1999**.
 [23] *SCALE3 ABSPACK*, An Oxford Diffraction Program, O. Diffraction, Ltd., UK, **2005**.
 [24] M. J. Frisch, G. W. Trucks, H. B. Schlegel, G. E. Scuseria, M. A. Robb, J. R. Cheeseman, G. Scalmani, V. Barone, B. Mennucci, G. A. Petersson, H. Nakatsuji, M. Caricato, X. Li, H. P. Hratchian, A. F. Izmaylov, J. Bloino, G. Zheng, J. L. Sonnenberg, M. Hada, M. Ehara, K. Toyota, R. Fukuda, J. Hasegawa, M. Ishida, T. Nakajima, Y. Honda, O. Kitao, H. Nakai, T. Vreven, J. A. Montgomery Jr., J. E. Peralta, F. Ogliaro, M. Bearpark, J. J. Heyd, E. Brothers, K. N. Kudin, V. N. Staroverov, R. Kobayashi, J. Normand, K. Raghavachari, A. Rendell, J. C. Burant, S. S. Iyengar, J. Tomasi, M. Cossi, N. Rega, J. M. Millam, M. Klene, J. E. Knox, J. B. Cross, V. Bakken, C. Adamo, J. Jaramillo, R. Gomperts, R. E. Stratmann, O. Yazyev, A. J. Austin, R. Cammi, C. Pomelli, J. W. Ochterski, R. L. Martin, K. Morokuma, V. G. Zakrzewski, G. A. Voth, P. Salvador, J. J. Dannenberg, S. Dapprich, A. D. Daniels, Ö. Farkas, J. B. Foresman, J. V. Ortiz, J. Cioslowski, D. J. Fox, *Gaussian 09, Revision A.1*, Gaussian, Inc., Wallingford CT, **2009**.

Received: October 26, 2018

Superacids

*D. Leitz, A. Nitzer, Y. Morgenstern,
F. Zischka, A. J. Kornath** 1–6

**Structural Investigation of Thiourea
Dioxide in Superacids**



Upon *O,O'*-diprotonation, thiourea dioxide (TDO) undergoes remarkable structural changes, which are discussed together with the fascinating structure of the $[\text{Ge}_4\text{F}_{20}]^{4-}$ anion.

DOI: 10.1002/ejic.201801298

Supporting Information

Table S1. Experimental vibrational frequencies [cm^{-1}] of $[(\text{H}_2\text{N})_2\text{CS}(\text{OH})_2]^{2+}2[\text{AsF}_6]^-$, and $[(\text{H}_2\text{N})_2\text{CS}(\text{OH})_2]^{2+}2[\text{SbF}_6]^-$, $[(\text{D}_2\text{N})_2\text{CS}(\text{OD})_2]^{2+}2[\text{AsF}_6]^-$ and calculated vibrational frequencies [cm^{-1}] of $[(\text{H}_2\text{N})_2\text{CS}(\text{OH})_2]^{2+}$ and $[(\text{D}_2\text{N})_2\text{CS}(\text{OD})_2]^{2+}$.

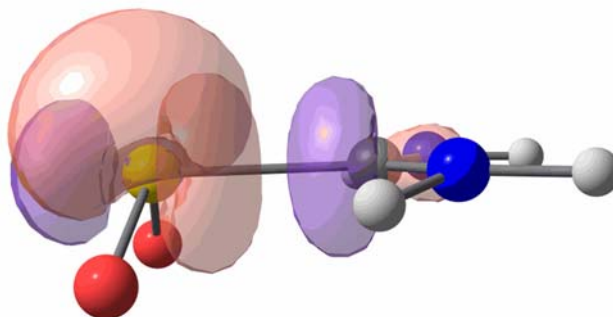
$[(\text{H}_2\text{N})_2\text{CS}(\text{OH})_2]^{2+}2[\text{AsF}_6]^-$		$[(\text{H}_2\text{N})_2\text{CS}(\text{OH})_2]^{2+}2[\text{SbF}_6]^-$		$[(\text{H}_2\text{N})_2\text{CS}(\text{OH})_2]^{2+}$	$[(\text{D}_2\text{N})_2\text{CS}(\text{OD})_2]^{2+}2[\text{AsF}_6]^-$		$[(\text{D}_2\text{N})_2\text{CS}(\text{OD})_2]^{2+}$	Assignment		
IR	Raman	IR	Raman	calcd. ^[a] (IR/Raman)	IR	Raman	calcd. ^[a] (IR/Raman)	[b]		
3401 (m)		3411 (w)		3633 (543/121)			2683 (152/20)	ν_{11}	A'	$\nu_s(\text{OX})$
3397 (w)		3400 (w)		3619 (497/51)		2578 (1)	2675 (61/8)	ν_{17}	A''	$\nu_{\text{as}}(\text{OX})$
3333 (w)	3333 (3)	3337 (w)		3618 (218/37)	2517 (m)	2520 (12)	2648 (289/57)	ν_2	A'	$\nu_{\text{as}}(\text{NX}_2)$
				3613 (68/5)	2448 (w)	2444 (5)	2636 (231/21)	ν_{18}	A''	$\nu_{\text{as}}(\text{NX}_2)$
3231 (s)	3237 (2)	3249 (m)	3240 (3)	3515 (297/171)		2409 (1)	2551 (143/76)	ν_3	A'	$\nu_s(\text{NX}_2)$
3118 (s)				3491 (393/19)			2528 (307/7)	ν_{19}	A''	$\nu_s(\text{NX}_2)$
1727 (s)		1714 (s)		1792 (375/0)	1720 (m)	1706 (1)	1766 (253/1)	ν_{20}	A''	$\nu_{\text{as}}(\text{CN}_2)$
1618 (w)	1622 (4)	1622 (m)	1626 (2)	1669 (69/2)	1173 (m)	1177 (9)	1195 (1/3)	ν_4	A'	$\delta(\text{NX}_2)$
1559 (w)	1563 (6)	1562 (m)	1571 (3)	1601 (66/6)	1136 (m)	1146 (3)	1174 (43/2)	ν_{21}	A''	$\delta(\text{NX}_2)$
1431 (w)	1427 (14)	1421 (w)	1424 (15)	1433 (29/13)	1423 (w)	1404 (41)	1431 (43/10)	ν_5	A'	$\nu_s(\text{CN}_2)$
		1226 (w)	1230 (2)	1172 (109/3)	885 (m)	888 (5)	888 (24/4)	ν_6	A'	$\delta(\text{SOX})$
1152 (w)	1158 (3)	1158 (m)	1165 (4)	1142 (81/3)		795 (12)	829 (115/1)	ν_{22}	A''	$\delta(\text{SOX})$
1122 (w)	1101 (20)		1114 (13)	1121 (22/12)	928 (3)	925 (22)	934 (18/10)	ν_7	A'	$\delta(\text{CNX})$
			1043 (5)	1043 (1/1)	803 (m)		804 (4/1)	ν_{23}	A''	$\delta(\text{CNX})$
968 (vw)	953 (2)	945 (w)		965 (231/2)	961 (m)	966 (9)	976 (119/4)	ν_{24}	A''	$\nu_{\text{as}}(\text{SO}_2)$
908 (vw)	905 (9)	904 (w)	908 (13)	915 (79/13)		909 (24)	913 (94/13)	ν_8	A'	$\nu_s(\text{SO}_2)$
	805 (13)		803 (9)	723 (14/1)			677 (28/1)	ν_9	A'	$\delta(\text{CN}_2)$
		672 (vw)		677 (332/1)	512 (w)	514 (5)	510 (126/1)	ν_{10}	A'	$\delta(\text{CN}_2)$
630 (w)				645 (4/0)		573 (23)	560 (17/6)	ν_{25}	A''	$\nu(\text{SC})$
	620 (2)			634 (52/5)		477 (2)	464 (36/0)	ν_{11}	A'	$\delta(\text{NX}_2)$
	573 (7)		567 (7)	594 (1/2)			342 (3/2)	ν_{12}	A'	$\delta(\text{NCS})$
			537 (6)	540 (113/3)	396 (m)		397 (45/1)	ν_{13}	A'	$\delta(\text{SOX})$
512 (vw)	498 (3)			511 (43/1)			421 (12/2)	ν_{26}	A''	$\delta(\text{SOX})$
431 (m)	432 (8)			414 (6/2)	374 (w)	379 (46)	390 (1/1)	ν_{14}	A'	$\delta(\text{CN}_2)$
			387 (10)	397 (8/0)			274 (1)	ν_{27}	A''	$\delta(\text{NX}_2)$
				381 (2/1)			333 (3)	ν_{15}	A'	$\delta(\text{SO}_2)$
			360 (15)	362 (6/3)			314 (18/1)	ν_{28}	A''	$\delta(\text{NX}_2)$
			284 (40)	285 (43/2)			263 (42/1)	ν_{16}	A'	$\delta(\text{CSO})$
				243 (0/0)		228 (3)	227 (0/0)	ν_{29}	A''	$\delta(\text{SO}_2)$
				44 (0/1)			40 (0/0)	ν_{30}	A''	$\omega(\text{CN}_2)$
698 (s)	686 (100)	658 (s)	653 (100)		700 (s)	687 (100)				$[\text{MF}_6]^-$
554 (m)	573 (7)	554 (m)	567 (7)			553 (10)				$[\text{MF}_6]^-$
390 (s)	370 (38)		283 (35)							$[\text{MF}_6]^-$

[a] Calculated at the PBE1PBE/6-311G++(3df,3dp) level of theory. IR intensity in [km/mol] and Raman scattering activities in [$\text{\AA}^4/\mu$]. Abbreviations for IR intensities: v = very, s = strong, m = medium, w = weak. Experimental Raman scattering activity is stated to a scale of 1 to 100. [b] X = H, D; M = As, Sb.

Table S2. Experimental and calculated vibrational frequencies (in cm^{-1}) of $(\text{H}_2\text{N})_2\text{CSO}_2$.

$(\text{H}_2\text{N})_2\text{CSO}_2$		$(\text{H}_2\text{N})_2\text{CSO}_2$	Assignment		
IR	Raman	calcd. ^[a]			
3273 (s)	3246 (0)	3663 (42/129)	ν_{15}	A''	$\nu_{\text{as}}(\text{NH}_2)$
		3632 (37/327)	ν_1	A'	$\nu_{\text{as}}(\text{NH}_2)$
3044 (s)	3065 (5)	3551 (58/231)	ν_2	A'	$\nu_{\text{s}}(\text{NH}_2)$
		3440 (159/60)	ν_{16}	A''	$\nu_{\text{s}}(\text{NH}_2)$
1701 (s)	1683 (2)	1751 (335/6)	ν_{17}	A''	$\nu_{\text{as}}(\text{CN})$
		1637 (31/10)	ν_3	A'	$\delta(\text{NH}_2)$
1477 (w)		1540 (28/6)	ν_{18}	A''	$\delta(\text{NH}_2)$
1435 (s)	1431 (10)	1391 (4/10)	ν_4	A'	$\nu_{\text{s}}(\text{CN})$
	1103 (38)	1207 (253/9)	ν_{19}	A''	$\nu_{\text{as}}(\text{SO}_2)$
1073 (m)	1076 (7)	1139 (23/13)	ν_5	A'	$\delta(\text{CNH})$
1026 (s)		1079 (61/12)	ν_6	A'	$\nu_{\text{s}}(\text{SO}_2)$
997 (s)	987 (100)	1063 (49/8)	ν_{20}	A''	$\delta(\text{NH}_2)$
734 (s)		795 (34/1)	ν_7	A'	$\delta(\text{NH}_2)$
689 (s)	688 (9)	710 (31/1)	ν_8	A'	$\delta(\text{CN}_2)$
620 (m)	621 (24)	623 (22/1)	ν_{21}	A''	$\nu(\text{SC})$
		575 (218/0)	ν_9	A'	$\delta(\text{NH}_2)$
		532 (29/6)	ν_{10}	A'	$\delta(\text{CN}_2)$
		498 (54/0)	ν_{11}	A'	$\delta(\text{NH}_2)$
501 (s)	498 (14)	463 (6/1)	ν_{22}	A''	$\delta(\text{NH}_2)$
		416 (15/3)	ν_{12}	A'	$\delta(\text{SO}_2)$
382 (m)	392 (17)	273 (22/3)	ν_{23}	A''	$\delta(\text{NCS})$
	326 (22)	258 (25/5)	ν_{13}	A'	$\delta(\text{NH}_2)$
	284 (1)	181 (7/4)	ν_{14}	A'	$\delta(\text{NH}_2)$
	172 (4)	28 (3/1)	ν_{24}	A''	$\delta(\text{CSO})$

[a] Calculated at the PBE/PBE/6-311G++(3df,3dp) level of theory. IR intensity in $[\text{km}/\text{mol}]$ and Raman scattering activities in $[\text{\AA}^4/\mu]$. Abbreviations for IR intensities: v = very, s = strong, m = medium, w = weak. Experimental Raman scattering activity is stated to a scale of 1 to 100.

**Figure S1:** Calculated structure of $(\text{H}_2\text{N})_2\text{CSO}_2$ with illustrated sulfur lone-pair and $\sigma^*_{(\text{C-S})}$ orbital.

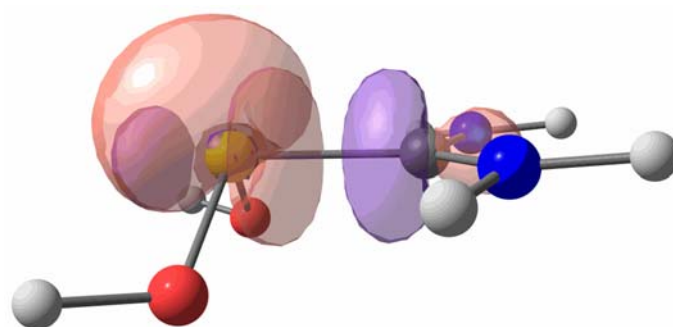


Figure S2: Calculated structure of the $[(\text{H}_2\text{N})_2\text{CS}(\text{OH})_2]^{2+}$ cation with illustrated sulfur lone-pair and $\sigma^*_{(\text{C-S})}$ orbital.

Table S3. Crystal data and structure refinement for and $2[(\text{H}_2\text{N})_2\text{CS}(\text{OH})_2]^{2+}[\text{Ge}_4\text{F}_{20}]^{4-} \cdot 4 \text{HF}$

Empirical formula	$\text{C}_2\text{H}_{16}\text{F}_{24}\text{Ge}_4\text{N}_4\text{O}_4\text{S}_2$
M_r	970.67
Crystal system	triclinic
Space Group	$P\bar{1}$
a [Å]	8.057(5)
b [Å]	8.598(5)
c [Å]	9.126(5)
α	85.619(5)
β	82.582(5)
γ	75.862(5)
V [Å ³]	607.3(6)
Z	1
ρ_{calcd} , [gcm ⁻³]	2.654
μ [mm ⁻¹]	5.280
$\lambda_{\text{MoK}\alpha}$ [Å]	0.71073
$F(000)$	464
T [K]	123(2)
hkl range	-10:10; -10:12; -11:13
refl. measured	6454
refl. unique	3700
R_{int}	0.0279
parameters	213
$R(F)/wR(F^2)^a$	0.0353/0.0594
weighting scheme ^{b)}	0.0170
$S(\text{GoF})^c$	1.016
residual density [eÅ ⁻³]	0.697/-0.765
device type	Oxford XCalibur
solution/refinement	SHELXS-97
CCDC	1869464

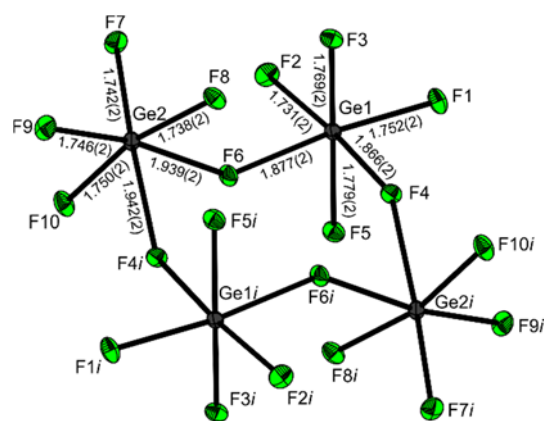


Figure S3: X-ray structure of the $[\text{Ge}_4\text{F}_{20}]^{4-}$ anion (thermal ellipsoids with 50% probability). Symmetry code: $i: -x, 1-y, 1-z$.

Table S4. Bond lengths [Å] and bond angles [°] of the $[\text{Ge}_4\text{F}_{20}]^{4-}$ anion in $2[(\text{H}_2\text{N})_2\text{CS}(\text{OH})_2]^{2+}[\text{Ge}_4\text{F}_{20}]^{4-} \cdot 4 \text{ HF}$.

Bond lengths [Å]			
Ge1–F2	1.731(2)	Ge2–F7	1.742(2)
Ge1–F1	1.752(2)	Ge2–F8	1.738(2)
Ge1–F3	1.769(2)	Ge2–F9	1.746(2)
Ge1–F5	1.779(2)	Ge2–F10	1.750(2)
Ge1–F4	1.866(2)	Ge2–F6	1.939(2)
Ge1–F6	1.877(2)	Ge2–F4	1.942(2)
Bond angles [°]			
F2–Ge1–F1	97.7(1)	F8–Ge2–F7	95.4(1)
F2–Ge1–F3	91.3(1)	F8–Ge2–F9	94.6(1)
F1–Ge1–F3	92.2(1)	F7–Ge2–F9	98.8(1)
F2–Ge1–F5	93.1(1)	F8–Ge2–F10	167.6(1)
F1–Ge1–F5	90.4(1)	F7–Ge2–F10	93.0(1)
F3–Ge1–F5	174.6(1)	F9–Ge2–F10	93.2(1)
F3–Ge1–F5	172.9(1)	F8–Ge2–F6	86.4(1)
F1–Ge1–F4	89.1(1)	F7–Ge2–F6	90.3(1)
F3–Ge1–F4	86.6(1)	F9–Ge2–F6	170.8(1)
F5–Ge1–F4	88.8(1)	F10–Ge2–F6	84.4(1)
F2–Ge1–F6	89.3(1)	F8–Ge2–F4	86.7(1)
F1–Ge1–F6	172.8(1)	F7–Ge2–F4	172.6(1)
F3–Ge1–F6	89.7(1)	F9–Ge2–F4	88.1(1)
F5–Ge1–F6	87.2(1)	F10–Ge2–F4	83.8(1)
F4–Ge1–F6	84.0(1)	F6–Ge2–F4	82.8(1)
Ge1–F4–Ge2	146.6(1)	Ge1–F6–Ge2	143.3(1)
Torsion angles [°]			
F1–Ge1–F4–Ge2	–114.1(2)	F2–Ge1–F6–Ge2	–77.3(1)
F3–Ge1–F4–Ge2	153.7(2)	F3–Ge1–F6–Ge2	14.0(1)
F5–Ge1–F4–Ge2	–23.6(2)	F5–Ge1–F6–Ge2	–170.6(1)
F6–Ge1–F4–Ge2	63.7(2)	F4–Ge1–F6–Ge2	100.6(1)
F8–Ge2–F6–Ge1	–47.9(1)	F10–Ge2–F6–Ge1	140.5(1)
F7–Ge2–F6–Ge1	47.6(1)	F4–Ge2–F6–Ge1	–135.0(1)